Targeting MAPK Signaling in Melanoma Cells

-

Implications for Immune Recognition and Cell Fate

Referees: Prof. Dr. Stephan Urban

PD Dr. Christine S. Falk

Dissertation

submitted to the
combined Faculties for the Natural Sciences and for Mathematics
of the Ruperto-Carola University of Heidelberg, Germany
for the degree of
Doctor of Natural Sciences

presented by
Diplom-Biologe
Stefan Maßen
born in: Freiburg im Breisgau

Oral examination: ……

Table of contents

Summary

To date, there are no encouraging treatment options for patients with malignant melanoma available. In search of therapeutic opportunities for these patients, the MAPK pathway called attention due to the discovery that components of this pathway are frequently mutated in cutaneous melanoma cells. 44% of melanoma patients have activating mutations in BRaf, and a single mutation, ^{V600E}BRaf, accounts for 90% of these BRaf mutations. Upstream, NRas is mutated in 22% of patients. The two mutations are mutually exclusive, indicating that one “driver” mutation is sufficient to constitutively activate the pathway. Several small molecule inhibitors have been developed to inhibit MAPK signaling by targeting BRaf or MEK. In a system comprising a ^{V600E}BRaf mutated melanoma cell line and three primary melanoma lines from one patient which carry a ^{G469R}BRaf mutation, I have comprehensively analyzed the effects of MAPK inhibition through U0126 and AZD6244 (specific MEK inhibitors) and Sorafenib (multi-kinase BRaf inhibitor) on recognition by NK cells, modulation of other cell signaling pathways in melanoma cells and their fate between apoptosis and autophagy.

Surface expression of NK cell ligands on melanoma cells was strongly modulated by MAPK inhibition. Expression of CD155, a ligand for the activating NK cell receptor DNAM-1 was decreased following MEK inhibition with U0126 and AZD6244 but increased by Sorafenib-mediated BRaf inhibition. This regulation of CD155 in melanoma cells had functional consequences for activation of NK cells because reduced CD155 expression following MEK inhibition correlated with reduced levels of NK cell cytotoxicity.

Besides the analysis of NK cell activation against treated melanoma cells, the tumor cell fate was also investigated in detail. The core of my comprehensive analysis was based on the simultaneous inspection of multiple cell signaling pathways in tight kinetics up to 96 hours. I was able to unravel differences in the mechanisms of action between the two MEK inhibitors and the BRaf inhibitor with respect to phosphorylation of MEK and kinase stability in general. In addition, I could identify consequences of MAPK inhibition on Akt, JNK, and p53 signaling pathways, which are all involved in the regulation of apoptosis and autophagy. *En route* to the evaluation of autophagy regulation in response to MAPK treatment, I have established a new ImageStream-based method for the quantification of autophagy, combining flow cytometry and single cell imaging. JNK was identified as a critical negative, and NFκB as a positive regulator of autophagy. The combination of this quantification of autophagy with an approach to measure apoptotic cells allowed the simultaneous detection of autophagy and apoptosis in the same cell under conditions of MAPK inhibition. These results indicate that Sorafenib, but not U0126 or AZD6244, effectively inhibits autophagy and promotes apoptosis.

Taken together, my studies clearly demonstrate that interference of the oncogenic MAPK pathway has consequences for immune recognition of tumor cells, the tumor microenvironment and the balance between autophagy and apoptosis.

Zusammenfassung

Derzeit existieren leider keine ermutigenden Therapiemöglichkeiten für Patienten mit metastasiertem Melanom. Auf der Suche nach gezielten Interventionen hat der MAPK Signalweg besonderes Aufsehen erregt, weil einige der Komponenten in Melanomen häufig mutiert sind. 44% der kutanen Melanome weisen aktivierende BRaf-Mutationen auf, wobei die ^{V600E}BRaf-Mutation mit 90% am häufigsten zu finden ist. NRas ist dagegen in 22% der Melanome mutiert. BRaf und NRas Mutationen schließen sich gegenseitig aus, was darauf hindeutet, dass eine Hauptmutation für eine konstitutive Aktivierung des Signalweges ausreicht. Seitdem wurden mehrere Inhibitoren für eine Blockade verschiedenen Stellen entwickelt. Ich habe die Effekte der MAPK Blockierung durch U0126 und AZD6244 (spezifische MEK Inhibitoren), sowie durch Sorafenib (multi-Kinase BRaf Inhibitor) auf die NK-Zell-Erkennung, die Modulation weiterer Zellsignalwege und das Zellschicksal im Hinblick auf Apoptose und Autophagie umfassend untersucht. Das von mir verwendete Zellsystem beinhaltet eine ^{V600E}BRaf mutierte Melanomlinie, sowie drei primäre Melanomlinien aus einem Patienten mit identischer ^{G469R}BRaf Mutation.

Die Inhibition des MAPK Weges führte zu einer deutlichen Modulation der Expression von NK Zell Liganden. Die CD155-Expression, ein Ligand des aktivierenden NK Zell Rezeptors DNAM-1, wurde nach MEK-Inhibition durch U0126 und AZD6244 verringert, durch die BRaf-Inhibition mit Sorafenib jedoch erhöht. Die funktionelle Relevanz dieser CD155-Regulation wurde in Degranulationsexperimenten gezeigt, wobei die verringerte CD155-Expression zu einer verringerten NK-Zellaktivierung führte. Neben der Untersuchung der NK-Zellaktivierung habe ich mich ausführlich mit dem Schicksal der Tumorzellen beschäftigt. Im Zentrum meiner Untersuchung stand die Analyse mehrerer Signalwege nach Behandlung mit MAPK Inhibitoren in 96-Stunden-Kinetiken. Dabei ließen sich unterschiedliche Wirkmechanismen zwischen MEK- und BRaf-Inhibitoren im Hinblick auf die MEK-Phosphorylierung und die generelle Stabilität der Kinasen feststellen. Die Blockierung des MAPK Wegs bewirkte weitreichende Effekte auf die Akt, JNK und p53 Signalwege, die an der Regulation von Apoptose und Autophagie beteiligt sind. Um die Auswirkungen der MAPK Blockierung auf diese Regulation zu untersuchen, habe ich eine neue ImageStream-basierte Methode für die Quantifizierung von Autophagie etabliert, die Durchflusszytometrie mit Mikroskopie kombiniert. JNK wurde als kritischer negativer Regulator, und NFκB als positiver Regulator von Autophagie identifiziert. Die parallele Quantifizierung von Autophagie und Apoptose in einem Ansatz habe ich angewandt, um die Auswirkungen der MAPK-Inhibition auf beide Wege definieren zu können. Meine Ergebnisse zeigen, dass Sorafenib, aber nicht U0126 und AZD6244, die Induktion von Autophagie deutlich verringert, und gleichzeitig die Apoptose begünstigt.

Meine Untersuchungen zeigen deutlich, dass die Störung des onkogenen MAPK-Signalweges Konsequenzen für die Immunerkennung der Tumorzellen, das Tumor-Milieu und die Balance zwischen Apoptose und Autophagie hat.

I. Introduction

Cancer is a leading cause of death worldwide. According to WHO (World Health Organization) statistics, cancer accounted for 7.9 million deaths in 2007, around 13% of all deaths. Deaths from cancer worldwide are projected to continuously rise, with an estimated 12 million deaths in 2030. By the broadest definition, cancer is a term used for diseases in which abnormal cells divide without control and, as malignant cells, are able to invade other tissues. Cancer cells can spread to other parts of the body through the blood and lymphatic systems. To date, there are more than 300 different defined types of cancer, depending on their type of origin. Research over the past decades has shown that cancer development and progression involves dynamic changes in the genome of cells and their microenvironment. Discovery of tumorspecific mutations which produce oncogenes with dominant gain of function mutations on the one hand, and tumor suppressor genes with recessive loss of function on the other hand, has opened an entire research field in the context of oncogenic signaling events. While cancer research has become a very complex field, and research is continuously adding to this with additional layers of complexity, it has become clear that the origin of cancer and its development follows logical rules, and thus the complexity is understandable in terms of underlying principles and driving forces:

Cancer progresses through aquisition of functional capabilities, leading to defects in regulatory pathways that govern cell proliferation and homeostasis. Hanahan and Weinberg suggested that the vast catalog of cancer cell genotypes is a manifestation of essential principles, referred to as the hallmarks of cancer [1], and proposed six essential alterations in cell physiology, that collectively dictate malignant growth: Self-sufficiency in growth signals, insensitivity to growth inhibitory signals, evasion of programmed cell death (apoptosis), limitless replicative potential, sustained angiogenesis, and tissue invasion and metastasis.

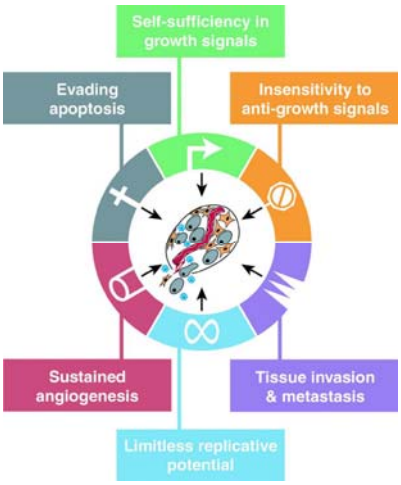

Figure I-1 - Hanahan and Weinberg suggested the "hallmarks of cancer", which include six essential alterations in cell physiology. They postulated the hypothesis, that cancer cell genotypes are a manifestation of essential principles, which collectively dictate malignant growth.

Cancer self-sufficiency in growth signals liberates cancer from the dependence on exogeneously derived signals from the normal tissue micronenvironment. This disrupts a critically important homeostatic mechanism, which normally functions to ensure proper behavior of various cell types within a tissue. Autonomy from growth signals can be achieved over three common molecular strategies, involving the alteration of (i) extracellular growth signals, of (ii) transcellular transducers of those signals, or of (iii) intracellular circuits that translate those signals into a cascade that leads to alterations in gene expression.
One of the driving forces for a variety of malignancies is the mitogen-activated protein kinase (MAPK) pathway, which plays a central role in the latter translational step: It integrates and processes signals from ligand activated growth factor receptors and integrins, resulting in increased gene expression and proliferation.

I.1 Melanoma

Skin cancer is the third most common human malignancy and its global incidence is rising at an alarming rate, with basal cell carcinoma, squamous cell carcinoma and malignant melanoma being the most common forms. There are an estimated 2–3 million new cases of skin cancer across the world each year, and although melanoma only accounts for about 132,000 of these (WHO), it is the most dangerous form, accounting for most skin cancer deaths due to its high prevalence and early metastasizing capacitiy. If melanoma is diagnosed before metastasis (Stage I and II), it can be cured by surgical resection, to about 80% of cases. However, metastatic malignant melanoma (Stage III and IV) is largely refractory to existing therapies and has a very poor prognosis, with a median survival rate of 6 months and a 5-year survival rate of less than 5% [2]. Therefore, new treatment strategies are urgently needed and under constant development.

I.1.1 Oncogenic MAPK signaling

The transmission of extracellular signals into their intracellular targets has been an intense field of research for more than three decades. It is generally accepted now, that this process is mediated by a network of interacting proteins (Serine/Threonine kinases in particular), and that this network regulates a large number of cellular processes. In 1995, Seger et al reviewed the pathway that has been newly elucidated by that time: The mitogen-activated protein kinase (MAPK) signaling cascade [3]. They described it as a cellular highway, which takes an extracellular stimulus, e.g. from growth factors, all the way from the plasma membrane to the cell nucleus: Extracellular growth factors bind to their cell-surface receptor tyrosine kinases (RTKs). There is a broad and diverse spectrum of RTKs in different tissues, including epidermal growth factor receptor (EGFR), c-KIT, platelet-derived growth factor receptor (PDGFR), vascular endothelial growth factor receptor (VEGFR), fibroblast growth factor receptor (FGFR) and fms-related tyrosine kinase-3 (FLT-3). The incoming signal is transduced via adaptor molecules such as growth factor receptor

bound 2 (GRB2) and exchange factors such as Son-of-sevenless (SOS) which lead to the activation of the Ras small guanine-nucleotide binding protein. Ras is attached to the inner face of the plasma membrane, and occurs in two activity states: It is inactive in its GDP-bound form, and becomes activated when GTP-bound [4-6]. The binding of GTP leads to a conformational change of Ras, and allows binding and activation of different effector molecules, two of the best-described are phosphatidylinositol-3-kinase (PI3K) and Raf.

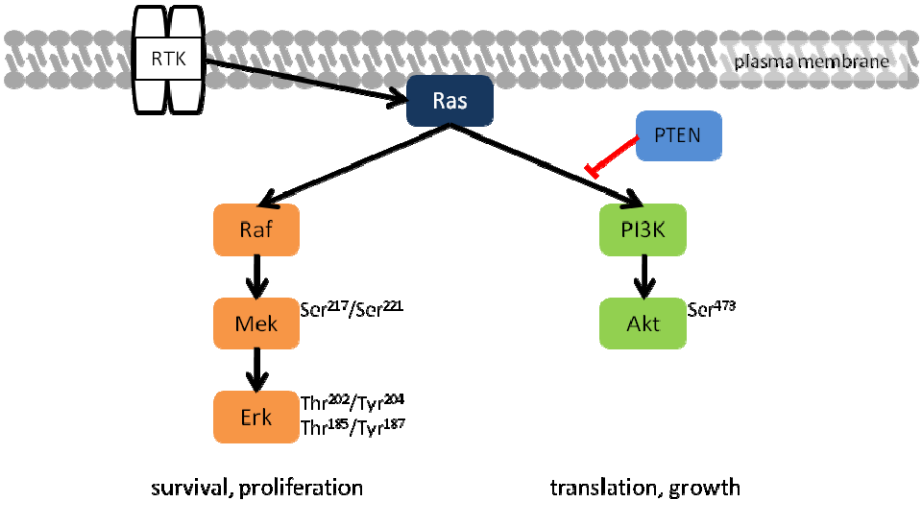

Figure I-2 - Basic schematic of Ras-ERK MAPK signaling. Extracellular growth factors bind to receptor tyrosine kinases (RTKs). This results in activation of Ras, which can activate Raf and PI3K. PI3K activation ultimately leads to Akt activation. The Akt pathway controls induction of apoptosis, as well as cell metabolism. Raf phosphorylates and activates MEK, MEK phosphorylates and activates ERK. Downstream effects of ERK include survival and control of proliferation.

Activation of PI3K leads to phosphorylation of phosphatidylinositol-4,5-biphosphate (PIP2) to phosphatidylinositol-3,4,5-triphosphate (PIP3) and ultimately results in activation of Akt. The Akt pathway controls cellular survival, apoptosis, cytoskeletal rearrangement and tumor cell chemo-resistance [7, 8]. Activation of Akt through PI3K can be inhibited by the tumor suppressor PTEN (phosphatase and tensin homologue), which is reportedly mutated in up to 25% of melanomas [9], leading to loss of its regulating function.

The Raf/MEK/ERK pathway represents the major signaling cascade initiated through Ras activation. Active Ras recruits Raf to the membrane for activation through a complex process involving changes in phosphorylation and binding to other enzymes and scaffold proteins, which stabilize and coordinate the assembly of the signaling complex [10]. Activated Raf in turn leads to the activation of the dualspecificity mitogen-activated protein kinase (MAPK) and extracellular signal-regulated kinase (ERK) kinases (MEK) and subsequently ERK. ERK phosphorylates many substrates and the duration and intensity of its activity affects how cells respond to extracellular signals [11]. The complexity of the pathway is further increased by the multiplicity of its components. The Ras family comprises HRas, NRas and KRas, the Raf family comprises ARaf,

BRaf and CRaf. In addition, there are two MEK isoforms (MEK1 and MEK2) and two ERK isoforms (ERK1 and ERK2) and the composition of these isoforms may vary between cells. These genes encode proteins with nonredundant functions.

Obviously, this pathway has to be carefully controlled to ensure appropriate responses to environmental stimuli. In normal cells, signaling results in survival and proliferation, but can also lead to senescence and differentiation. In cancer cells, the constitutive activation of the Ras/Raf/MEK/ERK pathway shifts the outcome towards proliferation and survival only. The MAPK pathway has been associated with several human tumor entities, because oncogenic mutations in Ras occur in ~15% of cancers [12] and ERK is hyperactivated in ~30% of cancers on average. Ras has been a main focus of cancer research for a long time, because it is mutated in around 50% of colon cancer, one of the most common-cancer forms. Raf recently took center stage when it was discovered that B-Raf is also very frequently mutated in human cancers particularly melanoma (44%), thyroid cancer (30–50%), colorectal cancer (5–20%) and ovarian cancer (~30%), but also at a low frequency (1–3%) in a number of other cancers. Therefore Ras-ERK signaling is particularly important in melanoma, because somatic mutations occur in BRaf, NRas, and KRas in 43%, 20% and 2% of melanomas respectively (www.sanger.ac.uk/genetics/CGP/cosmic/), which implies that Ras-ERK signaling represents one of the driving forces in melanoma.

I.1.2 MAPK mutations in melanoma

Ras mutations that have been observed in melanoma usually trap Ras in its GTP-bound active conformation and mostly involve glycine 12 (G12), glycine 13 (G13), and glutamine 61 (Q61). Even more important in melanoma is the mutational status of BRaf, mutated in 44% of melanomas. A glutamic acid substitution for the valine at position 600 (^{V600E}BRaf) accounts for over 90% of mutations in BRaf. ^{V600E}BRaf is a gain of function mutation, and has been shown to be constitutively 500-fold activated. It can stimulate constitutive MEK-ERK signaling in cells [13] and induce melanoma in mice [14, 15], showing that it can be quoted as a founder mutation in melanoma. However, more than 100 other rare mutations have been described for BRaf in melanoma, most of which cluster to the glycine-rich loop resulting in gate-keeper mutations, and to the activation segment in the kinase domain, resulting in “Kinase dead” variants. Normally, these regions trap BRaf in an inactive conformation, because they form an atypical intramolecular interaction. It is postulated, that mutations in the glycine-rich loop and in the activation segment disrupt this inhibiting interaction, thereby allowing the active conformation to prevail [16].

Functional studies have shown that most of the mutations in BRaf are activating and enhance its ability to directly phosphorylate MEK [16]. But ongoing research has shown, that the position of BRaf mutation matters, activating mutations are not all alike, and even inhibitory mutations can have activating effects [17, 18]:

Of 22 tested BRaf mutants, 18 proved to activate BRaf *in vitro* and stimulated ERK signaling *in vivo*, confirming the phenotype of an activated oncogene. Activity increases varied between the

different mutations. A high activity group showed 130-700 fold increases in kinase activity compared to wild-type. An intermediate activity group showed increases ranging from 1.3 to 64 fold which placed them above wild-type BRaf levels, but below mutationally activated Ras. The study also identified 4 mutants with only 30% to 80% of ^{wt}BRaf kinase activity *in vitro*, described as the impaired activity group. *In vivo* however, three of the four mutants still showed elevated levels of MEK signaling, through the transactivation of CRas in a Ras dependent manner, which then signals to activate MEK [17].

In BRaf, so-called “kinase dead” mutations occur at aspartic acid 594 (D594V). The carboxy oxygen of this highly conserved residue plays a critical role in chelating Mg^{2+} and stabilizing ATP binding in the catalytic site. As in other “kinase dead” mutations, D594V mutants appear catalytically and biologically inactive, so ^{D594V}BRaf for example cannot phosphorylate MEK, activate CRaf, or stimulate cell signaling. While ^{V600E}BRaf and NRas mutations occur in a mutually exclusive manner, in four of 34 BRaf kinase-dead mutants a second Ras mutations was found ($p<0,0001$). Elegant studies have shown, that kinase-dead BRaf in combination with mutant NRas cooperates to drive tumor progression through CRaf [17].

In conclusion, constitutively active Ras-ERK signaling plays a key role in melanoma development and progression. The downstream effects of this oncogenic pathway in human cancer include increased proliferation due to tumor suppressor inactivation and downregulation of cyclin-dependent kinases [19]. In addition, increased survival through modulation of MITF, a central regulator of melanocyte development [13, 20], and protection against FAS-induced apoptosis [21] are consequences of constitutively active MAPK signaling. Finally, invasion and metastasis are promoted through extracellular matrix remodeling [22] and angiogenesis [23]. These events are resulting from altered gene expression of direct downstream targets of Ras-dependent transcription factors. Furthermore, epigenetic changes in promoter DNA-methylation and histone-modification can be linked to this pathway. [24]. In addition, protein modifications like phosphorylation or acetylation modify signaling cascades as a consequence of this constitutively active pathway. Thus, the complexity of MAPK signaling allows the analysis of its relevance at different levels, and I have focused on immunological consequences of interference with this pathway.

I.1.3 Therapeutic strategies in melanoma treatment

As one of the central players in melanoma initiation, the oncogenic MAPK pathway represents one of the main targets for new therapeutic strategies. Various agents aim to inhibit either NRas, BRaf or MEK signaling in order to inhibit melanoma growth and to provide a therapeutic opportunity for patients with metastatic melanoma, alongside with chemotherapy and IFN-α treatment [25]. Many of them are small-molecule kinase inhibitors, which have been used to inhibit Raf or MEK in melanoma and other cancer types. During the last decade, a variety of small molecule inhibitors has been developed for experimental as well as clinical applications. The specificity ranges from multi-kinase inhibitors to the most recent drugs, i.e. mutation-specific inhibitors of BRaf.

Sorafenib (Nexavar®) is an example of a multikinase tyrosine kinase inhibitor whose spectrum of targets includes BRaf, in addition to CRaf, VEGFR-2, VEGFR-3, PDGFR, c-KIT and others. It has been shown to inhibit MAPK phosphorylation *in vitro* in most human tumor cell lines, but the inhibiting effect varies *in vivo* depending on the murine tumor model. Besides inhibition of MAPK phosphorylation it provides antiangiogenic activites [26].

Importantly, a phase II randomized trial showed that Sorafenib as a single agent did not provide any benefit in advanced stage melanoma [27]. Sorafenib has also been under evaluation in combination with chemotherapy and was well tolerated in Phase II trials [28, 29], but in conclusion, Sorafenib treatment disappointingly failed to produce objective responses in melanoma patients. All studies showed that BRaf mutational status did not prove to be associated with response rates [30], which is not surprising considering that Sorafenib inhibits independently from BRaf mutations. Therefore, it also showed effectiveness in renal cell carcinoma and hepatocellular carcinoma treatment, two tumors that do not possess BRaf mutations [31, 32].

Among the different MEK inhibitors, AZD6244 (Selumetinib®) has been described as a highly selective MEK1/2 inhibitor with good efficacy in *in vitro* and *in vivo* models [33]. Phase I studies showed inhibition of phosphorylated ERK in PBMC of the patients, as well as in paired tumor biopsies. Phase II studies are currently ongoing [34]. U0126 is another MEK specific inhibitor, which has been used to inhibit MEK phosphorylation *in vitro* and is only utilized experimentally.

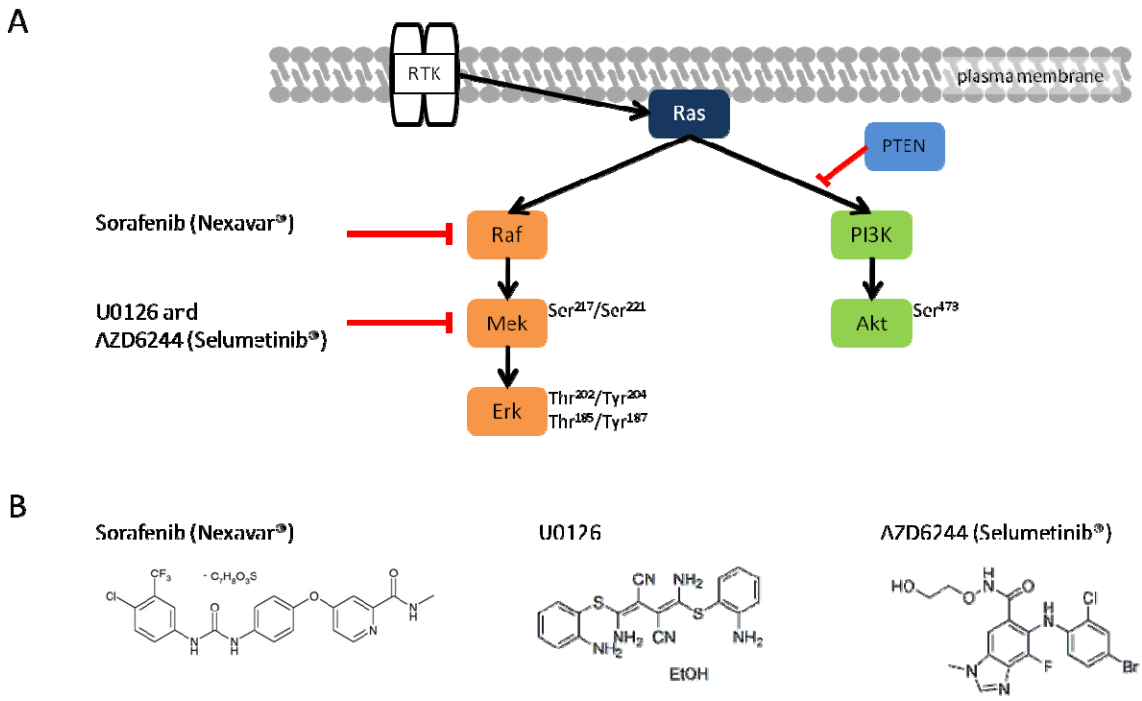

Figure I-3 - Small molecule inhibitors of MAPK signaling. Sorafenib is a multi-kinase inhibitor with anti BRaf activity. AZD6244 and U0126 are MEK-specific inhibitors. AZD6244 and Sorafenib are currently undergoing phase II trials for the treatment of melanoma patients.

Even though no clear clinical benefit in metastatic melanoma could be achieved so far, the search for new MAPK inhibitors to treat melanoma is ongoing. PLX4720 is a new selective BRaf inhibitor, due to its inhibition of mutated ^{V600E}BRaf [35]. It showed high selectivity for BRaf *in vitro* and preferentially inhibited BRaf signaling. PLX4720 has entered the clinic quite fast, and is now under evaluation in clinical trials. Despite some early success in phase I clinical trials, it remains to be seen if this new drug can achieve sustained benefit for metastatic melanoma patients. There is an increasing amount of adverse effects reported following treatment with PLX4720, and possible mechanisms are currently intensively investigated [17, 18, 36].

Sensitivity of tumor cell lines to different MAPK inhibitors varies to a great extent, independently of their mutational status. Just recently it was demonstrated that ^{V600E}BRaf melanoma lines showed large variations in susceptibility to PLX4720 [37], and other studies also suggested novel mechanisms of resistance to MEK or BRaf inhibitors [38]. The evaluation of new drugs usually focuses on the direct impact on MAPK signaling, measured as inhibited phosphorylation of MEK and ERK respectively. Yet, MAPK signaling plays a central role in tumor and normal cell signaling, and is connected to various other pathways. While most studies focus on intracellular consequences of MAPK inhibition such as phophorylation of kinases or induction of apoptosis, it is also relevant to address further downstream events like influence on chemokine and growth factor secretion, or modulated surface expression of immunological relevant molecules like HLA class I or NK receptor ligands. Thus, the effects of MAPK signaling perturbation should be

evaluated in kinetics over different time periods, taking into account immediate signaling events, as well as long-term effects of treatment.
With respect to the immune system, it has been reported that Sorafenib inhibits cytotoxicity and cytokine production of IL-2 treated and resting PBMC [39]. This is due to impaired NK cell reactivity, regulated directly through ERK and PI3K phosphorylation, which was inhibited with Sorafenib at pharmacological concentrations [40]. These studies implicate a connection between MAPK inhibition and immune recognition of tumor cells, an aspect which is investigated in detail in my thesis.

I.1.4 Natural Killer cells and recognition of melanoma cells

NK cells are a central component of the innate immune system, which acts as a first line of defense against pathogens or transformed cells. They are large granular lymphocytes, regulated by a big spectrum of activating and inhibitory receptors expressed on their surface. The existence of activating and inhibitory receptors implies that a delicate balance between these contradictory signals regulates NK cell effector function, i.e. cytotoxicity and cytokine/chemokine production. If a given target cell activates NK cell activity, they can induce apoptosis of target cells through release of cytotoxic molecules, perforin and granzyme a/b, or through triggering receptor mediated cell death pathways via Fas-ligand or tumor necrosis factor-related apoptosis-inducing ligand (TRAIL). Besides this natural cytotoxicity, NK cells can be activated by antibody-loaded target cells because CD16, the low affinity Fcγ receptor III, binds the Fc part of IgG-antibody complexes. Antibody-loaded target cells can then be eliminated through antibody-dependent cellular cytotoxicity (ADCC), which shows the tight connection between the innate (NK cells) and adaptive (IgG) immune system. NK cells can also modulate the immune response through the release of pro- and anti-inflammatory cytokines like IFN-γ, TNF-α, GM-CSF, IL-10, RANTES, MIP-1α and -1β, and chemokines CCL5, CCL3/4, CXCL9, CXCL10 and others.

NK cell activity depends on a tightly regulated balance between activating and inhibitory signals. In contrast to antigen specific T cells, they do not need priming for effector function, but depend on ligation of their activating and inhibitory receptors through target cells. Inhibitory receptors bind mostly HLA class I molecules, independently from presented peptides. This inhibition accounts for a NK cell “tolerance” of HLA class I-positive “self” cells.

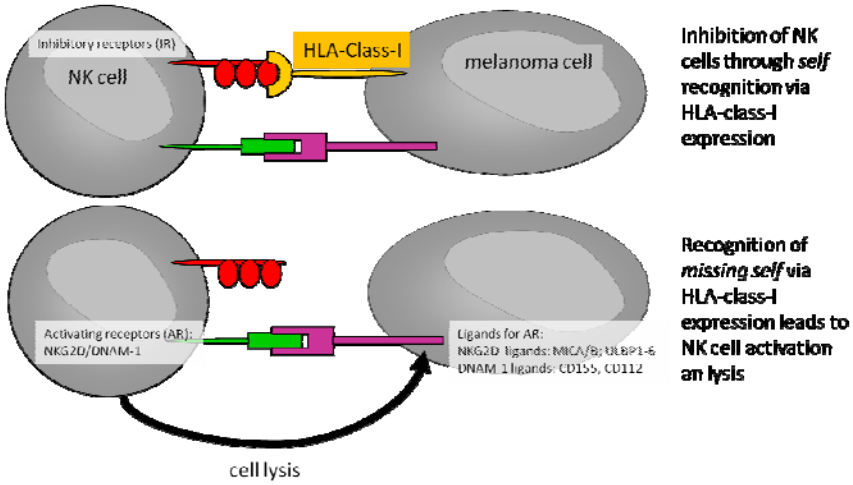

Figure I-4 - Activation of NK cells through missing self recognition. Expression of HLA class I on target cells, inhibits the cytotoxic potential of NK cells through ligation of inhibitory receptors. Reduced or lost HLA class I expression on target cells, activates NK cells through ligation of NKG2D or DNAM-1, which then lyse their target cells. The basis for this activation however, is the presence of ligands for activating receptors on the target cell side.

This concept of NK cell regulation was postulated as the “missing self” hypothesis by Klas Kärre [41]. Recent years have shown that this hypothesis alone can not account for NK-cell-self-tolerance: HLA class I molecules (chromosome 6p) and corresponding inhibitory NK-receptors (chromosome 19q13.4) are inherited indepent of each other. Theoretically this should lead to NK cells without an inhibitory receptor for self-MHC-molecules, but there are no known autoimmune diseases, founded exclusively on this NK cell phenotype [42]. This is why the “at least one” concept has been postulated, which tries to explain this phenomen through a selection process of NK clones taking place in the bone marrow. This selection allows only NK cells with at least one inhibitory receptor for missing self MHC molecules to differentiate and develop into the periphery. This selection process is not yet explained on a molecular level, and part of controversial discussion in the field. Three models are possible: (i) According to the “disarming” model, NK cells without an inhibitory receptor are actively shut down during development through a surplus of activating signals, and enter an anergic state [43]. (ii) Yokoyama described the “licensing” model, which requires interaction of an inhibitory receptor with self MHC molecules in order to aquire an activating signal for NK cell development, and to “license” the cell for function [44]. (iii) Vivier postulated the need of NK cell “education” in order to complete NK cell development. According to this model, NK cells only reach their full competence if they get a signal of an inhibitory receptor binding to a self-MHC-molecule, arguing that this step is required to switch on efficient activating signal pathways in the NK cell [45].

Besides inhibition of NK cells, mainly through MHC-class-I molecules, activating receptors play an important role in shifting this balance towards NK cell activity. Transformed or virus-infected cells can lose their MHC-class-I expression and additionally upregulate NK receptor ligands. The NKG2D receptor represents one of the most important activating receptors and recognizes eight ligands, MICA/B and ULBP1-6 [46-48]. The second activating NK cell receptor of interest for this

thesis is DNAM-1, which binds two ligands, CD155 (polio-virus resptor, PVR) and CD112 (Nectin-1). Since the ligands of these two receptors have been shown to be modulated by MAPK inhibition, I will focus on these molecules in this thesis.

The activating receptor NKG2D is a homodimer, which binds the MHC-class-I-like molecules ULBP1-6 and MICA/B. The receptor is expressed on all NK cells, as well as on $CD8^+$ $\alpha\beta^+$ and $\gamma\delta^+$ T-cells. Although it acts as an autonomous activating receptor on NK cells, NKG2D seems to have rather costimulatory function on T cells. NKG2D is of special interest in the human system, on the one hand, becasue many tumors express NKG2D ligands; on the other hand, tumor-derived soluble NKG2D ligands can be detected in serum of tumorpatients, which impairs NKG2D expression and function, associated with a worse prognosis [49, 50]

The polio virus receptor (PVR, CD155) is a transmembrane glucoprotein, which is widely expressed on normal cells, and overexpressed on many tumors, including melanoma. It acts as a ligand for the DNAX accessory molecule-1 (DNAM-1) receptor, which is involved in NK and T cell activation [51]. It has been shown that tumor-associated NK cells suffer from an impaired effector function, because DNAM-1 receptor expression is lower than in peripheral NK cells. The modified DNAM-1 expression is possibly due to chronic ligand exposure through the tumor cells, and supports the notion that tumor-induced alterations of activating NK cell receptor expression may hamper immune surveillance and promote tumor progression [52]. In case of melanoma, DNAM-1/CD155 interactions have been shown to be relevant for tumor recognition by NK cells [53].

We have previously shown that MAPK inhibition, in a concerted effort with DNA methyltransferases, can lead to the reconstitution of HLA class I and NKG2D ligand expression in colon cancer cell lines [24]. A careful comparison between colon cancer lines and melanoma lines revealed that the effects of MAPK inhibition on expression of HLA and NK ligands differ substantially between these tumor entities.

I.2 Integration of MAPK signaling, autophagy and apoptosis

Of note, the effects of MAPK perturbations can not only be judged by their ability to inhibit ERK or MEK phosphorylation respectively. Building on our experience from colon cancer cell lines and MAPK inhibitor treatment, we aimed to comprehensively analyze the effects of MAPK inhibition in melanoma cells on (I) cell signaling, including the PI3K/Akt pathway, effects on NFκB signaling, p53 signaling, and some transcription factors, (II) proliferation of tumor cell lines, (III) HLA class I and NK ligand surface molecule expression on tumor cells, (IV) chemokine and growth factor secretion and (V) balance between apoptosis and autophagy.

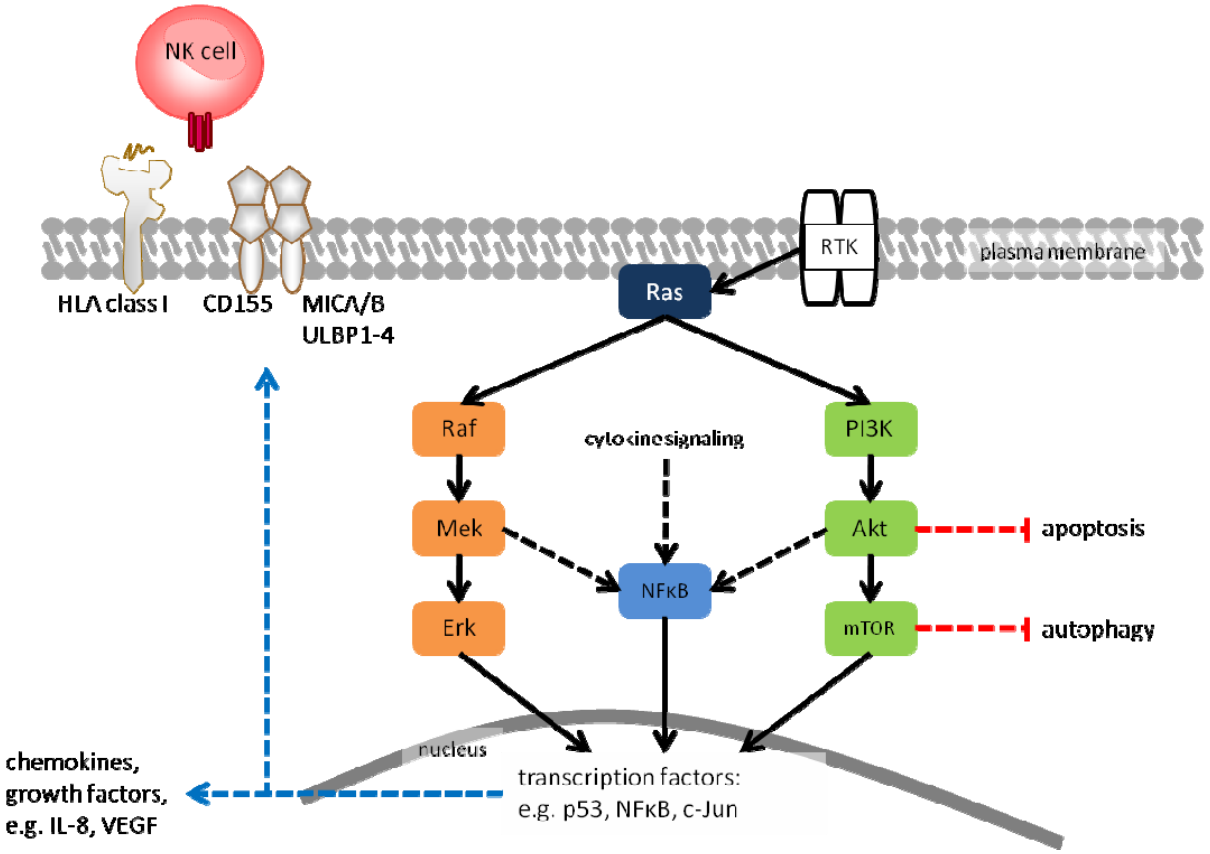

Figure I-5 - MAPK pathway perturbations are likely to affect whole cell signaling processes. Due to its multiple connections to other pathways, alterations in cell signaling and gene expression are presumably visible well beyond downstream ERK effects. Changes in gene expression of e.g. p53, NFkB and c-Jun affect the secretion of chemokines and growth factors, as well as the expression of surface molecules on the tumor cell. The PI3K pathway is directly connected to the regulation of autophagy via mTOR. It is not yet fully understood, if induction or inhibition of autophagy is beneficial for tumor cell progression.

Cell signaling and susceptibility to MAPK inhibitors can vary between different tumor cell lines, and most observed effects depend on the time period of treatment. We therefore decided to undertake a comprehensive approach for the analysis of a core set of melanoma cell lines. The A-375 melanoma cell line is a well-established tumor cell line that harbours the ^{V600E}BRaf mutation. Three primary melanomy cell lines have been established in the lab of Dirk Schadendorf (University Hospital, Essen), and carry the rare ^{G469R}BRaf mutation. Since those three primary melanoma lines originate from the same melanoma patient, they represent an excellent model system due to their limited genetic heterogeneity. It has been of special interest to me, to elaborate differences between the MAPK inhibitors Sorafenib, AZD6244 and U0126, as well as between the different cell lines with respect to signaling, autophagy and immune recognition by NK cells. I have made use of phosphoplex analysis, to evaluate cell signaling, measured chemokines and growth factor secretion with the Bio-Plex method, and used FACS analysis to determine changes on HLA class I and other surface molecule expression on tumor cells, and test those effects in the context of NK cell recognition of tumor cells.

I.2.1 MAPK inhibition and the balance between apoptosis and autophagy

Autophagy is an evolutionary well-conserved eukaryotic response to degrade portions of the cytosol and cytoplasmic organelles. This material is sequestered in unique organelles, called autophagosomes, which then fuse to lysosomes to form the autolysosome, which is then degraded together with its content by proteases. “Basal autophagy” is a homeostatic process and part of protein metabolism, which recycles long-lived proteins and organelles. “Induced autophagy” is a survival mechanism to produce amino acids under starvation conditions, degrade damaged mitochondria or even act as a bactericide defense mechanism [54].

Autophagy is a multi-step process, regulated on several different levels (compare Figure I-6). It starts with an isolation membrane, also called phagophore. It is likely derived from lipid bilayer, contributed by the endoplasmatic reticulum (ER) and/or the trans-Golgi and endosomes [55, 56]. The exact origin is not yet known, and the existence of a pre-autophagosomal structure (PAS) in mammalian cells, like it has been discovered in yeast, is still a matter of debate [57]. The phagophore enlarges to engulf intracellular cargo, sequestering it in a double-membraned autophagosome. Loaded autophagosomes then fuse with lysosomes to degrade the content by lysosomal acid proteases. Amino-acids and other by-products of degradation are then transported back to the cytosol, where they can be re-used for building macromolecules and for metabolism [58].

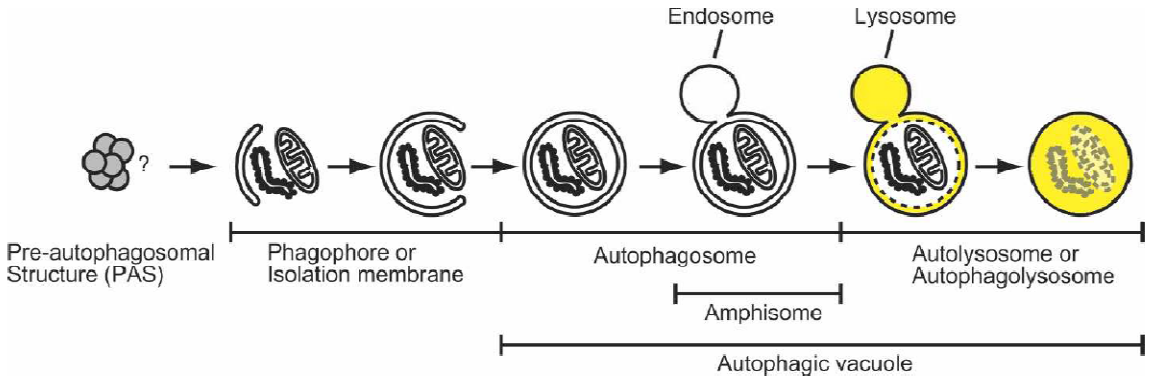

Figure I-6 - Process of autophagy. A double-layer membrane, called phagophore or isolation membrane enlarges to engulf long-lived proteins or organelles in the cytosol. The so-called autophagosomes then fuse with lysosomes to form the autophagolysosome (autolysosome), wherein the content is degraded by lysosomal acid proteases. Taken from Mizushima: Autophagy – process and function [58].

I.2.2 Autophagy quantification and monitoring

In the year 2000 Kabeya et al demonstrated that rat microtubule-associated protein 1 light chain 3 (LC3) is associated with the autophagosome membranes after processing. LC3 exists in two forms: LC3-I is cytosolic, but LC3-II is autophagosome-membrane bound, found on the inside and outside of autophagosomes [59]. The fusion of LC3 with green fluorescent protein (GFP) marked an important step in autophagy quantification at single-cell levels. It provides the possibility to detect autophagosomes based on GFP-LC3 fluorescence, which appears punctuated for LC3-II attached to autophagosomes, in contrast to an even distribution in its cytosolic LC3-I form.
Yet, precise quantification of autophagy is still a major problem in autophagy research. Among many different approaches, none of them yet proved to be sufficient [60, 61]. Western blotting is used to monitor the conversion of LC3-I to LC3-II, but lacks specificity, measures only population averages and gives semi-quantitative data. In contrast, high-resolution fluorescence microscopy allows for the examination of single cell autophagic activity, but its analysis is prone to subjectivity and the amount of cells usually analyzed is limited (≤300). It can only provide a snapshot of autophagic activity in a group of cells, which can not account for the amount of heterogeneity observed in populations of cells. In order to understand and further analyze regulation of autophagy on a molecular level, a method to accurately quantify autophagic activity is needed.

In addition to limitations of the methods that have been used thus far to measure autophagy, the number of autophagosomes in fully functional autophagy can not be used as a good measure to evaluate autophagy. That is because the formation of autophagosomes is followed by the degradation step, during which autophagosomes fuse to lysosomes and become degraded. Cell images can only provide a snapshot of the current number of autophagosomes, from which it is impossible to infer how many autophagosomes have just been formed and degraded. These normal physiological conditions of fully functional baseline autophagy have therefore been termed “steady-state” conditions. A cell with increased numbers of autophagosomes under steady-state conditions can on the one hand undergo induced autophagy with an enhanced rate of autophagosome formation, and the image has been taken before their degradation. On the other hand, autophagosome degradation might be dysregulated, which also leads to an accumulation of autophagosomes, even though the cell undergoes only “basal autophagy”. Accordingly, in GFP-LC3 expressing cells, a population of cells undergoing basal autophagy will comprise images with dotted cells (depicting autophagosomes), as well as images with homogeneous GFP expression in the cytosol (Figure I-7).
A possible solution to this problem is the use of lysosomal inhibitors. Bafilomycin A1 inhibits the fusion of autophagosomes and lysosomes and therefore artificially blocks degradation of autophagosomes. In addition, it reduces the quenching of acid-sensitive GFP-fluorescence, which otherwise occurs prior to the full degradation of autolysosomes. Conditions of lysosomal inhibiton have been termed “cumulative conditions”, because they lead to an accumulation of

autophagosomes. Accumulation of autophagosomes under cumulative conditions however will take place under “basal autophagy” as well as “induced autophagy”, only at different rates (Figure I-7). The comparison of steady-state conditions and cumulative conditions provides a good measure of true autophagic turnover, termed “autophagic flux”.

The problems with autophagic turnover, and the need for true autophagic flux measurements are evident in autophagy research, still, many studies are still carried out under steady-state conditions only, which is probably a main cause of contradiciting and confusing reports on the regulation of autophagy [60, 61].

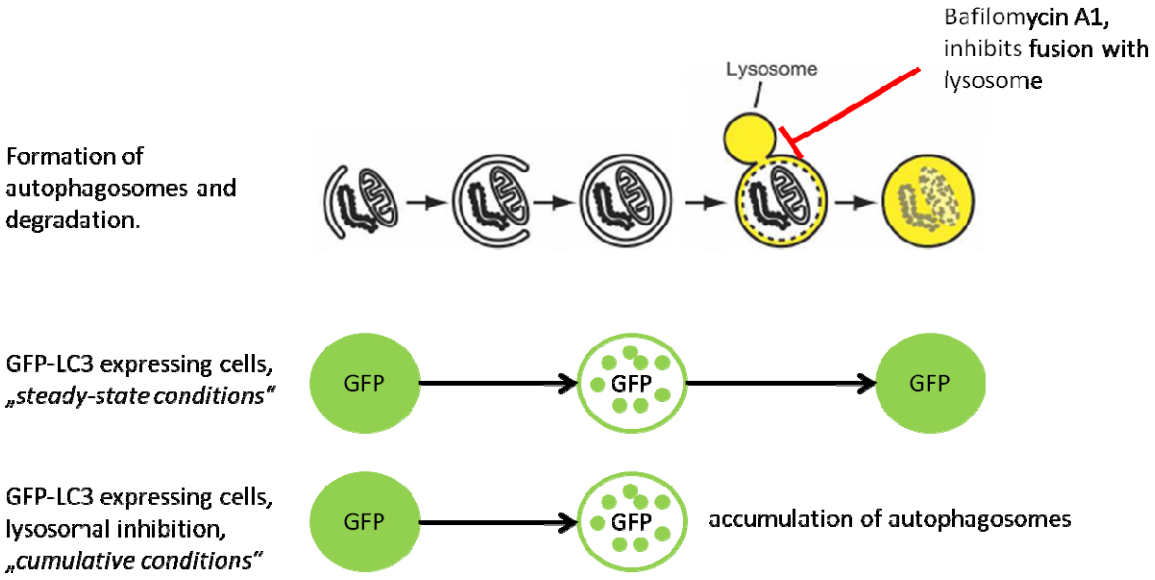

Figure I-7 - Autophagic flux measurements are necessary to determine autophagic turnover. Under steady-state conditions, the amount of autophagosomes is not a precise measurement of autophagic activity. Formed autophagosomes are immediately degraded upon fusion with lysosomes. Under “cumulative conditions”, lysosomal inhibitors like Bafilomycin A1 are used to block degradation of autophagosomes, leading to an accumulation of autophagosomes. Comparison of “steady-state” and “cumulative conditions” is necessary for the accurate assessment of autophagic activity.

I.2.3 Regulation of autophagy

Research over the past decade showed that regulation of autophagy is very complex. A proven central player in autophagy regulation is the mammalian target of rapamycin (mTOR). Amino acid and insulin/growth factor signaling seems to converge on mTOR, acting as a master regulator of nutrient signaling. mTOR is activated downstream of Akt, PI3K and growth factor receptor. When nutrients are available, this pathway signals to (I) promote growth through induction of ribosomal protein expression and increased protein translation and (II) to inhibit autophagy, even though it is not yet clear how this is carried out. Treatment with rapamycin effectively inhibits mTOR and promotes autophagic acitivity. Prior to the formation of the phagophore, the family of autophagy-

related genes (Atg family) is involved. Atg's have been discovered mainly in yeast, but the respective homologues have also been found in mammalian cells. Beclin-1 (Atg-6) is an essential protein for autophagy, it forms a complex with Vps34 (PI3K family), to control the formation of the phagophore, and in addition, it is also connected to the anti-apoptotic Bcl-2. Upon binding to Bcl-2, Beclin-1 is inactivated, which leads to inhibited autophagy [62]. Bcl-2 is just one of many examples for proteins with defined roles in regulation of apoptosis, which have now been shown to be involved in regulation of autophagy too. Nutrient deprivation and death receptor activation can both positively and negatively regulate autophagy through dynamic interactions of not only anti-apoptotic Bcl-2 members, but also pro-apoptotic BH3-only proteins, JNK signaling, p53 and NFkB pathways. The dual role of the involved proteins caused much debate in recent years:
Bcl-2 may directly [63] or indirectly [64, 65] suppress Beclin 1–mediated formation of autophagosomes. BH3-only proteins, sensors of cellular stress, are implicated in either the enhancement or activation of autophagy, presumably through the disruption of the Bcl-2:Beclin 1 complex [66], via LC3 binding. JNK activation of autophagy in response to starvation [67] and ceramide addition [68] may involve inhibition of Bcl-2 via phosphorylation. Finally, the pro-survival IKK pathway can either inhibit so-called autophagic cell death (described as programmed cell death type II) [69, 70], increase autophagosome formation via NFκB signaling [71], or activate autophagy independent of NFκB [72]. In addition to its functions in regulation of cell-cycle progression and induction of apoptosis, p53 has been shown to inhibit autophagy if it is located in the cytosol [73, 74].
Recently autophagy has also been connected to cancer development and progression: It can be stimulated by the tumor suppressors PTEN, TSC1 and TSC2 [75]. It was also shown to be inhibited by proto-oncogenes PI3K and Akt [75]. There is proof that defects in autophagy can lead to tumor development and the controversial view of autophagy as a cell death mechanism has also been supportive of a tumor-suppressing role of this pathway. A more plausible explanation for the tumor-suppressive function of autophagy can probably be dervived from its role as a selective degradation pathway [76]. Yet, just like other cells in the body, tumor cells can depend on autophagy to survive starvation and stress. So autophagy is a double-edged sword in cancer development and it is unclear whether it should be inhibited or induced as part of therapeutic strategies.

Autophagy is very likely to be affected by MAPK inhibition, not only due to oncogenic Ras signaling in tumor cells. Recently, hyperactivation of oncogenic BRaf (above "normal" oncogenic BRaf levels) was shown to induce growth inhibition and cell death by inducing autophagy, presumably through the inhibition of mTOR. The authors speculate, that the induction of autophagy might play a role in melanoma progression [77]. Contradictionary to this report, it has previously been shown, that high constitutive ERK phosphorylation found in many cancers, disrupts the maturation of autophagosomes and therefore may provide a malignant advantage, by impeding the tumor suppressive function of autophagy.

Many reports on autophagy regulation are contradicting each other. Autophagy is a vivid field of research and under heavy debate, yet a lot of ongoing discussion presumably stems from both, inaccurate measurements of autophagic activity, and from cell to cell variability which is not captured with population-average analyses, like Western Blot and FACS. Another reason for contradictory findings may be due to the assumption that autophagy regulation follows the same principles in each cell – from yeast to human tumor cells. Lessons from apoptosis and oncogenic MAPK signaling strongly suggest that the principles of cell survival, death and proliferation are significantly altered in tumor cells in particular, due to their oncogenic signaling status. These alterations may be specific for tumor entities as well as for the driver mutations that are responsible for their unlimited proliferative capacity. Since the role of autophagy in MAPK-driven tumor cells in not yet solved, one of the central aspects of my thesis was to establish a new method for the quantification of autophagy in the first place. Basing on this method, consequences of MAPK inhibiton could be addressed in detail.

I.2.4 ImageStream-based method for the quantification of autophagy and apoptosis

The ImageStream system is basically an imaging flow cytometer [78]. It integrates the features of flow cytometry and fluorosecence microscopy, allowing for the analysis of large numbers of cells, based on their fluorescent features, and providing the statistical power and analysis known from FACS. Additionally, the ImageStream allows the image analysis known from fluorescence microscopy for every measured single cell. This adds a new dimension of information to population analysis of cells. Simply stated, it combines the statistical power of FACS with the sophisticated analysis of high-resolution fluorescence microscopy, and uses advanced image analysis tools to extract single cell information for population level analysis.

We wanted to make use of the ImageStream to establish a new method to monitor autophagy, and to counter the previously described problems of autophagy research. The challenge was to quantitatively measure and analyze phenotypic responses within a defined population of cells. I established the method with stably-transfected MCF7 GFP-LC3 breast cancer cells derived from a single colony, i.e. with a minimized genetic variability. MCF7 GFP-LC3 cells are commonly used in autophagy research and were therefore selected in the first place, to allow comparison of the ImageStream with commonly used methods. For each cell, the number of GFP-spots, representing autophagosomes, can be counted. Subpopulations with different autophagosome numbers (spots) were systematically identified for each condition. Primary flux metrics were derived from differences between measurements under “steady-state conditions” (w/o Bafilomycin A1), and “cumulative conditions” (in the presence of the lyososmal inhibitor Bafilomycin A1). Secondary multi-parametric flux metrics were calculated within each subpopulation to further characterize autophagic responses at the single cell level. These metrics could then be applied, to further evaluate the regulation of autophagy in MCF7 GFP-LC3 cells,

and the impact of MAPK inhibition on melanoma cells using stably-transfected A-375 GFP-LC3 cells. We have combined our new method for autophagy quantification with an established ImageStream-based approach for quantification of apoptosis. Our method of simultaneous quantification of apoptosis and autophagy was used as a new powerful approach for the analysis of MAPK inhibition and its impact on the balance between apoptosis and autophagy.

Aim of the thesis

The general aim of this thesis was to improve the current understanding of the impact of MAPK inhibition in melanoma cells, regarding recognition by natural killer cells, signaling via other pathways and induction of apoptosis and autophagy, respectively.

In previous studies, our group has shown that inhibition of MAPK signaling in colon cancer cells altered the expression of several surface molecules relevant for T and NK cell recognition [24]. Although the MAPK pathway also represents an important pathway in melanoma, consequences of this oncogenic signaling differ substantially between different tumor entities. A set of well-characterized cell lines, comprising the established A-375 melanoma cells with the ^{V600E}BRaf mutation and three primary melanoma lines from one patient carrying the ^{G469R}BRaf mutation, was used to determine the surface expression of HLA class I molecules and NK receptor ligands, and their respective modulation during treatment with a BRaf and two MEK-inhibitors. Among the different human ligand-receptor pairs, I focused on the ligands for the two most relevant activating receptors in the context of melanoma, NKG2D and DNAM-1. The functional consequences of a possible modulation of these surface molecules should be investigated with respect to recognition and lysis by NK cells. Furthermore, the effects of these inhibitors on the secretion of chemokines and growth factors by these melanoma cell lines should be determined in order to argue for alterations in the microenvironment.
Using the novel phosphoplex technique, another aim was to investigate the effects of MAPK inhibition not only on the linear MAPK pathway, but also on various other interconnected pathways. Our panel included components of the PI3K, JNK and NFκB pathways. Tight kinetics were chosen for this pathway analysis, in order to demonstrate the importance of the dimension “time” for the regulation of cell signaling. The time-resolved analyses should help to improve our understanding of the impact on cell fate decisions like induction of apoptosis or autophagy.
Since the regulation of apoptosis and autophagy is still controversially discussed in the literature, one of the most important aims of this thesis was to establish a novel technology for the simultaneous detection of these two processes at the single cell level. For this purpose, the novel ImageStream technology should be tested for its suitability to quantify apoptosis and autophagy, and to address the important question whether tumor cells possess a delicate balance between autophagy and apoptosis, and whether this balance can be modulated by MAPK inhibition.

In the current literature, the rather simplistic view of identical effects of inhibitors within one “linear” pathway dominates the discussion – but for the long road to “individualized” therapy, detailed analyses of “side effects” will be necessary to improve future therapeutic approaches.

M. Materials and Methods

M.1 Materials

M.1.1 Cell culture

DMEM was purchased from Sigma-Aldrich. RPMI 1640, FBS, L-glutamine, sodium-pyruvate and non-essential amino acids (NEAA) were purchased from Invitrogen. Cell lines have been tested for mycoplasma contaminations at least once a month. In case of mycoplasma contamination, cell lines were treated with Myco-3 (Calbiochem) for three weeks, and tested again.

To isolate NK cells from peripheral blood of healthy donors, we used the NK cell negative isolation kits from Invitrogen. NK92 cells are human NK-leukemia cells that were originally derived by T. Tonn (Transfusion Medicine, DRK Frankfurt) and represent the most potent cytotoxic natural killer cell line.

Cell medium	Composition
TM	RPMI 1640, 10% FBS, 2mM L-Glutamin, 1mM Na-Pyruvat, 1x NEAA
RPMI III	RPMI 1640, 2mM L-Glutamin, 1mM Na-Pyruvat, 1x NEAA
DMEM	DMEM, 10% FBS, 2mM L-Glutamin, 1mM Na-Pyruvat, 1x NEAA
primary NK cell medium	RPMI III, 500U IL-2/ml
NK92 medium	RPMI 1640, 5% T cell growth factor (AG Falk), 15% FBS, 10% human serum, 200 U IL-2/ml
MCF7 GFP-LC3 selection medium	DMEM, 1mg/ml G418
A-375 GFP-LC3 selection medium	TM, 0,5mg/ml G418

Name	Origin	Medium	Source
Ma-Mel-48a	human primary melanoma line, patient ma-mel-48, established July 2002 from skin lesion	TM	D. Schadendorf
Ma-Mel-48b	human primary melanoma line, patient ma-mel-48, established January 2003 from lymph node metastasis	TM	D. Schadendorf
Ma-Mel-48c	human primary melanoma line, patient ma-mel-48, established July 2003 from lymph node metastasis, β2m-mutation, therefore HLA class I negative	TM	D. Schadendorf
Ma-Mel-48c GFP LC3	Ma-Mel-48c, stably transfected with GFP-LC3 vector	TM 0,25µg/ml Puromycin	N.R. Brady/ Bartenschlager
A-375	human malignant melanoma, skin-derived	TM	ATCC
A-375 GFP-LC3	A-375 GFP-LC3 cells, stably transfected with GFP-LC3 vector	TM 0,5mg/ml G418	N.R. Brady
MCF7 GFP-LC3	human, breast cancer cell line, Caspase-3 deficient	DMEM 1mg/ml G418	N.R. Brady
K-562	human erythroleukemia line, HLA class I negative	TM	D. Schendel
NK92	human NK cell leukemia line	NK92 medium	M. Uhrberg

Name	HLA/β2m	NRas	BRaf	PTEN	p53	p16/Arf
Ma-Mel-48a	HLA-A1, B8, Cw7	wt	G469R	wt	wt	wt
Ma-Mel-48b*	HLA-A1, B8, Cw7	wt	G469R	wt	wt	wt
Ma-Mel-48c*	HLA class I negative, β2m mutation	wt	G469R	wt	wt	wt
A-375	Cw06 (K80), Cw16 (N80)		V600E		wt	
MCF-7 GFP-LC3	HLA-A2, B18/44, Cw05			wt	wt	

HLA-typing, and mutational status of selected cell lines.

M.1.2 Antibodies

Antigen	Conjugation	Isotype	Clone	Concentration	Source
isotype control	-	IgG1	MOPC21	5 µg/ml	Sigma
isotype control	-	IgG2a	UPC10	5 µg/ml	Sigma
isotype control	-	IgM	MOPC104E	5 µg/ml	Sigma
HLA-Klasse-I	-	IgG2a	W6/32	hybridoma supernatant	J.Johnson
HLA-A2 + B17	-	IgG1	HB54	hybridoma supernatant	ATCC
HLA-A2 + A69	-	IgG2b	HB117	hybridoma supernatant	ATCC
HLA-A1	-	IgM		20:1	BMT
ULBP1	-	IgG2a	170818	5 µg/ml	R&D
ULBP2	-	IgG2a	165903	5 µg/ml	R&D
ULBP3	-	IgG2a	JFY02	5 µg/ml	R&D
ULBP4	-	IgG2a	7H7, Ratte	hybridoma supernatant	E.Kremmer
MICA	-	IgG2b	159227	5 µg/ml	R&D
MICB	-	IgG2b	236511	5 µg/ml	R&D
ICAM-1	-	IgG2a		hybridoma supernatant	J.Johnson
CD155	-	IgG1	PV.404	5 µg/ml	BC
HLA-E	-	Rat IgG2	4D1	hybridoma supernatant	E. Kremmer
isotype control	FITC	IgG2b	MOPC19	2 µl	BD
isotype control	PE	IgG2a	7T4-1F5	2 µl	BC
isotype control	PerCP	IgG2a	X39	2 µl	BD
isotype control	APC	IgG2a	X39	2 µl	BD
CD3	FITC	IgG1	UCHT1	2 µl	BC
CD4	APC	IgG1	13B8.2	2 µl	BC
CD8	PE	IgG1	B9.11	2 µl	BC
CD14	FITC	IgG1	M5E2	2 µl	BD
CD16	FITC, Pacific Blue	IgG1	3G8	2 µl	BC
CD25	FITC	IgG2a	B1.49.9	2 µl	BC
CD44	FITC	IgG1	37.51.1	2 µl	BC
CD56	APC, PE,	IgG1	NKH-1	2 µl	BC
CD107a	FITC, PE	IgG1	H4A3	10µl	BD
NKG2D	PE	IgG1	149810	2µl	R&D

Primary antibodies used for direct or indirect flow cytometry. BD: Beckton Dickinson, BC: Beckman Coulter

Antigen	Conjugation	Species	Concentration	Source
αMaus-IgG	PE	goat	1:100	Jackson ImmunoResearch
αMaus-IgG/M	PE, FITC	goat	1:100	Jackson ImmunoResearch

Secondary antibodies for flow cytometry

Antigen	Conjugation	Clone	Isotype	Source
Mouse anti-human p53	-	DO-1	IgG2a	Invitrogen
Mouse anti-human β-actin	-	B11V08		Promokine
Goat anti-mouse IgG	Peroxidase			Jackson ImmunoResearch

Antibodies used in Western blot analysis

M.1.3 Buffers, chemicals, reagents, special machines

Western Blot	Components, Source
Cell lysis kit + protease inhibitors	Bio-Rad
Gel electrophoresis running buffer	NuPage MOPS SDS running buffer 20x NP0001
10x transfer buffer	120 mM Tris base, 960 mM glycine
1x transfer buffer	10% 10x transfer buffer, 20% methanol, 70% water
6x Laemmli buffer	150 mM Tris-HCl, pH 6.8, 6% SDS, 30% glycerine, 0.15% bromphenolblue, 0.3 M DTT
blocking buffer	PBS, 0.1% Tween 20, 5% nonfat dried milk, AppliChem A0830
wash buffer	PBS, 0.05% Tween 20
first Ab dilution buffer	PBS, 5% BSA fraction V, 0.2% Tween 20
second Ab dilution buffer	PBS, 2.5% nonfat dried milk, 0.1% Tween 20
Precision Plus Protein Standards All Blue	Bio-Rad 161-0373
Super Signal West Dura Extended Duration Substrate	Thermo Scientific 34075

Cytokine multi-plex measurements	Source
Reagent Kit A (wash buffer, assay buffer, detection antibody diluents)	Bio-Rad
human cytokine tests: M-CSF, MIF, SCGF-b, SDF-1a (CXCL12), HGF, ICAM-1, IL-8 (CXCL8), VEGF	Bio-Rad
96-well filter plates	Millipore

Phosphoprotein multi-plex measurements	Source
Cell lysis kit + protease inhibitors	Bio-Rad
PMSF (Phenylmethylsulfonfluorid)	Sigma
phosphoprotein reagent kit	Bio-Rad
96-well filter plates	Millipore
total-protein tests: Akt, p53, IκB-α, ATF-2, c-Jun, ERK1/2, JNK, MEK1, p38 MAPK, CREB	Bio-Rad
phospho protein tests: Akt (Ser^{473}), GSK-3α/β (Ser^{21}/Ser^{9}), p53 (Ser^{15}), IκB-α (Ser^{32}/Ser^{36}), NF-κB p65 (Ser^{536}), ATF-2 (Thr^{71}), c-Jun (Ser^{63}), ERK1/2 (Thr^{202}/Tyr^{204}, Thr^{185}/Tyr^{187}), JNK (Thr^{183}/Tyr^{185}), MEK1 (Ser^{217}/Ser^{221}), p38 MAPK (Thr^{180}/Tyr^{182}), CREB (Ser^{133})	Bio-Rad

MAPK Inhibitors	Source
DMSO (solvent)	Sigma
U0126, MEK inhibitor	Promega
AZD6244	Lab D. Schadendorf
Sorafenib (Nexavar, BAY 43-9006)	Bayer

Autophagy tools and pathway perturbation	Source
Earles balanced salt solution (EBSS)	Invitrogen/Gibco
Krebs-Henseleit solution	Sigma
Bafilomycin A1	Calbiochem
Puromycin	Sigma
G418	Sigma
SP600125 (JNK inhibitor, 50μM)	Calbiochem
QNZ (NFkB inhibitor, 10μM)	Calbiochem
HA14-1 (Bcl-2 inhibitor, 50μM)	Calbiochem
TNF-a (43ng/ml)	Calbiochem

Special machines	Source
xCELLigence system	Roche Diagnostics
Luminex/Bioplex system	Bio-Rad
ImageStream System	Amnis corporation

M.2 Methods

M.2.1 Cell culture

All cells were grown at 37°C with 5% CO_2 under sterile conditions. Adherent tumor cells were split every two to three days, cell culture flasks were changed at least once a week. In general, cells were frozen in 50% FBS/RPMI III / 10% DMSO at -80°C. Prior to use, FBS was inactivated by incubation at 56°C for 45 minutes.

NK cell isolation

We isolated NK cells from peripheral blood mononuclear lymphocytes (PBMC) using the magnetic Dyna-bead untouched human NK cells kit from Invitrogen/Dynal. In principle a mixture of biotinylated monoclonal antibodies against the non-NK cells is added to PBMC. During a short incubation time, depletion MyOne SA Dynabeads bind the non-NK cells. The bead-bound cells are then separated from NK cells with a magnet. Bead-bound cells are discarded, and the remaining untouched NK cells used. Purity of the NK cell fraction was checked by FACS with CD3 and CD56 stainings.

Tumor cell treatment with MAPK inhibitors

More then 60% of malignant melanomas carry activating mutations in the MAPK pathway, leading to uncontrolled proliferation. Therefore MAPK signaling in melanoma cell lines was inhibited using small molecule inhibitors, in order to study their effects on various signaling pathways, surface molecule expression and immune recognition by T and NK cells.

U0126 is a MEK inhibitor, which binds the MAPK-kinase MEK1/2, inhibiting its catalytic activity and therefore activation of downstream kinases ERK1/2. It is solved in DMSO (stock solution, 10mM), and used at a final concentration of 10µM. Sorafenib (Nexavar, BAY 43-9006) inhibits Raf-1, B-Raf and other receptor tyrosine kinases (e.g. VEGFR-2,3; PDFR-b, Flt-3 and c-KIT) [79] which also leads to inhibition of MEK/ERK signaling. One pill of Sorafenib was solved in 31,4ml DMSO (stock solution, 10mM) and used at a final concentration of 5µM. AZD6244 (Selumetinib, ARRY-142886) is a selective, non-ATP competitive inhibitor of MEK1/2 [80], solved in DMSO (stock solution, 10mM), and used at a final concentration of 3µM.

To capture short-term as well as long-term effects of MAPK inhibition, the following timepoints were chosen for analysis: 30min, 6h, 12h, 24h, 48h, 72h and 96h. For Luminex and FACS analysis, $0{,}1x10^6$ cells per sample were seeded in 6-well plates, one 6-well plate for each timepoint. Cells were seeded the day before treatment and allowed to adhere and grow over night. For treatment with MAPK inhibitors, the medium was discarded and cells washed with 2ml PBS per well, then the drug-containing medium was added. Since most of the inhibitors are not stable at 37°C, medium was changed after 48 hours of treatment. Cell culture medium supernatants were harvested for the detection of chemokines and growth-factors. For flow

cytometry evalutation, cells were detached after their respective incubation time using Accutase (PAA, Germany). For phosphoplex and Western Blot analysis, we lysed the cells using the cell lysis kit for phosphoprotein detection from Bio-Rad, Germany.

Flow cytometry (FACS)

We used flow cytometry analysis to characterize melanoma cell lines surface expression of ligands of T and NK cells. In addition, subpopulations of cells within PBMC were defined as effector cells. HLA class I expression, CD155 expression and various other markers were used in indirect staining FACS assays to identify changes in surface expression following exposition to MAPK inhibitors. For cytotoxicity assays with NK cells, it was necessary to define the NK cell population, and other subpopulations within PBMC for specific analysis. CD107a staining, was used as marker for detection of degranulating effector cells following contact with target cells. Measurements were performed with BD FACSCalibur or BD LSR II and analyzed using the BD CellQuest software and BD FACS Diva software respectively.

Indirect staining protocol with secondary antibodies

At least 10000 cells per well in 96-well plates were resuspended in 50µl FACS-buffer. 50µl of primary antibody (hybridoma supernatant) was then added (5µg/ml) to the cell suspension, and incubated on ice for 45 minutes. Following a washing step with FACS-buffer, secondary anti-mouse goat PE antibody was added in 50µl FACS-buffer. After a further incubation period of 20 minutes on ice, cells were washed in FACS-buffer and measured immediately, or fixed with 1% PFA/PBS. Isotope control monoclonal antibodies were used to determine nonspecific background staining.

Direct staining of cells and FACS analysis

Direct antibody staining was performed in 96-well u-bottom plates. At least 50000 cells per sample were resuspended in 50µl FACS-Buffer, and respective antibodies in different combinations were added. After incubation on ice and in the dark for 45 minutes, cells were washed with 150µl FACS-buffer, and if necessary, cells were fixed using 1% PFA/PBS. Isotope controls for each color were used to determine background staining.

CD107a Degranulation Assay

If NK cells and T cells recognize their specific target cells, they release cytotoxic granules into the immunological synapse, in order to induce programmed cell death in target cells. With the fusion of lysosomes to the cell membrane, lysosomal-associated protein-1 (LAMP-1, CD107a), which is associated with the granula membrane, becomes transiently detectable at the cell surface of activated NK cells and T cells [81]. During co-incubation of NK cells and/or T cells with target cells, specific antibodies were used to detect CD107a expressing effector cells as a marker for

target cell-induced cytolytic activity. This marks effector cells which have released granula in order to kill their taget cells.
Isolated NK cells from PBMC were stimulated for 24h with 500U IL-2. In 96-well plates target and effector cells were mixed in a 1:1 ratio in 200µl medium, and 10µl CD107a antibody (PE-labeled) per well was immediately added. After 1h of incubation, Monensin was added (2mM, BD Bioscience) to minimize the internalization of CD107a during incubation. Monensin prevents the acidification of endocytic vesicles, thus avoiding the degradation of reinternalized CD107a proteins from the surface, and allowing for the visualization of this marker following stimulation [81]. 3h later, after a washing step, further antibody staining was used to characterize the effector cell population, with e.g. DNAM-1 FITC, CD3 PerCP, CD56 APC and CD16 Pacific blue, as described previously.

M.2.2 Protein biochemistry

SDS-Polyacrylamid gel-electrophoresis (SDS/PAGE)

We denaturated the samples in Laemmli buffer, and put them on ice after boiling them for 5 minutes at 95°C. Next, we separated the samples on NuPage gels, running at 150V constant for 50-90 minutes in 1x MOPS buffer.

Western Blot

After SDS/PAGE proteins were transferred to a polyvinylidene difluoride (PVDF) membrane for 90 minutes at 200mA in Western Blot transfer buffer. Prior to use, the PVDF membrane was activated in methanol and washed in transfer buffer. After blotting, we placed the membrane in blocking buffer for 2h at RT or over night at 4°C. Primary antibody was then added and incubated over night at 4°C. After rinsing the membrane in wash buffer, we incubated the blot with horseradish peroxidase (HRP)-conjugated secondary antibody for 1 hour at RT, and following a washing step, we developed the blot in SuperSignal Substrate Working Solution for approximately 5 min.

M.2.3 ImageStream system

The ImageStream Multispectral Imaging Cytometer combines the advantages of high-resolution microscopy and flow cytometry in one system (www.amnis.com). It is a flow-based system like FACS, but collects multisprectral fluorescence images of every collected cell [82, 83]. I used it to establish a solid monitoring technique of autophagic activity, and to further elucidate the complex regulation of autophagy. In principal, cells labeled with 405, 488 or 658nm excitable fluorochromes are hydrodynamically focused, excited with laser light and imaged on a time dealy integration (TDI) CCD camera (Figure M-1). Light passes through a spectral decomposition element that directs different spectral bands to spatially distinct channels on the TDI CCD

detector. A single cell image is optically decomposed into a set of sub-images, each corresponding to a different color component.

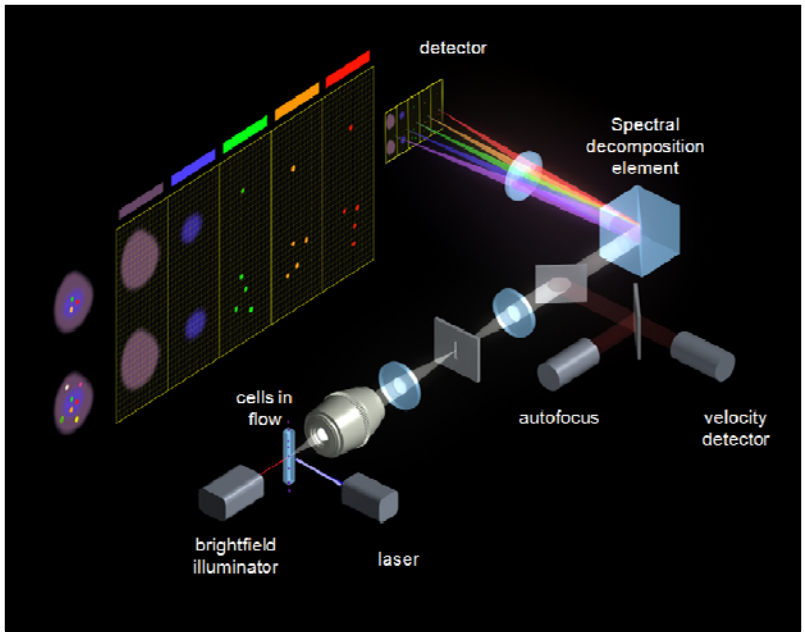

Figure M-1 - Operation principle of the ImageStream (www.amnis.com)

Quantification of apoptosis

Experimental procedure and analysis

The method of detecting apoptotic cells has previously been established [84]. We have established the quantification of apoptosis in A-375 wild-type cells. Cells were seeded in 6-well plates to ~90% confluency and treated with DMSO (solvent control) and high-dose Sorafenib (20µM) for 24 hours. After detaching the cells with Accutase, cells were fixed in 1,5% PFA for 10min at RT, and permeabilized in 0,1% Saponin/PBS. DNA was then stained with Hoechst, and afterwards washed and imaged with the ImageStream. The identification of apoptotic cells relies on detection of fragmented DNA in apoptotic cells. This is quantified using the two features (I) “Bright detail intensity threshold” to quantify nuclear fragmentation and (II) “area threshold” to quantify nuclear condensation. We have imaged 10000 cells per sample. This method was applied to quantify apoptosis in A-375 GFP-LC3 cells in response to MAPK inhibition.

Quantification of autophagy

Experimental procedure

The ImageStream System was applied to establish a new method for the monitoring of autophagy. For sample preparation, stable GFP-LC3-expressing cells were seeded in 6-well plates and grown to 90% confluency. Following a wash step with PBS, the cells were incubated in EBSS and drug cocktail, with or without lysosomal inhibitor Bafilomycin A1 (100 nM). Following a 3h treatment period, cells were detached using 2% Trypsin/EDTA, then diluted in ice-cold PBS, and fixed in 4% paraformaldehyde (PFA) for 20 minutes at 37°C. For ImageStream measurements, cells were then resuspended in 50µl PBS.

Analysis principle

Side scatter, bright-field and GFP fluorescence were collected. For all image analysis and classification steps, the Amnis Software IDEAS© 3.0.233 was used, which contains a large amount of features and masks for combinatorial analyses. To discriminate single cells from cell aggregates and cells out of focus, a dot plot of the features “aspect ratio” versus “area” was created. Aspect ratio is the minor axis divided by the major axis, and therefore describes the extent to which an object is round or oblong. The area feature is equal to the number of square microns within a mask. The dot plot clearly separates a single cell population from cell aggregates that are either too large or too elongated to be included in the single cell gate (Figure M-2, A).

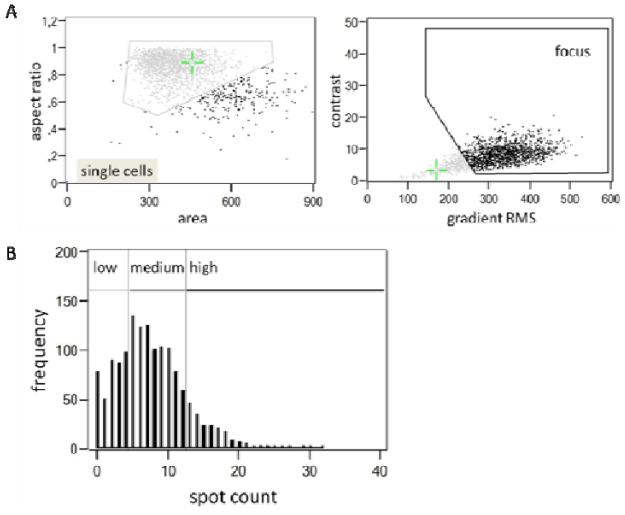

Figure M-2 - ImageStream workflow. A Gate on single cells, using the object features area and aspect ratio. Using the single cell population, cells in focus were determined with the gradient RMS and contrast features to filter out cells out of focus. **B** Cells in focus analyzed for autophagosomal content. Based on the number of detected spots we created populations of low (0-4 spots), medium (5-12 spots) and high (more than 12 spots) autophagic activity.

The contrast feature and the gradient RMS calculation were then used to determine the focus quality of images in the single cell population. The contrast feature measures the image sharpness by detecting large changes in pixel values. For every pixel the slopes of the pixel intensities are computed from the surrounding 3x3 pixel block. The Gradient RMS feature was computed using the average gradient of a pixel normalized for variations in intensity levels. This is similar to the contrast calculation with differently weighted assignments to the pixel arrays. The combination of gradient RMS and contrast allowed the detection of cells in focus (Figure M-2, A) [78].

The population of “cells in focus” was analyzed to measure autophagic activity, which can be determined because LC3-II binds to the membrane of autophagosomes. Once LC3 is fused to GFP and stably expressed, autophagosomes become visible as GFP-labeled spots. The ‘spot mask’ feature was used to determine spots and the ‘count’ feature utilized to measure the number of spots, i.e. individual and clustered GFP-labeled autophagosomes. After manual inspection of more than 100 cells, the spot to background ratio was set to 6 and the radius of spots to 2, to achieve comparable results between manual inspection and automated analysis. Depending on autophagosomal content three states of autophagic activity were defined: Low, (0-4 spots, I) medium (5-12 spots, II) and high (more than 12 spots, III). An example subpopulation distribution for spot count measurements is shown in Figure M-2B.

Compared to high resolution fluorescence microscopy the resolution of the ImageStream system is still low. Sometimes, clusters of autophagosomes were observed, that count as just a single spot. To overcome this misinterpretation, the differences between autophagosome clusters and single autophagosomes were incorporated into our analysis: Clusters of autophagosomes are bigger than single autophagosomes, and the GFP intensity in autophagosome clusters is higher compared to single autophagosomes. Therefore, secondary metrics were added, to take into account the area of spots within a cell as well as the intensity of spots compared to the total GFP intensitiy of a cell. I called those secondary metrics “normalized area” and “normalized intensity”. For the calculation of both - normalized area and normalized intensity a tight object mask on the bright field pictures was used to determine the extent of the whole cell. For normalized area the area of this tight object mask was calculated, as well as the total area of all spots within this cell. Normalized area then calculates as the ratio of area of spots and area of the object. For normalized intensity the ratio of intensity of spots divided by the intensity of the whole cell was calculated (determined as mean fluorescence GFP intensitiy of the object mask). Clusters of spots show higher normalized area and normalized intensity values compared to single spots. Importantly, there was a positive correlation between normalized area and spot count, indicating the validity of our metrics (Figure M-2, B).

M.2.4 Luminex-based multiplex system

The Luminex/Bioplex technique

The Luminex/Bioplex system allows for the simultaneous detection of several proteins, like cytokines, chemokines or kinases in cell culture supernatants or cell lysates respectively. This method uses a panel of up to 100 fluorescence-labeled-beads, which can be differentiated from another due to their color by the Luminex machine (Figure M-3, A). The bead sets are colored in different ratios of red dye and infrared dye. 10 different levels of fluorescence intensity for each dye creates a panel of 100 beads which can be distinguished from another by the classifier laser. This bead set allows the simultaneous detection of different proteins within one sample: Differently colored beads are specific for different proteins because of their coating with specific antibodies. Each bead carries thousands of capture antibodies for one specific protein. Quantification of the protein of interest occurs by the addition of a second biotinylated specific antibody, which binds to another epitope of the protein, and thus addition of SAPE enables quantificiation according to fluorescence intensity (Figure M-3 C). The Luminex reader is equipped with two lasers, a classification laser (635nm) which excites the beads and allocates them into specific regions, and a reporter laser (532nm) which excites the molecular tags, i.e. PE. The amount of fluorescent intensity (reporter laser) is proportional to the amount of the captured molecule. With default settings, the system is calibrated to analyze 25-100 beads for each region, and reports the median fluorescence intensity of these beads.

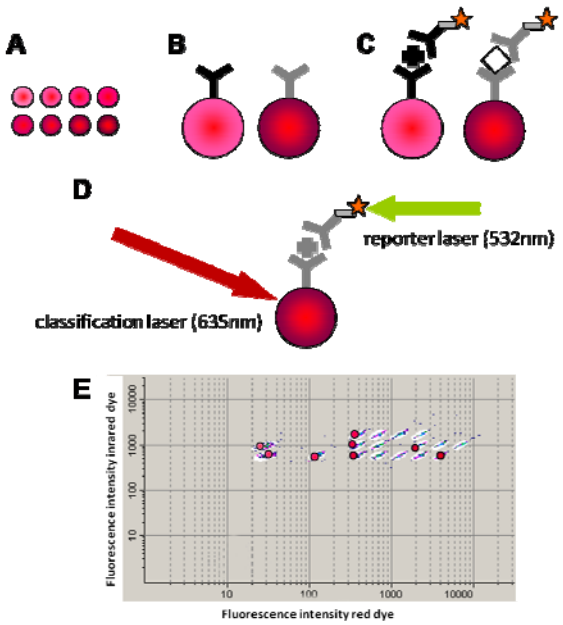

Figure M-3 – the Luminex technique. A The bead set is internally dyed with combinations of two spectrally different fluorophores. 10 different levels of fluorescence intensity for each fluorophore create a panel of 100 distinguishable beads. **B** Thousands of capture antibodies are bound to each bead; different beads carry different capture antibodies. **C** bead-bound antibodies collect proteins in the sample; reporter biotinylated secondary antibodies bind to sample molecules. **D** The classification laser excites the beads, fluorescence of the beads identifies the region (**E**). The reporter laser excites molecular tags, i.e. SAPE. The amount of fluorescence intensity is proportional to the amount of analyte captured.

Cytokine detection and quantification from culture supernatants

We used the Luminex technique to create a cytokine and chemokine secretion profile for melanoma cell lines, and to determine the effects of MAPK inhibiton on this profile. Following MAPK inhibitor treatment as described in 0, cell culture supernatants were collected, and stored at -80°C until the measurement. Bio-Plex assays (Bio-Rad) contain standard concentrations of each analyte, and the calculation of respective standard curves allows calculation of protein concentrations in the culture supernatants of treated melanoma cells.

We performed the assay according to the manufacturers protocol. Lyophilized cytokine standard was resuspended in 500µl RPMI III, and incubated on ice for 30 minutes. Serial dilution series to generate standard curves of each chemokine/growth factor of interest were performed. The bead mixture, specific for the analyzed chemokines and growth factors was incubated with 50µl supernatant in a 96-well filter plate for 30 minutes at RT. This incubation step, as well as all following incubation steps, have been carried out on a plate shaker in the dark, to avoid bead aggregations, as well as bleaching of the beads and SAPE-labeled detection antibodies. Wells which contained only medium served as background controls. Several washing steps were performed with 100µl wash buffer, to remove unbound proteins. We used a vacuum pump for all washing steps to remove the fluid in the wells. Since the beads are bigger (5nm) than the filter pores, they remain in the wells. After addition of secondary biotinylated antibody mix for 30 minutes at RT, and three more washing steps SAPE was added for 10 minutes at RT (1:125 dilution). After three final washing steps and addition of 125µl assay buffer, standards and samples were analyzed for bead and SAPE fluorescence.

Analysis of standard curves and samples

We used the Bio-Rad Manager 5.0 and 6.0 software for analysis. Standard curves are automatically calculated by the software using a 5 parameter logistic plot formula, which allows the calculation of protein concentrations in the samples (pg/ml), according to the linear relationship between FI and concentration. The software permits the definition of two outliers, which differ strongly from the standard curves. Usually this only occurs at very high or low standard concentrations. Only values within the linear regression range of the standard curves were qualified as concentrations. Linear concentration range was between 1-50000pg/ml.

Phosphoplex measurements

Besides chemokine detection assays, the Multiplex technology was also used to determine the phosphorylation status of kinases and transcription factors from whole cell lysates. The technique was applied to analyze the effects of MAPK inhibition by small molecule inhibitors in melanoma cell lines on various signaling pathways, in addition to the Ras/Raf/MEK/ERK pathway. On separated plates, the total content of kinases as well as the phosphorylated protein fraction in our samples was determined.

Preparation of cell lysates

We used the cell lysis kit from Bio-Rad for the preparation of tumor cell lysates, because this lysis procedure maintains the binding site for both, capure and detection antibody. The treatment with different small molecule inhibitors of the MAPK pathway was performed as described in 0. After treatment, the supernatant was collected for chemokine detection, and cells were washed with 2ml icecold PBS per well. After adding 150µl cold lysis-buffer to each well, cells were detached with a cell scraper and lysates were transferred to 1,5ml Eppendorf tubes. Next, the tubes were incubated during gentle rotation at 4°C for 20 minutes, and then shock-frozen at -80°C to increase cell digestion. After thawing the lysates on ice, they were centrifuged at maximum speed for 25 minutes at 4°C. The supernatant was transferred to a new tube, and stored at -20°C. 10µl lysate aliquots were stored in separate tubes for detection of total protein concentrations.

Detection of lysate protein concentrations and adjustment to assay concentrations

For the quantification of total protein, we used the Pierce BCA Protein Assay Kit (Thermo Scientific). 10µl of each sample was pipetted into a 96-microplate well. 200µl of the working reagent were added to each well, and mixed with the sample on a plate shaker for about 30 seconds. The plate was covered and incubated at 37°C for 30 minutes. After the incubation period, the absorption was measured at 562nm with an Elisa reader. The use of a standard dilution series and the calculation of standard curves, allowed for the exact determination of protein concentrations in each sample.

Protein concentrations were set to the lowest necessary concentration amongst all lysates within one group, diluted with assay buffer: To allow for the comparison of drug perturbations as well as comparison between cell lines, we detected the lowest protein concentration within this set of samples, and adjusted all other sample concentrations accordingly. 50µl of lysates were incubated on a plate shaker at RT in the dark with bead mixtures over night. The following day biotinylated detection antibodies were added after three washing steps, and plates were incubated at RT for 30 minutes. For quantification SAPE was added, and after three further washing steps plates were measured and analyzed in 125µl assay buffer with the Luminex machine and the Bio-Rad Manager 5.0 and 6.0.

Phosphoplex analysis

For phosphoprotein detection, Bio-Rad does not provide standards with defined protein concentrations, but positive control lysates to test for general assay performance. We collected at least 50 beads for each analyte region. Reported median fluorescence intensity values for each analyte are a measure for the total or phosphorylated protein content in the samples. It is important to quantify changes in phosphorylated kinase protein in comparison with corresponding total protein content. Usually total-kinase levels are used to prove correct protein quantifications, e.g. in Western Blotting, where they serve as loading controls. Due to the higher sensitivity of the phosphoplex assay, changes in total kinase content are also detected.

M.2.5 xCELLigence system

The xCELLigence system monitors cellular events in real time without incorporation of labels or dyes. It measures electrical impedance across interdigitated micro-electrodes integrated on the bottom of tissue culture E-plates. The impedance measurement provides quantitative information about the biological status of the cells, including cell number, viability and morphology (adherence) [85, 86]

The presence of cells on top of the electrodes affects the local ionic environment at the interface between electrode and solution, leading to an increase in the electrode impedance. The gold electrodes at the bottom of E-plates cover about 80% of the bottom of the wells. The more cells attached to the electrodes, the larger the increases in electrode impedance. In addition, the impedance depends on the quality of the cell interaction with the electrodes. For example, increased cell adhesion or spreading will lead to a larger change in electrode impedance. Thus, electrode impedance, which is displayed as cell index (CI) values, can be used to monitor cell viability, cell number, morphology, and degree of adhesion (Figure M-4), it is however not possible to discriminate between these events.

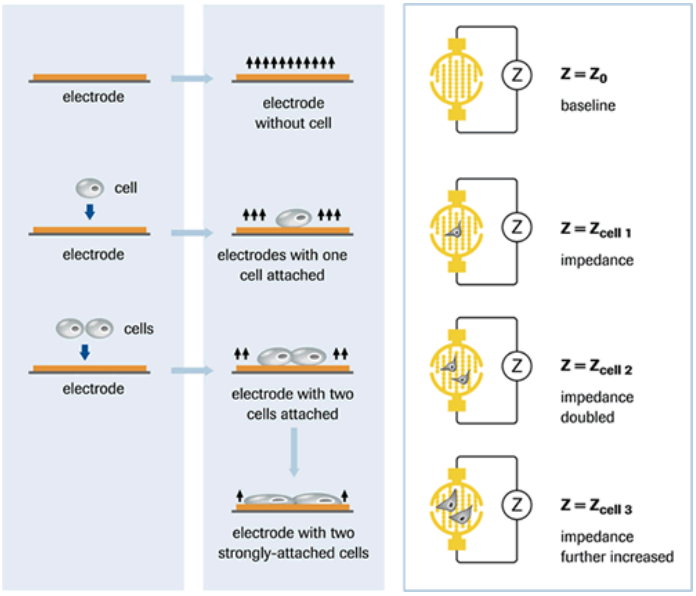

Figure M-4 - xCELLigence technology and derivation of Cell Index (CI). Cell Index is a relative metric, and requires a background measurement as a starting point for evaluation. Changes in impedance by cell adhesion and proliferation lead to higher impedance and higher values of CI. Image used from Roche Diagnostics.

CI is a dimensionless parameter derived as a relative change in measured electrical impedance to represent the status of cells in the wells. When cells are not present or are not well-adhered on the electrodes, the CI is zero. Under the same physiological conditions, when more cells are attached on the electrodes, the CI values are larger. Thus, CI is a quantitative measure of cell number present in a well. Additionally, change in cell status, such as cell morphology, cell adhesion, or cell viability will lead to changes in CI.

We used the real-time cell analyzer dual plate (RTCA DP) instrument to perform proliferation assays, measure the effects of drug perturbations and the extent of NK cell killing. We placed the instrument in an incubator set to 37°C and 5%CO_2, and used this incubator only for xCELLigence analysis. This minimizes temperature and CO_2 changes during cell incubation times, and therefore reduces artificial changes in Cell Index values.

Proliferation assays

For proliferation tests over 96 hours, we seeded between 1250 to 10000 cells in duplicate wells for each cell line. Control wells contained only TM, and the initial background measurement was performed with 100µl TM only in each well. After addition of the cells, they were allowed to sink for 30 minutes at RT, before initiating the measurement. Incubation of the cells occurred at 37°C and 5% CO_2 for the indicated times. In the absence of inhibitors or other drugs, increasing impedance correlates with cell proliferation. As shown in Figure M-5, higher cell numbers at timepoint 0 resulted in increased curves.

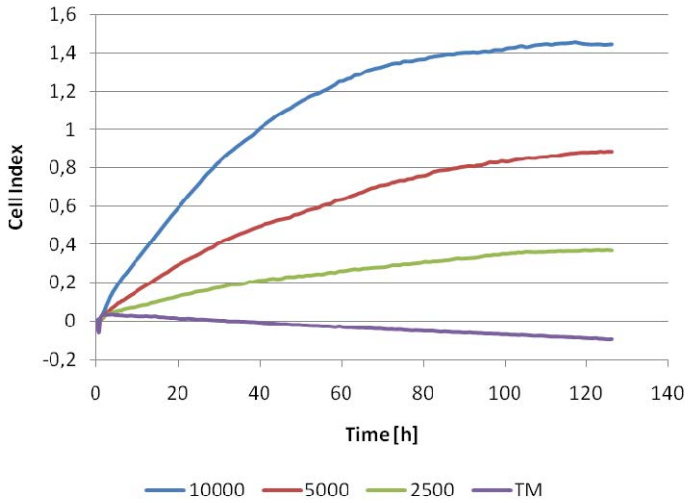

Figure M-5 - Example of real-time monitoring of proliferation with xCELLigence system. Electrode impedance is displayed and recorded as Cell Index (CI). It reflects the biological state of monitored cells, including cell number, cell viability, morphology and adhesion degree. Ma-Mel-48a was tested with 10000, 5000 and 2500 cells per well. Values shown are averages of duplicate measurements. TM served as negative control without cells.

MAPK inihibition and effects on cell status and proliferation

One of the features of therapeutic agents like MAPK inhibitors can be detected as reduced proliferation of tumor cells and possibly the induction of cell death. The real-time monitoring technique of the xCELLigence system is especially suited to continuously analyze the effects of MAPK inhibition on cell status and proliferation without any further intervention over long incubation periods.

Cells were seeded one day before addition of inhibitor or solvent control. After adjusting the background measurement, 5000 cells were added in a total volume of 100µl TM per well, and

rested for 30 minutes at RT. Then the E-plate was placed in the RTCA instrument and the measurement was started. On Day 0, MAPK inhibitors were diluted in 20µl TM and added to the E-Plate wells. Final concentrations in these wells were 10µM for U0126, 3µM AZD6244 and 5µM for Sorafenib. These concentrations were chosen on the basis of prior flow cytometry experiments, in order to utilize concentrations with high biological activity, but without immediate induction of cell death. The measurement was immediately continued for 96 hours.

NK cytotoxicity assays

The xCELLigence system can also be used for cytotoxicity assays, since lysis of adherent target cellx by killer cells results in decreasing values of CI. Suspension cells like lymphocytes do not influence CI values, because their adherence to the E-plates is to low to interfere with the impedance of tumor cells. After the background measurement, melanoma cell lines were added in a total volume of 100µl, containing 5000 cells per well. Adhesion of the tumor cells was allowed for 4-6 hours, before primary NK cells were added in a 5:1 effector:target ratio in 50µl TM per well. NK cells were either isolated from PBMC the day before use, stimulated for 24h in RPMI III supplemented with 500 U IL-2/ml; or NK92 NK leukemia cells were used.

R.Results

R.1 Melanoma and MAPK pathway

R.1.1 Characterization of melanoma cell lines

For the analysis of MAPK inhibition in melanoma cell lines we used a core set of cell lines for all experiments. This set includes A-375 cells, a well-established melanoma cell line, carrying the V600E BRaf mutation (^{V600E}BRaf), and three primary melanoma lines: Ma-Mel-48a, -48b and -48c, carrying the G469R BRaf muation (^{G469R}BRaf). Importantly, the Ma-Mel-48 cell lines have been established from different melanoma lesions of one patient, one skin lesion and two from lymph node metastases.

The set of melanoma cell lines was characterized using FACS analysis, using different antibodies to test for HLA class I expression (W6/32, B9.12), HLA-A1, HLA-A2 (HB54), β2-microglobulin (HB28) and HLA-E (4D1), as shown in Figure R-1.

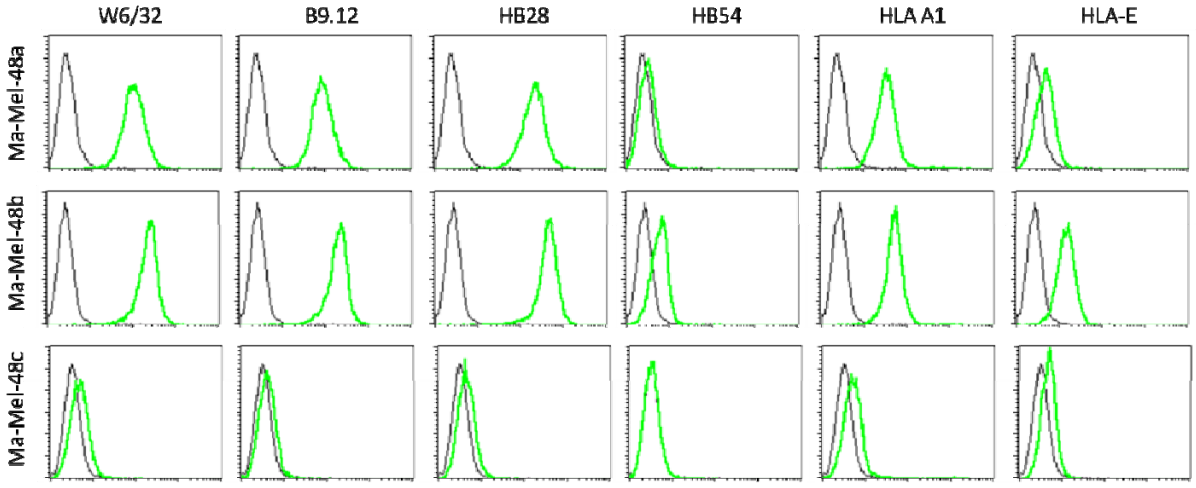

Figure R-1 - FACS characterisation of Ma-Mel-48 W6/32 recognizes only correctly folded HLA/β2m/peptide complexes; B9.12 recognizes HLA-Classe-I heavy chain alone, HB28 recognizes β2m which is non-covalently associated with HLA class I heavy chains. HB54 binds specifically to HLA-A2, 4D1 antibody binds the non-classical HLA molecule HLA-E.

Ma-Mel-48a and -48b cells show strong expression of HLA class I (W6/32 and B9.12) with β2-microglobulin surface expression recognized by HB28 antibody. Ma-Mel-48a and -48b are HLA-A1 positive, HLA-A2 negative and show a little background expression of HLA-E. In contrast, Ma-Mel-48c cells show a complete loss of HLA class I expression (negative for W6/32, B9.12, HLA-A1) probably due to a loss of β2-microglobulin, as seen with HB28 staining. This assumption has been confirmed by A. Paschen (Lab D. Schadendorf, University hospital Essen), who identified a deletion combined with a mutation in the β2m gene (unpublished results). HLA-E expression is

comparably low in both, Ma-Mel-48a and -48b. Without β2-microglobulin, HLA-peptide/ β2m-complexes can not be expressed at the cell surface.
A-375 cells are HLA class I positive, HLA-A2 positive and do not show any defects in β2m expression. HLA-E is expressed similarly low to Ma-Mel-48 cells. We have summarized the characterization of melanoma cell lines in Table R-1. In addition to HLA expression, we have investigated the expression of ligands for the activating NK cell receptors NKG2D and DNAM-1.

Surface molecule	General expression	Weighting
HLA class I	++	48a=48b>A-375<48c; (48c are negative)
ULBP2	+	A-375>48a>48b>48c
MICA	(+)	A-375>48a>48b>48c
CD155	+	48b>48a>48c>A-375
ICAM-1	+++	48a>48b>48c>A-375
ULBP1	-	
ULBP3	-	
ULBP4	-	
MICB	-	

Table R-1 - Evaluation of important ligands for NK cells in melanoma cell lines. In addition to HLA class I, we have tested the expression of ULBP1-4, MICA/B, CD155 and ICAM-1 using FACS analysis. In addition to general expression levels, we have classified these expression levels in a descending direction.

Remarkably, especially the expression of ULBP1-4 and MICA/B, which bind to NKG2D, is low in all melanoma cell lines. Only ULBP2 and MICA are expressed, we could not find any expression of ULBP1,3,4 and MICB. CD155 is expressed by all melanoma cell lines.
Loss of HLA class I expression is a common phenomenon in tumor cells. HLA class I negative cells can not be recognized by cytotoxic $CD8^+$ T cells, and therefore, loss of HLA class I is often postulated to be a survival benefit for tumor cells. Then again, loss of HLA class I can also lead to loss of NK cell inhibition, which in turn can lead to enhanced NK cell cytotoxicity.
Therefore, a loss of HLA class I expression should render Ma-Mel-48c cells, compared to Ma-Mel-48a, -48b, and A-375 cells, more sensitive to cytolysis by NK cells, since no inhibition of NK cells can be achieved in Ma-Mel-48c, but could work in Ma-Mel-48a, -48b and A-375.
The xCELLigence system is a real-time monitoring system for cell proliferation and adhesion *in vitro*. Impedance measurements allow the analysis of proliferation, adhesion, morphological changes and also cell death. Cell death, induced either through drugs or killer cells, ultimately leads to detachment of cells from the well bottom, which leads to decreasing impedance. Therefore, I utilized the xCELLigence system to perform NK cell cytotoxicity assays, whereby melanoma cells were seeded in E-plates, and afterwards NK92 cells were added at an effector to target ratio of 5:1. NK92 is used as killer cell because of its high cytotoxic activity, due to its high expression of many activating receptors. In contrast to classical 4 hour chromium release assays, the xCELLigence method does not directly show lysis of cells but indirectly quantifies decreasing

adherence to the plate as a consequence of being killed. The advantage of this system is that slow lysis processes can be monitored for >24 hours.

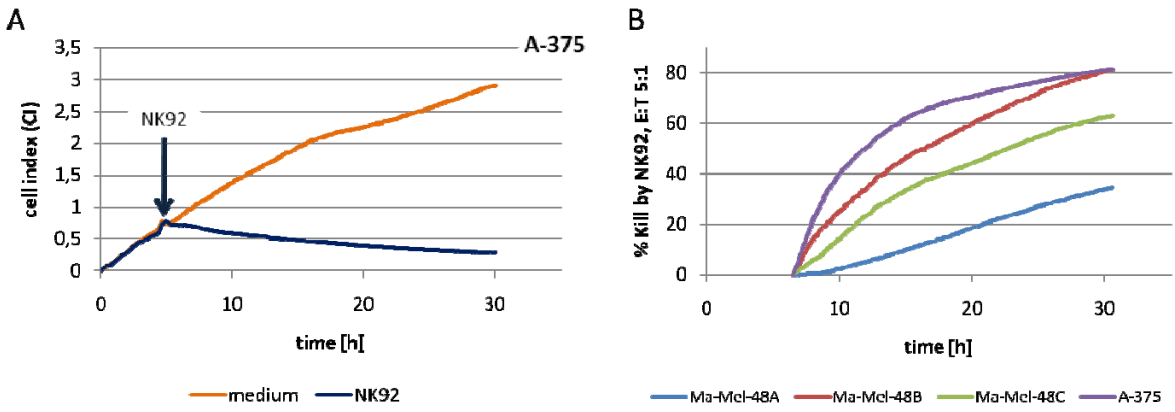

Figure R-2 - NK92 lyse melanoma cells slowly and independent of target HLA class I expression. A Raw cell index values for A-375 cells in NK92 and medium control wells. After addition of NK92 cells, cell index values decrease rapidly. B Calculation of % Kill values (division of "treated" cell index through control cell index, and substraction from 100) reveals different kinetics and extents of cell lysis.

Figure R-2A shows the raw curves of cell index values for A-375 cells after addition of NK92 cells and in medium control wells. Obviously, the addition of NK92 cells led to a rapid decrease in cell index values, corresponding to cell lysis. Figure R-2B integrates the relation between NK92 and control wells, showing %lysis values, which are calculated by division of "treated" cell index through control cell index, and substraction from 100. This graph shows that relative to control, A-375 cells were killed efficiently and to a high level of 80% within 24 hours. Ma-Mel-48a cells showed the smallest changes and were killed slowly by NK92 only to a degree of 30% within 24 hours. 48b cells have been killed to a similar extent as A-375 but not as quickly in the beginning, and the kill of Ma-Mel-48c ranges between 48a and 48b. Surprisingly, Ma-Mel-48c cells were not killed more effectively than Ma-Mel-48b cells, even though are HLA class I negative. Although all melanoma lines express at least some ligands for activating NK receptors, this seems to be insufficient to increase NK lysis in the absence of HLA class I molecules.

***In conclusion**, this experiment showed that inhibition of NK cell activity through HLA class I expression of melanoma cells is not the only mechanism that regulates NK cell cytotoxicity. The absence of NK cell inhibition does not necessarily lead to enhanced activation of NK cells, which also depends on the expression of ligands for activating receptors. Melanoma cells have been killed with different kinetics and to a different extent by a highly cytotoxic NK line, arguing that they activate NK cells to different levels.*

R.1.2 MAPK inhibiton limits melanoma cell proliferation

We have shown in a previous study of MAPK inhibition in colon-cancer cell lines, that MAPK signaling perturbations can have immediate effects, like inhibition of phosphorylation of downstream targets, but also longterm effects like alterations in HLA class I expression and DNA-methyltransferase activity [24]. Therefore, I was interested in the evaluation of this situation melanoma cells. In order to allow for treatment periods of up to 96 hours, the concentrations of the inhibitors had to be titrated for each cell line. Our goal was to find concentrations of each inhibitor that could be used for all cell lines, with maximum biological activity, but limited occurrence of cell detachment and cell death in longterm experiments. As expected, these effects proved to be dose-dependend and different between the cell lines. For a treatment period of 96 hours, concentrations of 10μM for U0126, 3μM for AZD6244 and 5 μM for Sorafenib were chosen for all cell lines. These concentrations showed pronounced biological activity with limited toxic effects, like detachment of dead cells in cell culture experiments and FACS analysis (data not shown). Since the BRaf inhibitor Sorafenib and the two MEK inhibitors U0126 and AZD6244 target the MAPK pathway at two kinases that are directly connected in the signaling cascade, it was of interest to see whether differences in proliferation and adhesion could be detected between inhibitors and between cell lines respecetively.

The xCELLigence system is especially suited to analyze basic effects of MAPK inhibition on melanoma cell lines, because the effects of treatment are followed in real time. Figure R-3 shows the effect of MAPK inhibition for Ma-Mel-48a, -48b, -48c and A-375. The xCELLigence system measures effects on proliferation, morphology changes, adhesion and cell death. Graph analysis shows the effects of drug treatment relative to DMSO control, which was set to 100% living cells.

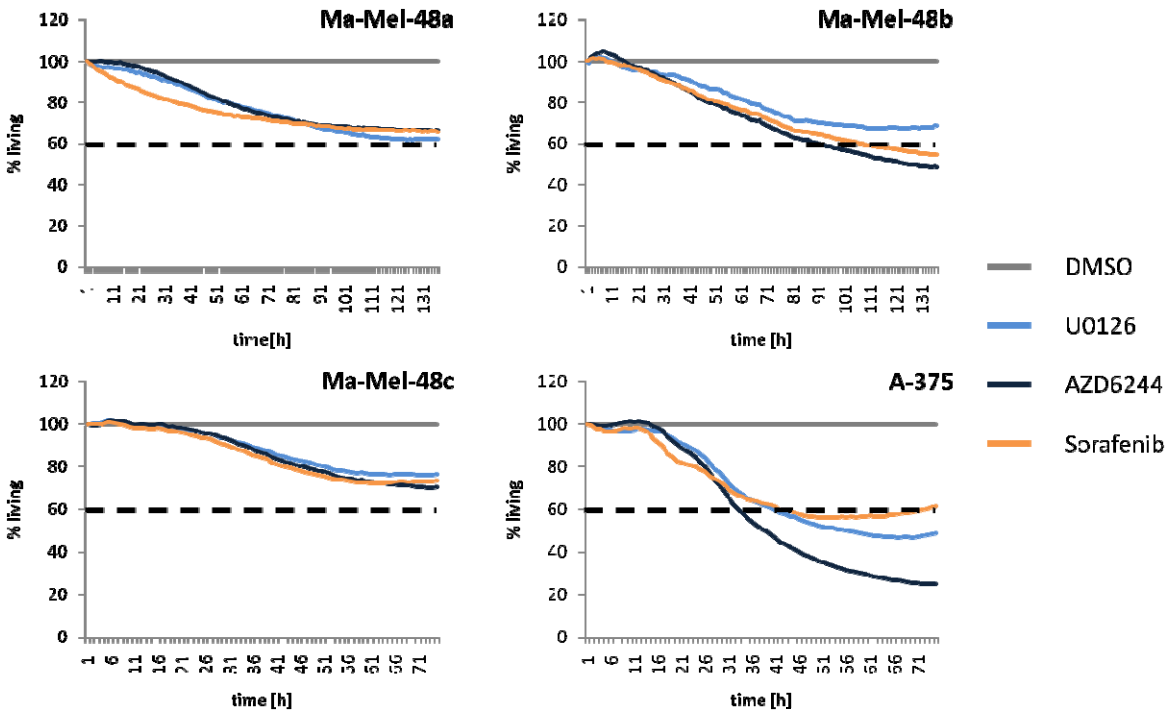

Figure R-3 - Sensitivity of melanoma cell lines to MAPK inhibitors. Cell index values were normalized at the starting point of treatment. Percent living is then calculated as the ratio between treatment and control, times 100. Control DMSO-treated cells were set to 100% living cells. Cells have been treated with U0126 [10µM], AZD6244 [3µM] and Sorafenib [5µM] for the indicated times. In Ma-Mel-48c and A-375 cells, the experiment was stopped earlier, due to 100% confluency in control wells.

Ma-Mel-48a and -48c show decreased proliferation as an effect of U0126, AZD and Sorafenib treatment, the three drugs acted very similar. i.e. compared to DMSO, proliferation decreased to ~70%. Ma-Mel-48b showed a similar trend, but AZD6244 and Sorafenib affected the cells more than U0126. A-375 cells generally reacted more sensitive to MAPK inhibition. After 16h of treatment, cell proliferation in all treated wells decreased significantly. Sorafenib and U0126 lead to strong decreases in cell index compared to DMSO. While AZD6244 reduced the cell index level further to 25% of DMSO control cells after 70 hours.

The susceptibility of melanoma cells to MAPK inhibition has previously been linked to the state of BRaf mutations. A-375 cells are the only cells in our set which carry the ^{V600E}BRaf mutation, while Ma-Mel-48 cells carry the “gate-keeper” mutation G469R. If the mutation of BRaf is responsible for the different susceptibililty to MAPK treatment, this opens up a lot of questions regarding the functional concequences of BRaf mutations, and especially ^{V600E}BRaf. What are the differences in oncogenic signaling between ^{G469R}BRaf and ^{V600E}BRaf, and how does it affect the expression of surface molecules or the secretion of cytokines, chemokines and growth factors? To answer these questions, I analyzed several parameters in the course of MAPK inhibition.

R.1.3 Influence of MAPK inhibition on HLA, CD155 and NKG2D ligands expression

The effects of MAPK inhibition on cell proliferation could not be determined immediately after the beginning of treatment. Differences between the inhibitors U0126, AZD6244 and Sorafenib appeared later than 30 hours after treatment. Due to the proliferation rate of melanoma cells, this might not be surprising, because differences between normal proliferating cells and cells with induced cell-cycle arrest or inhibited proliferation may arise only after a whole cell cycle. But it also holds the possibility that the effects of MAPK inhibition can not only be captured within short periods of time. To capture short-term as well as longterm effects of MAPK inhibition in FACS and multiplex analysis, we decided to include early measurements of 30min, 6h and 12h, and then continued monitoring of our cell lines after 24h, 48h, 72h and 96h.

As shown in Figure R-2, HLA class I expression on Ma-Mel-48a, -48b, -48c and A-375 does not provide a sufficient explanation for different levels of NK cell lysis. NK cell cytotoxicity against these melanoma lines can also be due to a lack of NK cell activation. Thus, I focused on ligand expression of the activating receptor NKG2D, including MICA/B and ULBP1-4, as well as CD155 expression, which can activate NK cells via the DNAM-1 receptor (compare Table R-1). Additionally, effects of MAPK inhibition on these cell surface molecules were addressed by monitoring ligand expression over 96 hours of treatment. Figure R-4 demonstrates the time and inhibitor-dependent alterations of CD155 surface expression.

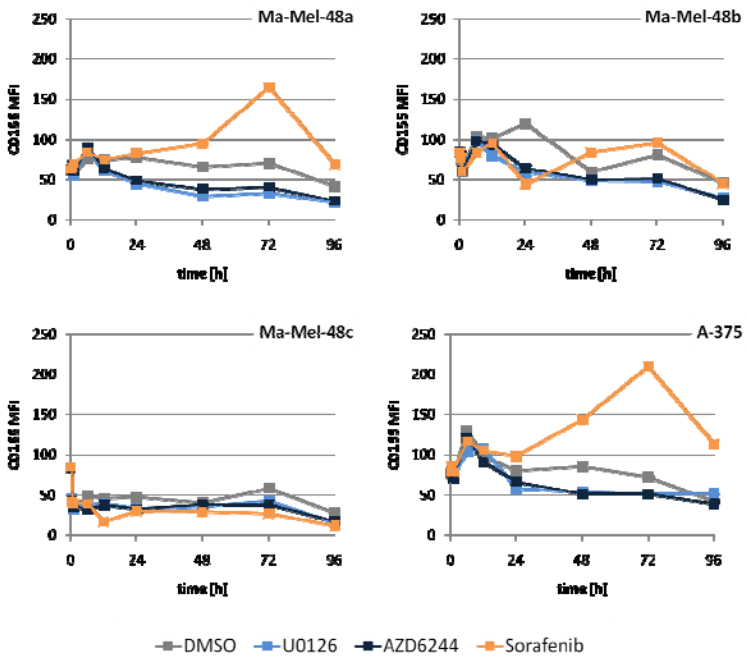

Figure R-4 - CD155 is expressed on all melanoma cells, and modulated through MAPK pathway perturbations. Cells were treated with MAPK inhibitors (U0126 10µM, AZD6244 3 µM, Sorafenib 5µM) and analysed in FACS staining after 30', 6h, 12h, 24h, 48h, 72h and 96h. Graphs show the mean fluorescence of CD155 antibody stainings for Ma-Mel-48a, -48b, -48c and A-375 melanoma cell lines.

Ma-Mel-48a and A-375 show identical patterns: Stable expression of CD155 within the first 12 hours of treatment: At 24 hours, U0126 and AZD6244 treated cells show decreased levels of CD155 expression, compared to DMSO control treatment and Sorafenib. Later timepoints show that the decrease of CD155 in U0126 and AZD6244 samples is sustained over 96 hours. DMSO control expression levels are stable over 96 hours. Surprisingly, Sorafenib treatment strongly increased CD155 expression, peaking at 72 hours of treatment. Ma-Mel-48b cells showed similar effects but to a limited extent. After 48 hours, Sorafenib samples show a slightly higher expression of CD155 than DMSO control samples, and U0126 and AZD6244 again seem to slightly inhibit CD155 expression levels. I could not detect a modulated expression of CD155 in Ma-Mel-48c cells, where the expression level was generally lower than in Ma-Mel-48a and -48b, but remained stable over 96 hours for all treatments.

The analysis of HLA class I expression over a timecourse of 96 hours also reveals differential modulating effects of MAPK inhibition (Figure R-5). In Ma-Mel-48a and A-375 cells, U0126 and AZD6244 treatment led to a slightly upregulated HLA class I expression after 48 hours, which decreases again to baseline levels after 72 and 96 hours. Since this upregulation in HLA class I is also seen in DMSO treated cells, but not to the same extent, it seems to be cell cycle-associated. Ma-Mel-48b cells, show a similar effect, but the increase after 48 hours is not as pronounced as in Ma-Mel-48a and A-375. Sorafenib seems to have an inhiting effect on HLA class I expression in all three HLA class I positive cell lines. Ma-Mel-48a and -48b show a more pronounced inhibition with Sorafenib than A-375 cells. The HLA class I negative Ma-Mel-48c show of course no influence of MAPK inhibition, since HLA class I is not expressed.

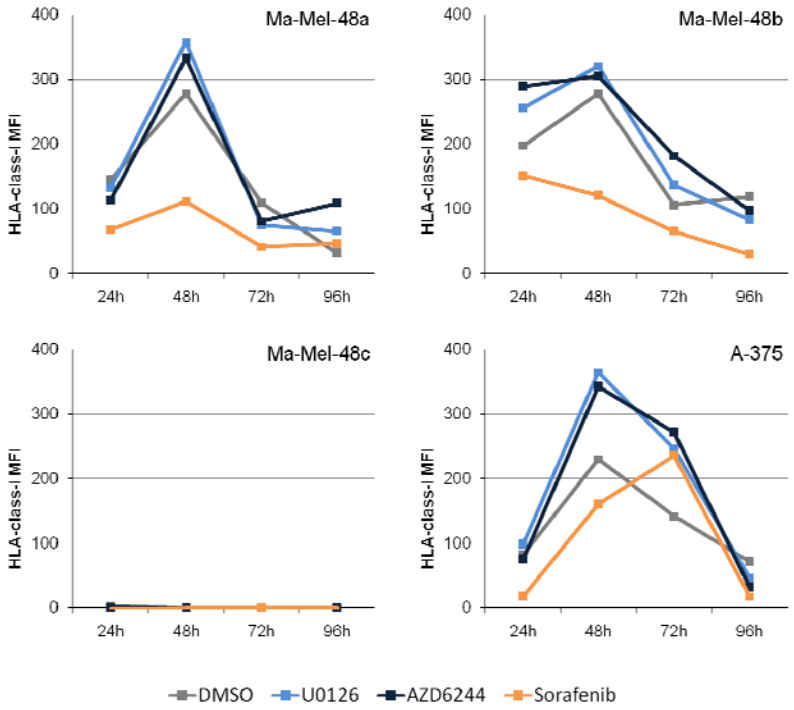

Figure R-5 - HLA class I is modulated by MAPK pathway perturbations. Treatment effect of melanoma cells with U0126 (10μM), AZD6244 (3μM) and Sorafenib (5μM) was analyzed for HAL class I expression using W6/32 and goat α mouse antibodies.

We have also tested the expression and modulation of NKG2D ligands MICA/B and ULBP1-4. Expression of these ligands on Ma-Mel-48 and A-375 cells turned out to be generally very low (Table R-1) and does not show any substantial modulating effects of MAPK inhibition (data not shown).

***In conclusion**, we could show that MAPK inhibition by these drugs in melanoma cell lines surprisingly leads to different expression levels of CD155, an important ligand for the NK cell activating receptor DNAM-1. Additionally, U0126, AZD6244 and Sorafenib proved to modulate this expression differently, showing even opposing effects of increased CD155 expression in Sorafenib treated cells and decreased levels of CD155 expression in U0126 and AZD6244 treated cells (Ma-Mel-48a and A-375). Interestingly, the modulation of HLA class I surface expression by the three MAPK inhibitors follows a mirror image of CD155. In contrast to CD155, U0126 and AZD6244 treated cells displayed increased HLA class I levels and Sorafenib-treataed cells showed decreased expression. Therefore, CD155 and HLA class I seem to be regulated by different mechanisms that are differentially influenced by BRaf (Sorafenib) and MEK (U0125, AZD6244) inhibition.*

R.1.4 Consequences of altered HLA and NK ligand expression for NK cell degranulation

I have shown that untreated melanoma cell lines were killed slowly by NK92 cells independently from their HLA class I expression (Figure R-2). Additionally, I observed changes in cell surface molecule expression in response to treatment with MAPK inhibitors. The modulation of CD155 expression (Figure R-4) was of special interest, as it might induce changes in NK cell recognition by binding to the DNAM-1 receptor. Since the xCELLigence system showed a strong influence of the inhibitors on cell proliferation, this assay was not suited to address NK cell cytotoxicity to treated cells, due to indistinguishable overlapping effects. Therefore, we performed CD107a degranulation assays with NK cells from PBMC, co-cultured with treated melanoma cell lines (Figure R-6A). NK cells, which recognize their targets and get activated, release cytotoxic granula into the immunological synapse. During this process, lysosomes, containing granzymes and perforin, fuse with the NK cell plasma membrane, and lysososmal associated protein-1 (LAMP-1, CD107a) becomes transiently visible on the surface of NK cells. NK cell degranulation assays make use of this mechanism to identify active NK cell subsets. Since NK92 are leukemic cells with a constant high turnover of vesicles and permanent high levels of surface CD107a expression, they are not useful for degranulation assays. Therefore, PBMC were used as effector cells, and degranulation of NK cells was determined by gating on the $CD3^-/CD56^+$ population only. In order to lower the degranulation threshold, PBMC were pre-activated for 24 hours with IL-2, which did not alter their phenotype, but allowed stronger degranulation in response to target cells.

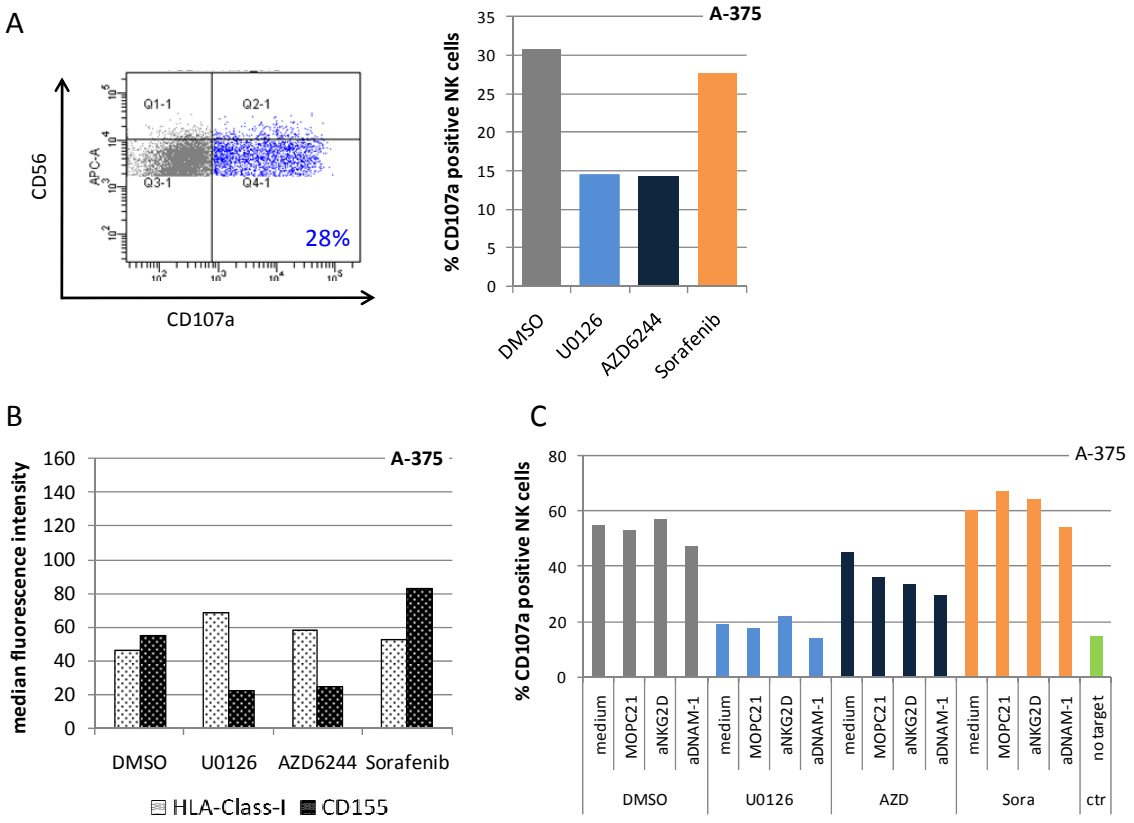

Figure R-6 - In A-375 cells, CD155 expression correlates with NK cell cytotoxicity. Degranulation of NK cells is detected as $CD56^{bright}$ and $CD56^{dim}$ $CD107a^{+}$cells (Q2-1 and Q4-1), and calculated from 100% NK cells. **A** Shows an representing dot plot of FACS analysis, and a quantification of percent $CD107a^{+}$ NK cells targeting MAPK inhibited A-375 cells. **B** Shows a quantification of corresponding target FACS analysis to detect HLA class I and CD155 expression levels. **C** Quantification of $CD107a^{+}$ NK cells in blocking experiments with mAb binding to MOPC21 (Isotype), NKG2D and DNAM-1 receptors.

In A-375 melanoma cells treated for 48 hours with MAPK inhibitors, a modulated NK cell degranulation was observed. DMSO and Sorafenib treated samples showed 30% of CD107a positive NK cells. Degranulation was substantially decreased in U0126 and AZD6244 treated melanoma cells. Simultaneously to the degranulation assay, A-375 cells were tested for their modulation of HLA class I and CD155 expression in inhibitor-treated cells, as shown in Figure R-6B. In DMSO and Sorafenib treated cells, CD155 expression was relatively stronger than HLA class I expression. Whereas HLA class I expression remains stable in U0126 and AZD6244-treated samples, a decrease in CD155 was observed. Thus, CD155 expression correlates well with the lower NK cell recognition of U0126 and AZD6244-treated samples (compare Figure R-6A and B). This suggests CD155 as a possible regulator of NK cell activity in A-375 melanoma cells. Its expression is modulated in response to MAPK inhibitor treatment, which seems to influence NK cell cytotoxicity.

To further assess the regulatory role of CD155, blocking experiments were performed. To avoid ADCC (antibody-dependent cytotoxicity) by binding of CD155-antibodies to the Fc-receptor CD16, blocking antibodies against the relevant receptors DNAM-1 and NKG2D as control were used. Before co-culture with A-375 target cells, NK cells were incubated with blocking antibodies

against (I) DNAM-1 (receptor for CD155), (II) NKG2D, as control receptor, to inhibit activation through NKG2D ligands, and (III) compared to the isotype antibody (MOPC21), and untreated NK cells respectively. As shown in Figure R-6C, the experiment confirmed the inhibited NK cell cytotoxicity in U0126 and AZD6244 treated samples. In the presence of DNAM-1 specific mAb, degranulation was slightly decreased by ~10-15% which resembles an inhibition of ~30% in all samples. NKG2D-specific mAb had only a minor effect on degranulation, indicating that DNAM-1 is more involved in the recognition of melanoma cells than NKG2D. This hierarchy follows nicely the higher expression of DNAM-1 ligand CD155, compared to NKG2D ligands.

Although they were slowly killed by the NK line NK92, Ma-Mel-48 cells, in contrast to A-375, activated NK cells only to a very limited extent (Figure R-7). Ma-Mel-48a, -48b and -48c primary melanoma cells were treated for 48 hours with MAPK inhibitors, and co-cultured with pre-activated NK cells from three different PBMC for 4 hours. K-562 cells were used as positive control for NK cell activity, because K-562 cells are HLA class I negative and strongly activate NK cells. Figure R-7 shows that with K-562 target cells all three NK cell populations from different PBL show high values of CD107a degranulation, ranging from 60% to 75%. Negative control samples without target cells show a baseline degranulation in less than 10% of NK cells. Interestingly, NK cells from PBL I-III show different amounts of CD107a degranulation with Ma-Mel-48a, -48b and -48c target cells, but in comparison to K-562 cells, only a small subpopulation of CD107a positive NK cells was induced. For all target cells, PBL I NK cells show highest amounts of activity, PBL III NK cells the lowest amount of activity, and PBL II NK cells range in between.

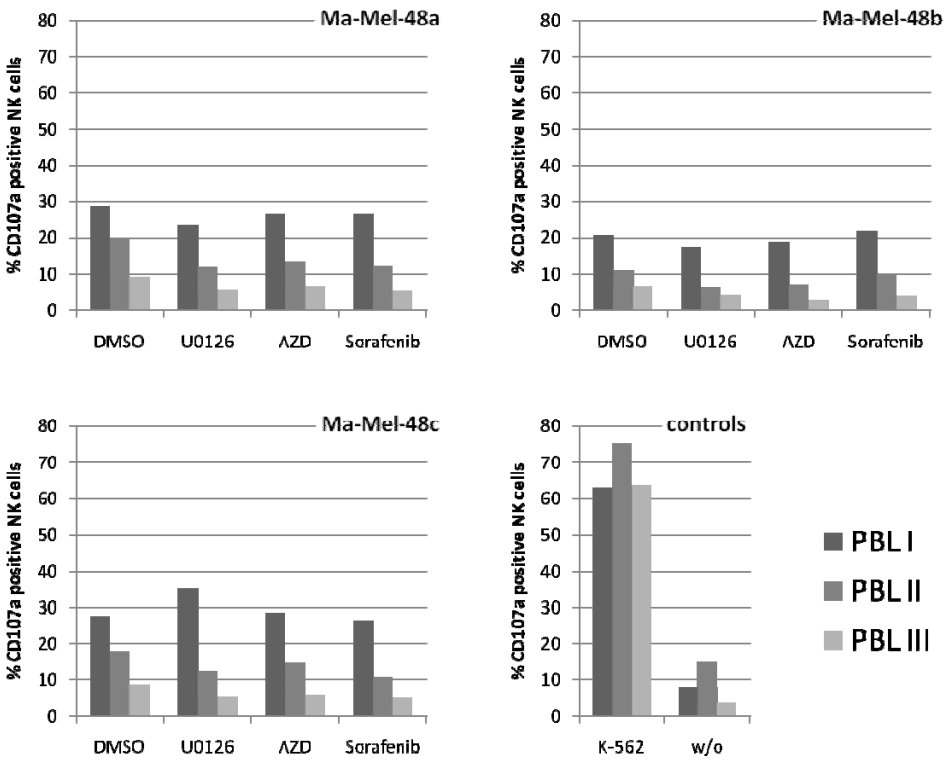

Figure R-7 - Ma-Mel-48 cells induce limited NK cell cytotoxicity. NK cells were isolated from three different PBMC of healthy donors, preactivated and then co-cultured with Ma-Mel-48a, -48b and -48c cells in CD107a degranulation experiments. The HLA class I negative cell line K-562 was used as a positive control for NK cell recognition, and shows high amounts of CD107a positive NK cells for all three PBL. Ma-Mel-48 cell all induced only limited amounts of NK cell degranulation, but where recognized to different extents by the PBL. PBLI showed the highes NK cell degranulation, followed by PBL II and PBL III.

Treatment of melanoma cells with U0126, AZD6244 and Sorafenib did not have strong effects on NK cell cytotoxicity for all Ma-Mel-48 cell lines. Even though Ma-Mel-48c cells are HLA class I negative, again primary NK cells do not display higher degranulation compared to HLA class I positive Ma-Mel-48a and -48b cells. This observation confirms the previous finding that the absence of HLA class I alone, is insufficient to increase NK activity, probably due to low NK ligand expression, especially of CD155.

***In conclusion**, I could show that the modulating effects of MAPK inhibitors on CD155 expression, can result in effects on NK cell recognition as seen in U0126 and AZD6244-treated A-375 samples, which show downregulation of CD155, and decreased NK cell cytotoxicity accordingly. Blocking the interaction between CD155 and DNAM-1 was shown to slightly inhibit cytotoxicity of primary NK cells. Importantly, the effects of the different MAPK inhibitors are not consistent, e.g. in A-375 cells, U0126 and AZD6244 treatment led to reduced expression of CD155, while Sorafenib induced CD155 expression*.

R.1.5 Influence of MAPK inhibitors on secretion of chemokines and growth factors

Transformation of tumor cells does not only include changes in tumor cells themselves, but also impacts the tumor microenvironment, which is composed of various cell types, e.g. fibroblasts, blood vessels, infiltrating immune cells and growth factors, chemokines and cytokines. Immune cell infiltration of tumors strongly depends on the chemokine and cytokine milieu in the tumor. Since many growth factors and chemokines are produced by tumor cells, the secretion of chemokines, cytokines and growth factors of Ma-Mel-48 cells was analyzed to determine changes in their secretion profile in response to MAPK inhibition. Cell culture supernatants following treatment were therefore stored before subjecting the cells to lysis for Phosphoplex or Western Blot analyses. The secretion of M-CSF, MIF, HGF, ICAM-1, SCGF-β, SDF1-α, IL-8 and VEGF, in Ma-Mel-48a, -48b and -48c cells after 48 hours of treatment with DMSO, U0126, AZD6244 and Sorafenib was determined. In Bio-Plex measurements these factors are quantified simultaneously. Remarkably, the three melanoma lines differed substantially in their secretion profile. HGF (hepatocyte growth factor), IL-8 (CXCL8), M-CSF and SDF-1α (CXCL12) were highly secreted by Ma-Mel-48a cells, and to a fractional amount by Ma-Mel-48c. In contrast, Ma-Mel-48b does not produce these factors at all. Treatment of MAPK inhibitors inhibited secretion of these factors almost completely. In contrast, VEGF was produced by all three cell lines to a different extent and was almost completely inhibited following treatment with the MAPK inhibitors. A similar picture was seen with soluble ICAM-1, which is procued by the three lines and strongly decreased by MAPK inhibitors. The observation that SCGF secretion by Ma-Mel-48a and -48c was not influenced by the inhibitors demonstrates that the strong inhibition of the other factors was not due to a general suppression of protein secretion. Thus, only factors that are presumably MAPK-dependent were influenced by inhibition of this pathway. Interestingly, MIF was the only factor out of 50 tested that showed an increased release in Ma-Mel-48b cells following treatment with Sorafenib. Since MIF is involved in several resistance pathways of tumor cells, this effect may be responsible for resistance of tumor cells to MAPK inhibition *in vivo*.

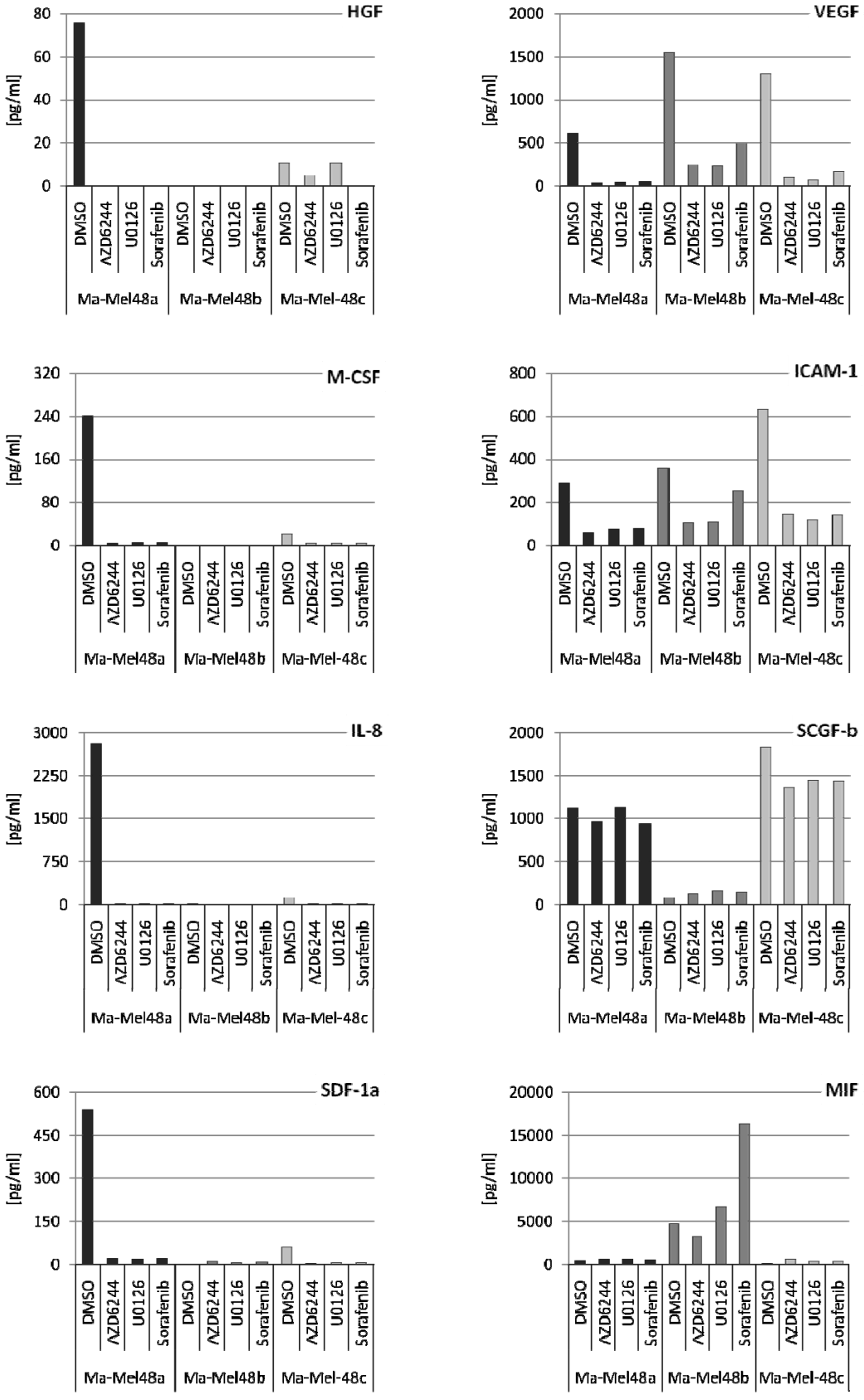

Figure R-8 - Cytokine, chemokine and growth factor profile of Ma-Mel-48 cells in response to MAPK pathway perturbations. Supernatants of Ma-Mel-48a, -48b and -48c cells were harvested following 48 hours of treatment with MAPK inhibitors, and subjected to multiplex analysis. Cells have been treated with U0126 [10µM], AZD6244 [3µM] and Sorafenib [5µM].

Macrophage inhibitory factor (MIF) was produced in large amounts by Ma-Mel-48b cells, and treatment with Sorafenib increased the secretion to more than 15.000pg/ml. Ma-Mel-48a and -48c did not show any secretion of MIF. ICAM-1 and VEGF show secretion profiles similar to each other: In DMSO controls, we could detect substantial amounts of ICAM-1 and VEGF in cell culture supernatants of all three cell lines. But ICAM-1 and VEGF are both efficiently downregulated with U0126, AZD6244 and Sorafenib treatment. SCGF-β in contrast to that did prove to be unaffected of MAPK inhibition. We detected substantial amounts of SCGF-b in Ma-Mel-48a and -48c, and low amounts in Ma-Mel-48b. The secretion remained stable after MAPK inhibition.

***In conclusion**, the secretion profiles can be grouped into four different schemes. M-CSF, HGF, SDF-1α and IL-8 are only produced by Ma-Mel-48a, and decreased in response to treatment. Since these chemokines and growth factors represent important factors for the tumor microenvironment, the inhibition of the MAPK pathway results in a substantial alteration. ICAM-1 and VEGF are secreted by all three cell lines in substantial amounts, and treatment with MAPK inhibitors leads to efficient downregulation of ICAM-1 and VEGF. VEGF was shown to be of prognostic relevance in melanoma patients. Thus, the decrease in VEGF secretion following MAPK inhibition may be of clinical relevance. MIF was only produced by Ma-Mel-48b cells and upregulated with Sorafenib. SCGF-b is secreted by primary Ma-Mel-48a and -48c cell lines, and production remained stable over 48 hours of treatment with U0126, AZD6244 and Sorafenib. Taken together, secretion of VEGF, M-CSF, IL-8, SDF1-α, HGF and M-CSF is highly dependent on MAPK signaling in melanoma cells*.

R.2 Kinetics of phosphorylation patterns during MAPK pathway inhibition

The perturbation of MAPK signaling with U0126, AZD6244 and Sorafenib is the basis for all observed effects – i.e. alterations in surface molecule expression, NK cell cytotoxicity and secretion profiles. Notably, substantial differences in some of these read-out systems were observed between the BRaf inhibitor Sorafenib, and the MEK-inhibitors U0126 and AZD6244. Therefore, we aimed to elucidate the effects of MAPK inhibitor treatment on MAPK signaling itself, but also on various connected pathways, e.g. JNK and Akt signaling or p53 stabilization. In order to capture the effects comprehensively and to possibly find explanations for the observed phenomena, we chose to utilize the Luminex system to perform phosphoplex analysis, which allows the simultaneous measurement of several different proteins in one sample. We quantified phosphorylated and total content of ERK1/2, MEK1, CREB, Akt, NFκB, IkB-α, JNK, c-Jun, p38 MAPK, GSK3α/β, Atf-2 and p53. Using this technique we were able to monitor the effect of MAPK inhibitors on various pathways over a time course of 96h.

R.2.1 Effects of MAPK inhibition on MEK/ERK proteins

R.2.1.1 Modulation of MEK1 and ERK1/2 phosphorylation in response to MAPK inhibition

A commonly used readout for the performance of MAPK inhibitors is the inhibition of phosphorylation of downstream kinases. Inhibition of MEK or Raf impairs their own kinase activities, which are involved in the kinase cascade that finally leads to phosphorylation of ERK, which then signals to various transcription factors to control cell proliferation. Thus, inhibited activity of Raf (by Sorafenib) or MEK (by U0126 and AZD6244) leads to dephosphorylation of MEK and ERK respectively. Due to the assumed linear signaling within the MAPK pathway, dephosphorylation of MEK with Sorafenib, should also lead to dephosphorylation of ERK. Therefore, all three inhibitors are supposed to mediate inhibition of ERK phosphorylation. The antibody that has been used in Phosphoplex analysis binds to both, ERK1 and ERK2 (Thr^{202}/Tyr^{204}, Thr^{185}/Tyr^{187}). Figure R-9 shows the effects of treatment of Ma-Mel-48a, -48b, -48c and A-375 with U0126, AZD6244 and Sorafenib for 96h, on phoshpo-ERK1/2 levels.

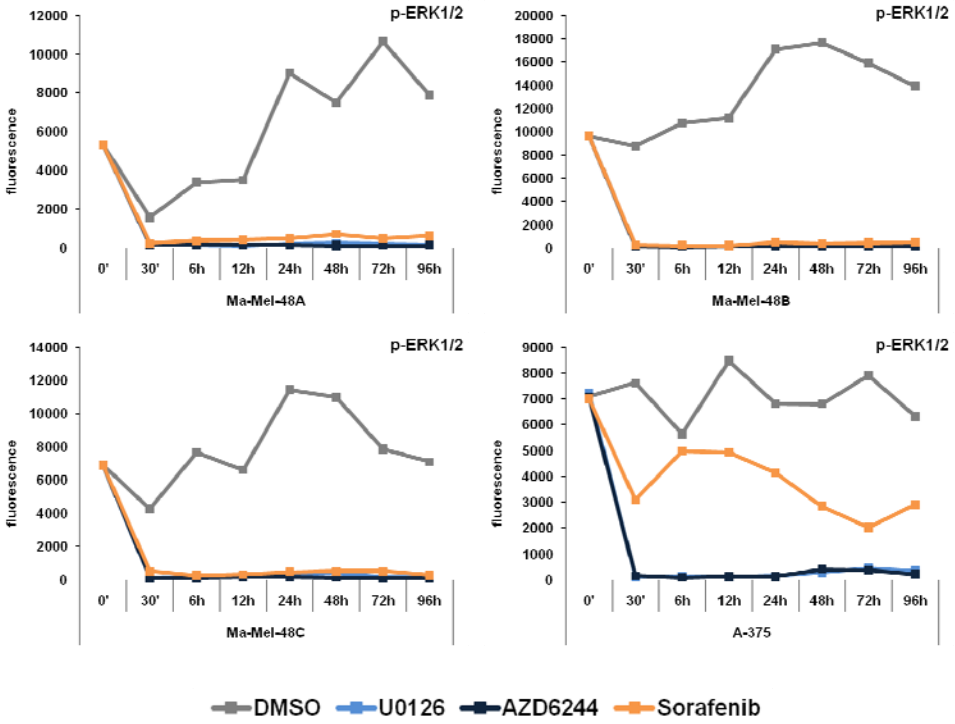

Figure R-9 - ERK phosphorylation inhibited with all MAPK inhibitors Melanoma cells were treated with U0126 (10µM), AZD6244 (3µM) and Sorafenib (5µM) or DMSO as solvent control.

Ma-Mel-48a, -48b and -48c show a very similar kinetic of ERK phosphorylation in response to treatment. ERK1/2 is constitutively phosphorylated in all three cell lines in large amounts. In DMSO control samples, phospho-ERK levels increased over the treatment period of 96 hours, probably due to cell-cycle dependent signals. The treatment with all three MAPK inhibitors led to a rapid and sustained inhibition of p-ERK1/2 in Ma-Mel-48a, -48b and 48c. In A-375 cells, DMSO control samples showed a more constant phospho-ERK level compared to Ma-Mel-48 cells. U0126 and AZD6244 achieved a rapid and sustained inhibition of ERK acitivity, but Sorafenib treatment could only partially inhibit ERK1/2 phosphorylation.

The read-out of ERK phosphorylation proved effectiveness of all three drugs in our set of melanoma cell lines. The substantial inhibition of phospho-ERK levels was achieved within 30 minutes of treatment, and was sustained over 96 hours. Since Ma-Mel-48a cells carry the ^{G469R}BRaf mutation, and A-375 cells the ^{V600E}BRaf mutation, the mutation status of BRaf seems to be irrelevant for MEK inhibitors. In A-375 cells, Sorafenib showed only a partial inhibition of phospho-ERK acitivity, which might be dependent on their ^{V600E}BRaf mutation.

The analysis of p-MEK1, upstream of ERK1/2, revealed more pronounced differences between the inhibitors and cell lines (Figure R-10). Sorafenib is the only inhibitor, which inhibits Raf activity, directly upstream of MEK. U0126 and AZD6244 are both MEK inhibitors, which are supposed to inhibit kinase activity of MEK, although they bind at different sites. MEK inhibition is

not necessarily associated with a decrease MEK phosphorylation itself. This difference depends on the mutation status, as e.g. ^{V600E}BRaf has been shown to suppress p-MEK in AZD6244-treated cells. Along those lines, differences in p-MEK levels between both MEK inhibitors, U0126 and AZD6244 were observed. U0126 inhibited p-MEK1 levels in all four melanoma cell lines tested, in Ma-Mel-48c cells not as strongly and sustained as in 48a, 48b and A-375.

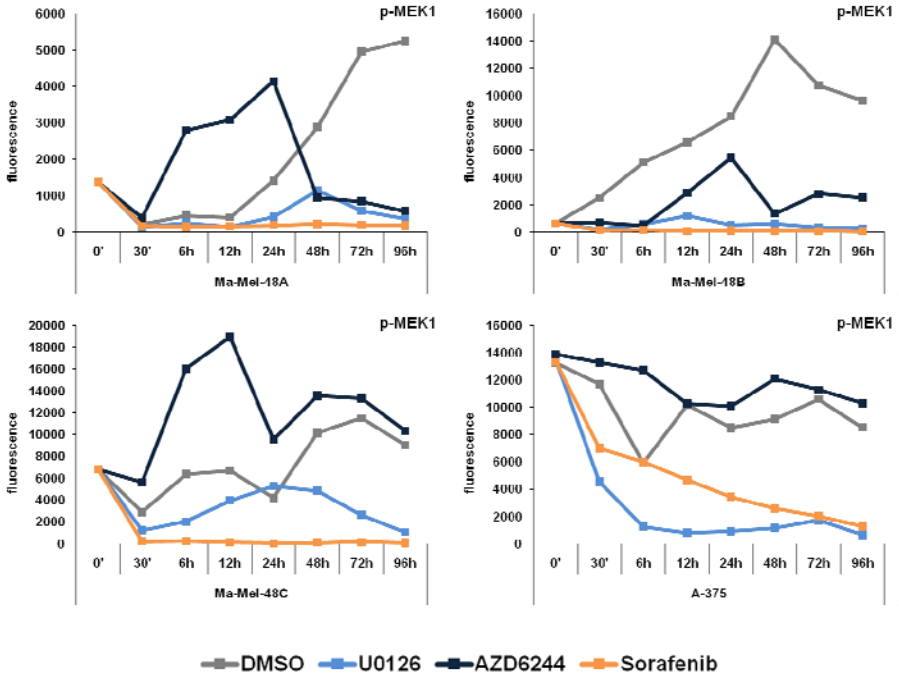

Figure R-10 - p-MEK1 expression varies between different inhibitors and cell lines. Cells have been treated with U0126 [10µM], AZD6244 [3µM] and Sorafenib [5µM] for 96 hours, and subjected to phosphoplex analysis.

In contrast, AZD6244 treatment – even though shown to be very effective in inhibition of ERK activity before, resulted in increased p-MEK1 levels compared to DMSO in Ma-Mel-48a and -48c lines. This increase in p-MEK1 levels was suppressed in ^{V600E}BRaf A-375 cells. Surprisingly, only in Ma-Mel-48b cells, AZD6244 treated samples showed phospho-MEK levels lower than in DMSO control cells. Sorafenib, as expected, effectively inhibited p-MEK1 expression in all cell lines, due to its upstream inhibition of Raf.

***In conclusion**, the analysis of p-MEK levels reveals different mechanisms of action of the two MEK inhibitors. U0126 binds to MEK1/2 proteins to inhibit their activity, and obviously blocks phosphorylation of MEK1 at Ser^{217}/Ser^{221}. AZD6244, which is a non-ATP competitive inhibitor, does not block phosphorylation sites of MEK1, but somehow inhibits dephosphorylation of MEK1, which leads to increasing levels of phospho-MEK1. For obvious reasonsm this underlines the necessity to test downstream ERK phosphorylation to assess the effectiveness of MEK inhibitors. Sorafenib proved to be very effective at inhibition of MEK activity, due to the directly upstream inhibited kinase activity of Raf, which normally functions to phosphorylate MEK.*

R.2.1.2 Modulation of total ERK1/2 and MEK1 protein levels in response to MAPK inhibition

Total protein concentrations of the lysates have been equalized between all cell lines and treatments before phosphoplex analysis, to ensure that total protein changes are not due to different amounts of lysate. Therefore, changes in total protein levels observed with Phosphoplex analysis can either be due to degradation processes in case of reduction of total protein levels, or stabilization of proteins and increased metabolism in the case of increasing total protein levels. Short and long term kinetics strengthen the interpretation of drug-induced effects on total kinase levels. Figure R-11 shows the course of total ERK1/2 protein levels in the four cell lines. There is no evident correlation between the inhibition of phosphorylation and the amount of total ERK1/2 proteins.

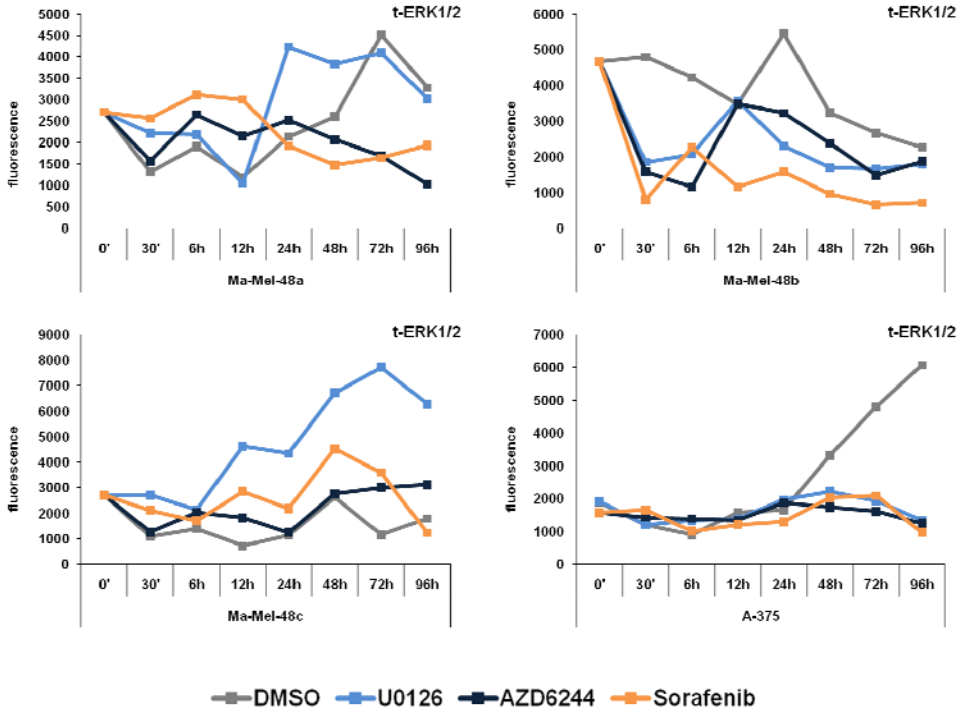

Figure R-11 - Heterogenous levels of total ERK1/2 protein in response to MAPK inhibition. Total protein concentrations across all cell lines and treatments were adjusted to 150µg/ml before analysis. Cells have been treated with U0126 [10µM], AZD6244 [3µM] and Sorafenib [5µM] for 96 hours and subjected to phosphoplex analysis.

A-375 cells show homogenious levels of t-ERK1/2 for the different treatments, which demonstrates the correct adjustment of the lysates. After 24h, DMSO samples show an increasing amount of t-ERK1/2, that is not visible with MAPK inhibitor treatment. Such changes are likely to be cell cycle-dependent since they often occur after 24 hours of treatment. For Ma-Mel-48a, -48b and -48c cells, the total ERK1/2 curves are less homogeneous, which raises the question whether protein concentrations were adjusted correctly. This problem could be excluded by the analysis of total protein levels of e.g. c-Jun (Figure R-14). Thus, total ERK1/2 curves in

Ma-Mel-48 cells most likely reflect fluctuations of the kinases during cell-cycle progression. While Sorafenib seems to stabilized these fluctuations, U0126 causes a strong increase in t-ERK1/2 in Ma-Mel-48a and -48c. In contrast, Ma-Mel-48b show the highest t-ERK1/2 in DMSO samples, and rather decreased levels with the inhibitors. Remarkably, these t-ERK1/2 fluctuations occur independently from the constant and sustained inhibition of phosphorylated ERK1/2. It is also important to mention that the changes in kinase concentrations are basically not detected by Western Blot analyses, because they are balanced by different exposure times in case of high or low signals.

The evaluation of total MEK1 levels reveals a unique feature of AZD6244 treatment (Figure R-12). Across all cell lines, AZD6244 effectively decreases t-MEK1 levels, which is in contrast to the increased or sustained MEK1 phosphorylation we have detected (Figure R-10). So binding of AZD6244 to MEK1 leads to the disappearance of total protein on the one hand, and increasing levels of phosphorylated MEK1 on the other hand. Since U0126 has a different binding site, and does not show similar effects, the binding site may be responsible for these opposing AZD6244-specific effects on p-MEK1 versus t-MEK1. This hypothesis is currently investigated using a third MEK inhibitor.

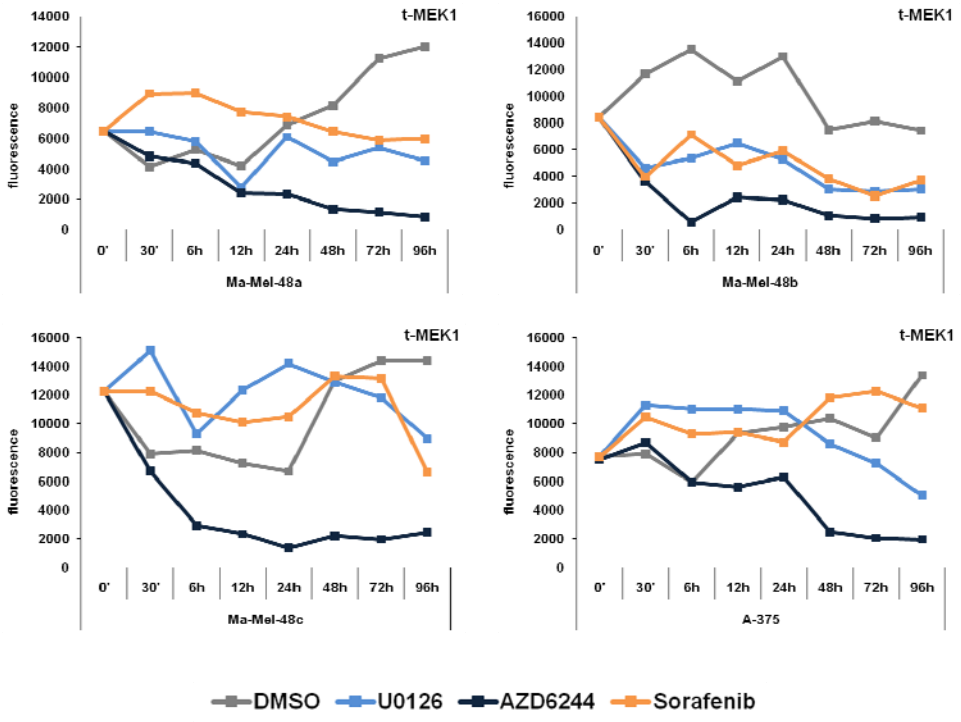

Figure R-12 - Only AZD6244 reduced total MEK1 content. Total protein concentrations across all cell lines and treatments were adjusted to 150µg/ml before analysis. Cells have been treated with U0126 [10µM], AZD6244 [3µM] and Sorafenib [5µM] for 96 hours and subjected to phosphoplex analysis.

U0126 and Sorafenib seem to lower total MEK1 levels in Ma-Mel-48b cells a bit, but do not show clear inhibiting or activating characteristics in Ma-Mel-48a, -48c, and A-375 cells. Overall MEK1 total protein levels are high for all cell lines, supporting the role as a driving signaling force.

***In conclusion**, within MAPK signaling, the inhibitors U0126, AZD6244 and Sorafenib all inhibit ERK phosphorylation effectively. The inhbiting effect is achieved within minutes, and sustained over a treatment period of 96 hours. Sorafenib achieved only a partial inhibition of phospho-ERK1/2 in A-375 cells, but showed full inhibition in Ma-Mel-48 cells. AZD6244 showed a striking characteristic with elevated levels of phosphorylated MEK1 in Ma-Mel-48a and -48c cells, together with decreasing levels of total MEK1 protein in all cell lines. Generelly, phosphorylated MEK or ERK can be stabilized while total kinase levels are decreased during inhibitor treatment, suggesting that phosphorylated and unphosphorylated kinases can be regulated independently. Both specific MEK inhibitors, U0126 and AZD6244, showed two different mechanisms of action, but both achieved the goal of inhibited ERK phosphorylation.*

R.2.2 JNK, Akt and p53 phosphorylation and stabilization are affected by MAPK inhibition

R.2.2.1 JNK and c-Jun signaling is altered in response to MAPK inhibition

C-Jun N-terminal kinases (JNK) were first characterized as stress-activated members of the MAPK family, and are involved in the regulation of cell-cycle progression and induction of apoptosis, through the control of various downstream substrates, e.g. c-Jun and p53. Phospho-JNK levels in Ma-Mel-48 and A-375 cells were constantly low over the timecourse of 96 hours of MAPK treatment (Figure R-13). Ma-Mel-48a and Ma-Mel-48b show a slight inhibition of JNK phosphorylation with the three MAPK inhibitors.

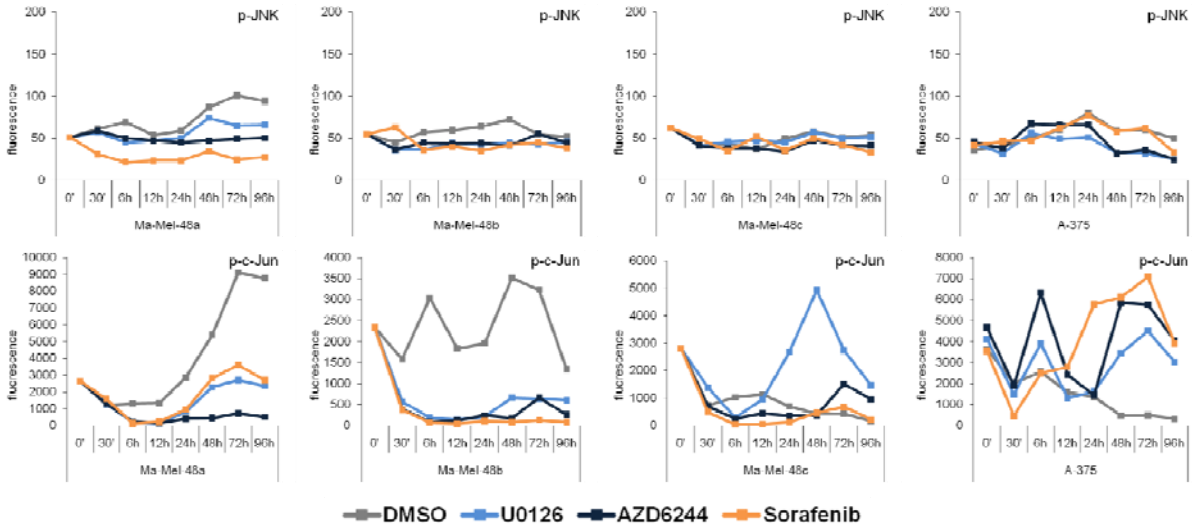

Figure R-13 - Phosphorylation of JNK and c-Jun is modulated in response to MAPK inhibition. Cells have been treated with U0126 [10µM], AZD6244 [3µM] and Sorafenib [5µM] for 96 hours and subjected to phosphoplex analysis.

Downstream of p-JNK, p-c-Jun levels showed more pronounced effects. In Ma-Mel-48a, p-c-Jun levels in DMSO-treated control cells steadily increase after 12 hours and peak at 72 hours. This effect is efficiently suppressed by U0126, AZD6244 and Sorafenib treatment. Ma-Mel-48b cells show similar effects: Phospho-c-Jun levels in DMSO-control cells remain at high values over 96 hours and are strongly inhibited in response to inhibitor treatment. In Ma-Mel-48c we detected an increase in phospho-c-Jun only in U0126-treated cells; DMSO as well as Sorafenib and AZD6244 show low c-Jun phosphorylation levels. In A-375, phospho-c-Jun levels seem to be upregulated early (6h) and after 24 hours with MAPK inhibitors. DMSO control cells show decreasing levels of phospho-c-Jun.

The parallel analysis of total JNK and c-Jun protein content revealed two important aspects of this highly sensitive quantificiation method: First, MFI values for total-c-Jun were much lower than those of phosphorylated-c-Jun (Figure R-14). We have made similar observations for Akt and some other proteins. This puzzling observation was clarified based on our data with the manufacturer (Bio-Rad). While the capture mAb on the bead is identical for phospho- and total-assays, the phospho-specific detection mAb always detects all isoforms of the kinase or transcription factor, while the total-specific detection mAb sometime only binds to some but not all isoforms. In the case of total-c-Jun, only c-Jun and not its other variants like junB is detected in the total assay. In the case of total Akt, only Akt1 but not Akt2/3 are detected (Figure R-16). Second, JNK and c-Jun nicely display a direct correlation between phosphorylated and unphosphorylated proteins (compare Figure R-13 and Figure R-14), supporting the interpretation, that the relationship between phosphorylated and total kinases and transcription factors follows an individual regulation.

Regarding JNK, only a small portion occurs in its active phosphorylated state, and here total JNK levels are generally higher than phospho-JNK levels (Figure R-14), confirming that all JNK isoforms are detectable.

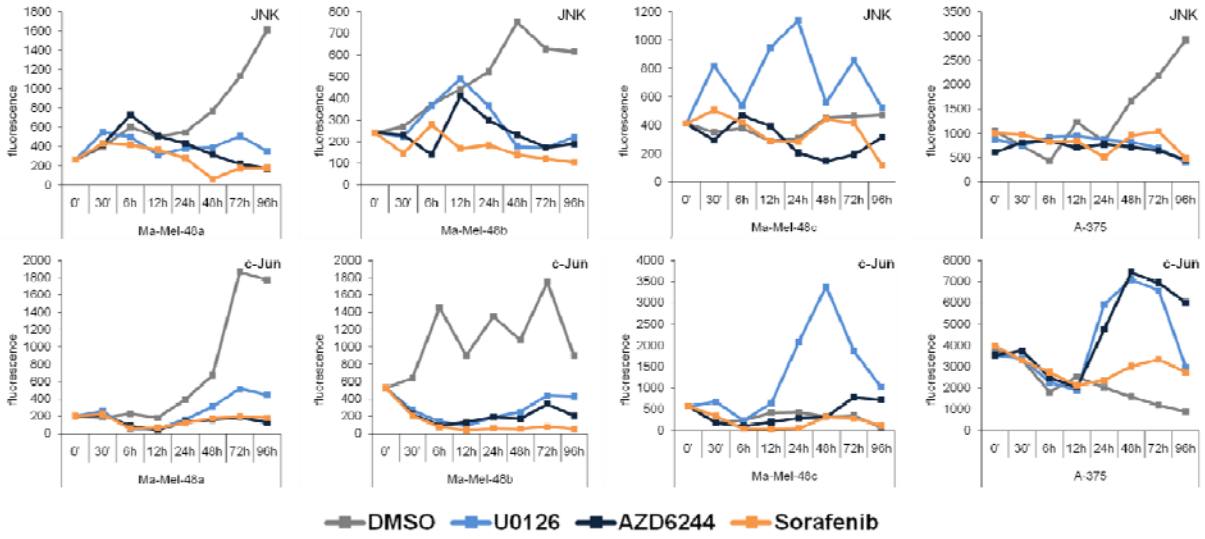

Figure R-14 - Total amounts of JNK and c-Jun follow the observed modulation in phospho JNK and c-Jun. Cells have been treated with U0126 [10µM], AZD6244 [3µM] and Sorafenib [5µM] for 96 hours and subjected to phosphoplex analysis.

In Ma-Mel-48a and -48b the picture of total JNK regulation looks very similar to the phosphorylation pattern of JNK. DMSO control samples show increasing levels of total JNK after 24 hours, which are reduced with MAPK inhibitors. Even though the JNK-phosphorylation patterns of A-375 cells were different from Ma-Mel-48a and -48b, total JNK seems to be regulated the same way, i.e. DMSO control cells show an increase in total JNK content, which was prevented in U0126, AZD6244 and Sorafenib samples effectively.

The analysis of total c-Jun levels revealed that the patterns of c-Jun phoshporylation and total protein content correlate nicely. The increase in phospho c-Jun in DMSO-treated Ma-Mel-48 cells is accompanied by a parallel increase in total c-Jun protein that was suppressed by the three inhibitors. Obviously, inhibition of the MAPK pathway has consequences for the natural regulation of the transcription factor c-Jun. This may be one of the reasons for the decreased secretion of growth factos and chemokines in Ma-Mel-48 cells, since VEGF and CXCL8, for example, possess AP-1 binding sites in their promoters.

R.2.2.2 Degradation of total protein levels is independent of caspase activity

One of the big surprises was the extent to which total protein levels were regulated in response to MAPK inhibition. While c-Jun was an example in which the kinetic of an increase in total and phospho c-Jun over 96 hours was suppressed, other kinases were clearly degraded in MAPK

inhibitor-treated cells, p38 MAPK for instance. We wondered, whether this degradation is protein specifically regulated, or if it occurs in the context of apoptosis and caspase activity. In order to test this, I have used the pan-caspase inhibitor zVAD fmk in further phosphoplex experiments, to inhibit caspase activity in addition to treatment with MAPK inhibitors for 48 hours. The results clearly show that caspase activity is not responsible for protein degradation, because neither in phospho-protein levels, nor in total protein levels, inhibition of caspase activity could reverse the effects of MAPK treatment. Figure R-15A shows that total c-Jun levels are unaffected by the addition of zVAD FMK, in A-375 cells as well as in Ma-Mel-48a. Besides c-Jun, we have also checked phosphorylated and total amounts of Akt, Atf-2, IκB-α, p38MAPK, p90RSK, ERK1/2, p53 and MEK1 for the influence of caspase inhibition. None of these proteins showed changes in response to addition of zVAD fmk. Figure R-15B exemplarily shows the kinetic of total p38 MAPK. All three inhibitors lead to a strong degradation of total p38 MAPK, which is unaffected by the addition of zVAD, as tested for the timepoint of 48 hours of treatment. Additionally, this data nicely shows that even though the amount of fluorescence changes between different phosphoplex assays, the tendency remains the same between measurements (compare fluorescence between left and right graph in Figure R-15B).

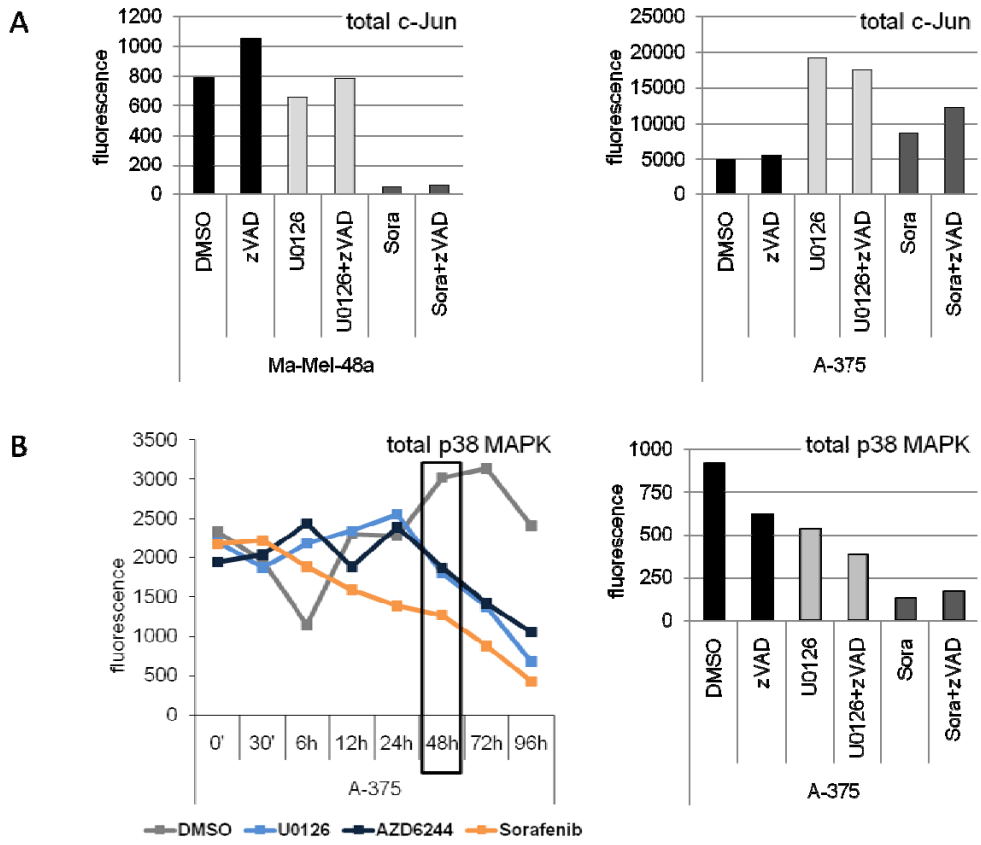

Figure R-15 - Caspase inhibition does not alter protein degradation levels. zVAD fmk was added additionally to the respective wells, in a final concentration of 40µM. For the zVAD assay, we have used U0126 and Sorafenib in final concentration of 10µM. Total p38 MAPK kinetic included the treatment with U0126 (10µM), AZD6244 (3µM) and Sorafenib (5µM).

R.2.2.3 Influence of MAPK inhibition on PI3K/Akt signaling

Akt signaling, alongside p53, plays a central role in controlling cell fate decisions. MAPK signaling is tightly connected to Akt, since Ras signals also activate PI3K, which signals via PIP3 to phosphorylate and activate Akt. On the one hand, Akt signals to inhibit apoptosis, e.g. via inhibition of BAD, or via regulation of pro-survival transcription factors. On the other hand, Akt activates the mammalian target of rapamycin (mTOR), which controls cell metabolism, and is a central regulator of autophagy. In its active phosphorylated state, mTOR inhibits autophagy, via yet unclear mechanisms.

Even though the MAPK inhibitors we use inhibit MAPK signaling downstream of Ras, it seems likely that dysregulation of MAPK signaling also alters PI3K/Akt signaling. Indeed, our evaluation of phosphorylated and total amounts of Akt protein implicates that MAPK perturbations can lead to dysregulation of Akt signaling (Figure R-16), presumably via feedback-loops from Akt/mTOR to the MAPK pathway [87]. The observation that all cells possess a weak baseline phosphorylation of Akt (<500 MFI), is an indicator for a non-mutant PI3K pathway, since PI3K-mutated cells are characterized by much higher intrinsic Akt levels, e.g. PI3K-mutated MCF7 cells (Appendix Figure 1).

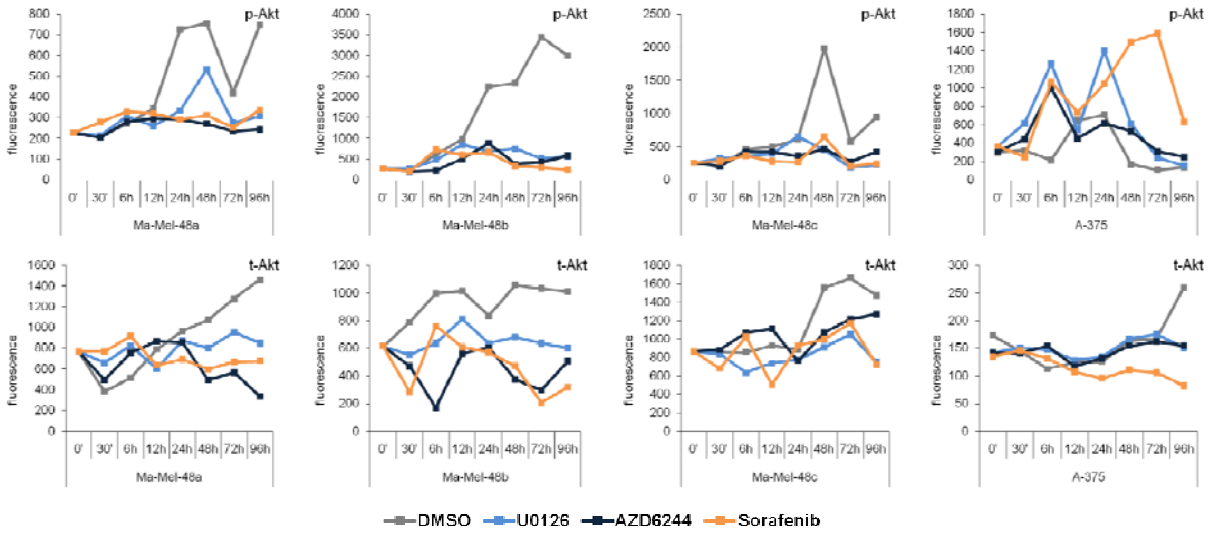

Figure R-16 - Total and phosphorylated amounts of Akt are altered in response to MAPK inhibitor treatment. Kinetics include the treatment with U0126 (10µM), AZD6244 (3µM) and Sorafenib (5µM).

In Ma-Mel-48a and -48b cells, phosphorylated Akt (Ser473) levels increase in DMSO controls cells at 24 hours of MAPK inhibitor treatment, and remain stable. However, this increase is suppressed by the three inhibitors in Ma-Mel-48 cells. The phosphorylated picture is partially reflected in corresponding total Akt levels of Ma-Mel-48a and -48b. Ma-Mel-48c seem to follow the trend of Ma-Mel-48a and -48b cells, but the increase in phosphorylated Akt is not as pronounced in Ma-Mel-48c. A-375 show a different regulation of Akt: Phosphorylated levels first

seem to increase with U0126 and Sorafenib treatment, in contrast to Ma-Mel-48 cells. In DMSO-treated cells, phospho-Akt levels slightly increase after 12 hours, but return to baseline levels after 24 hours of treatment. In sharp contrast to Ma-Mel-48 cells, Sorafenib treatment in particular results in late Akt-phosphorylation that peaks at 48 hours and 72 hours respectively. Total levels of Akt in A-375 cells are low and stable across all samples. Of note, the observation of lower total Akt levels than phospho-Akt values can be explained by the detection of total Akt1 only. However, like in most melanoma cells, Akt3 is primarily expressed but not detectable (personal communication by A. Paschen, University Hospital Essen).

***In conclusion**, the primary melanoma lines Ma-Mel-48 and the established A-375 line differ in their kinetics of phosphorylated and total levels of JNK, c-Jun and Akt, despite the fact that homogeneous inhibiton of ERK1/2 is achieved by all three inhibitors. In addition, there is variability between the three melanoma lines although they carry the same ^{G469R}BRaf mutation and were derived from one single patient. Thus, inhibition of phospho-ERK1/2 is a common denominator of MAPK inhibition at BRaf or MEK, but it is not at all reflecting individual reactions to other kinases or transcription factors*.

R.2.2.4 Influence of MAPK inhibition on phosphorylated and total amounts of p53

P53 signaling and transcriptional activity results in three major outputs; cell cycle arrest, cellular sensescence and/or apoptosis. The tightly regulated p53 protein is not only under control of JNK signaling, but also induced by a number of stress signals, including DNA damage, oxidative stress and activated oncogenes. Therefore, dysregulation of p53 through MAPK inhibition could have major effects on cell fate. Figure R-17 shows the kinetics of phophorylated and total protein p53 levels (phosphorylation at Ser15). In all cell lines, and for phosphorylated as well as total protein levels, an upregulation of p53 during the first 12 hours is detectable, which then decreases again to initial levels after 24 hours. This is probably due to a cell cycle dependent stabilization of p53. As we have shown in Figure R-3, inhibition of proliferation in comparison to DMSO controls starts to be visible as early as 20 hours after the start of treatment, some effects are dependent on the cell cycle, and become detectable only in thight kinetics.

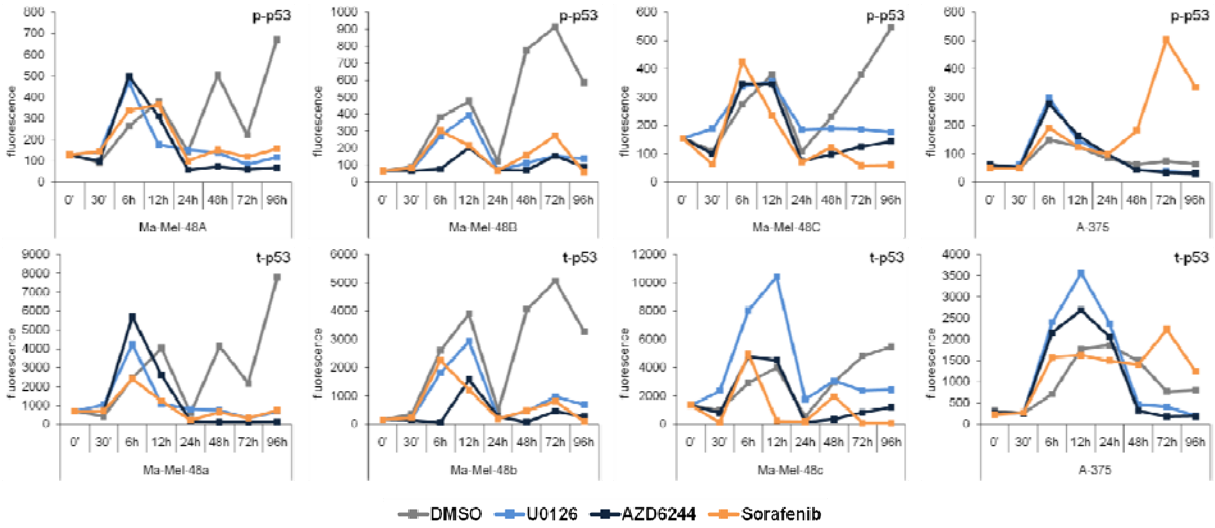

Figure R-17 - Phosphorylated and total amounts of p53 are tightly connected and modulated with MAPK inhibitors. Cells have been treated with U0126 [10µM], AZD6244 [3µM] and Sorafenib [5µM] for 96 hours and subjected to phosphoplex analysis.

All Ma-Mel-48 cells show a similar regulation of p53 in response to treatment with MAPK inhibitors. During the first 24 hours of treatment, a transient increase in both, phospho- and total-p53 levels is detectable that can be somewhat stronger in the presence of inhibitors. After 24 hours, phosphorylated levels in DMSO controls further increase substantially. Remarkably, this effect is not seen in MAPK inhibitor treated samples. In this setting, the comparison of phophorylated and total protein levels shows a strong correlation for all three cell lines. In contrast to Ma-Mel-48 cells, A-375 cells shows a different behavior. After 24 hours, only Sorafenib-treated cells show a strong upregulation of p53 phosphorylation and to a lesser extent total p53 too.

***In conclusion**, the analysis of Phosphoplex data shows a strong impact of MAPK inhibition on various pathways, which play central roles in the control of cell fate, like p53, Akt, and JNK. In addition, the use of MAPK inhibitors has to be thoughtfully evaluated before treatment, on the one hand because the inhibitors U0126, AZD6244 and Sorafenib showed different effects on the regulation of phosphorylated and total amounts of proteins, which in conclusion means that the choice of inhibitor does matter - even small differences in mechanisms of action or target specificity can lead to large changes. On the other hand, the target cells have to be evaluated as well, because the effects of treatment varied between cell lines, even if the genetic heterogeneity is as limited as in Ma-Mel-48 cells. Our approach also reveals the need for analysis of immediate as well as long-term effects of MAPK inhibition.*

This comprehensive approach of pathway analysis underlines the interconnectivity of the MAPK pathway with JNK, PI3K/Akt and p53 signaling. Even specific inhibition of single proteins, as seen with U0126 and AZD6244, has widespread effects on cell signaling, which have to be taken into account.

R.2.2.5 Western Blots confirm Phosphoplex findings

Phosphoplex assays are a newly established and improved method to analyze cell signaling. In order to confirm our Phosphoplex findings, we performed Western blots from the same lysates which have been used for Phosphoplex analysis. We picked A-375 cells and p53 protein to test the reproducibility of our findings, and tested all lysates from 0-96 hours in response to MAPK treatment. Figure R-18 shows that the results of Western blot (Figure R-18A) and phosphoplex analysis (Figure R-18B) correlate well.

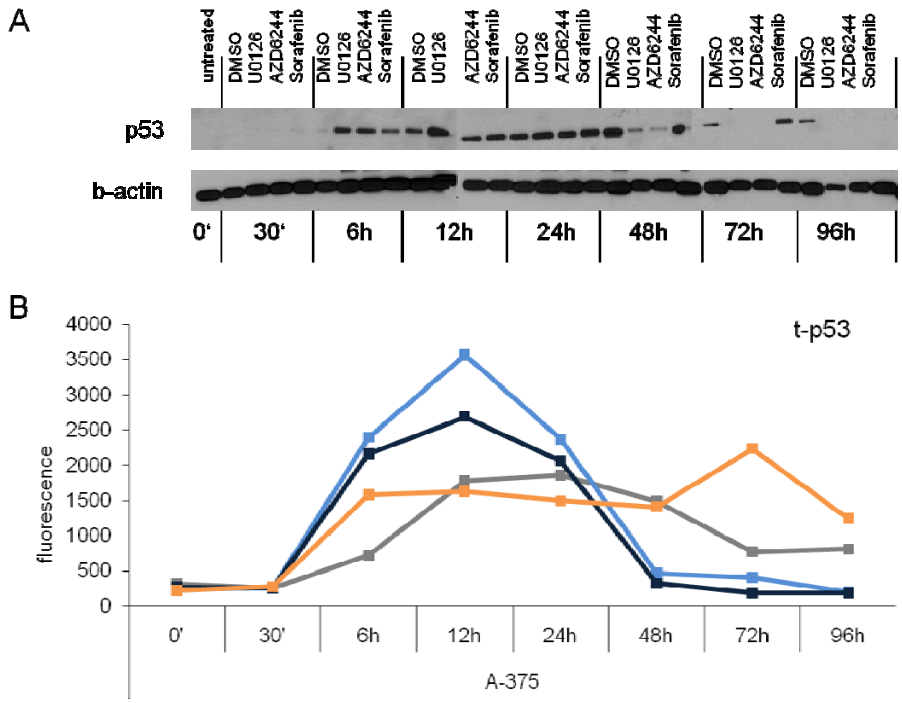

Figure R-18 - Western Blot analysis confirms Phosphoplex analysis of total p53. The same lysates which have been used in Phosphoplex analysis were used to confirm our results in Western Blot experiments. The comparison of Western Blot and Phosphoplex analysus reveals a strong correlation between both methods. Phosphoplex analysis proves to be more sensitive and quantifiable than Western Blot measurements.

Phosphoplex analysis shows low fluorescence values for p53 within 30 minutes. Accordingly, there is no detectable p53 in Western Blot analysis at this timepoint. After 6 hours we see increases in p53 content for U0126, AZD6244 and Sorafenib treated cells, and only a slight band of p53 in the DMSO control sample. This fits nicely to Phosphoplex analysis, with low amounts for DMSO, and higher amounts for MAPK inhibitor treated cells. The correlation of Western Blot and Phosphoplex data remains tight over the course of 96 hours. At 12h and 24h, a high amount of p53 is detectable in all 4 samples. After 48 hours, until the end of treatment, p53 is reduced in U0126 and AZD6244-treated samples, and even increased in the Sorafenib-treated sample, compared to DMSO. In Western Blots, p53 becomes undetectable from 72 hours to 96 hours in inhibitor-treated cells. DMSO levels of p53 remain stable in Western Blot until the end of treatment; Sorafenib is still detectable after 72 hours, but not anymore at 96 hours of treatment.

***In conclusion**, the comparison of Western Blot and Phosphoplex analysis shows a perfect correlation of protein levels for all samples and timepoints. Phosphoplex analysis is more sensitive than Western Blot analysis, and thus, even slight differences between the samples are easily visible and quantified*.

R.3 MAPK inhibition influences balance between apoptosis and autophagy regulation

P53, Akt and JNK play dual roles in the critical regulation of autophagy and apoptosis. P53, known as the guardian of the genome, controls cell-cycle progression and the induction of apoptosis in response to DNA damage, and other cell stress signals. It has also been shown that cytoplasmic p53 inhibits autophagy induction, whereas nuclear p53 does not [73]. Akt was shown to inhibit apoptosis, as well as autophagy, and JNK was shown to induce apoptosis, as well as autophagic cell death [88]. In addition, other proteins well-known for their role in regulation of apoptosis, e.g. Bcl-2, have been implicated in autophagy regulation.

The role of autophagy as such, is proposed to have cytoprotective functions, but in parallel, dysregulation of autophagy can lead to cell death, described as programmed cell death type II. These discrepancies are controversely and intensively discussed in current research in this field. As autophagy is currently limited by the established methods to quantifiy its activity, I wanted to develop an approach that allows the simultaneous monitoring of apoptosis and autophagy at single cell levels. I took advantage of the ImageStream System, which is a flow-based imaging cytometer. Like FACS analysis, it provides high content measurements with high statistical significance, and combines this with the advantages of single cell inspection in fluorescence microscopy.

R.3.1 Monitoring apoptosis with the ImageStream

The approach of monitoring apoptosis with the ImageStream system is based on DNA staining, and the occurrence of DNA fragmentation and nuclear condensation in response to induction of apoptosis, and has previously been established for the ImageStream [84]. Measurements of nuclear fragmentation correlated with secondary methods of detection of apoptosis over time, which indicated that it is also an early marker for apoptosis. I used this method to establish the quantification of apoptosis in A-375 cells, following treatment with Sorafenib, which induced apoptosis more efficiently compared to AZD6244 and U0126. Therefore, A-375 cells have been treated with DMSO and Sorafenib for 24 hours, and then analyzed with the ImageStream system.

Nuclear fragmentation (Bright detail intensity threshold) and nuclear condensation (area threshold) analysis of 10000 cells per sample identified only a small population of apoptotic cells

after DMSO treatment (Figure R-19A). With high-dose [20µM] Sorafenib treatment however, we observed a large shift in distribution towards apoptotic cells, with a total of 67%.

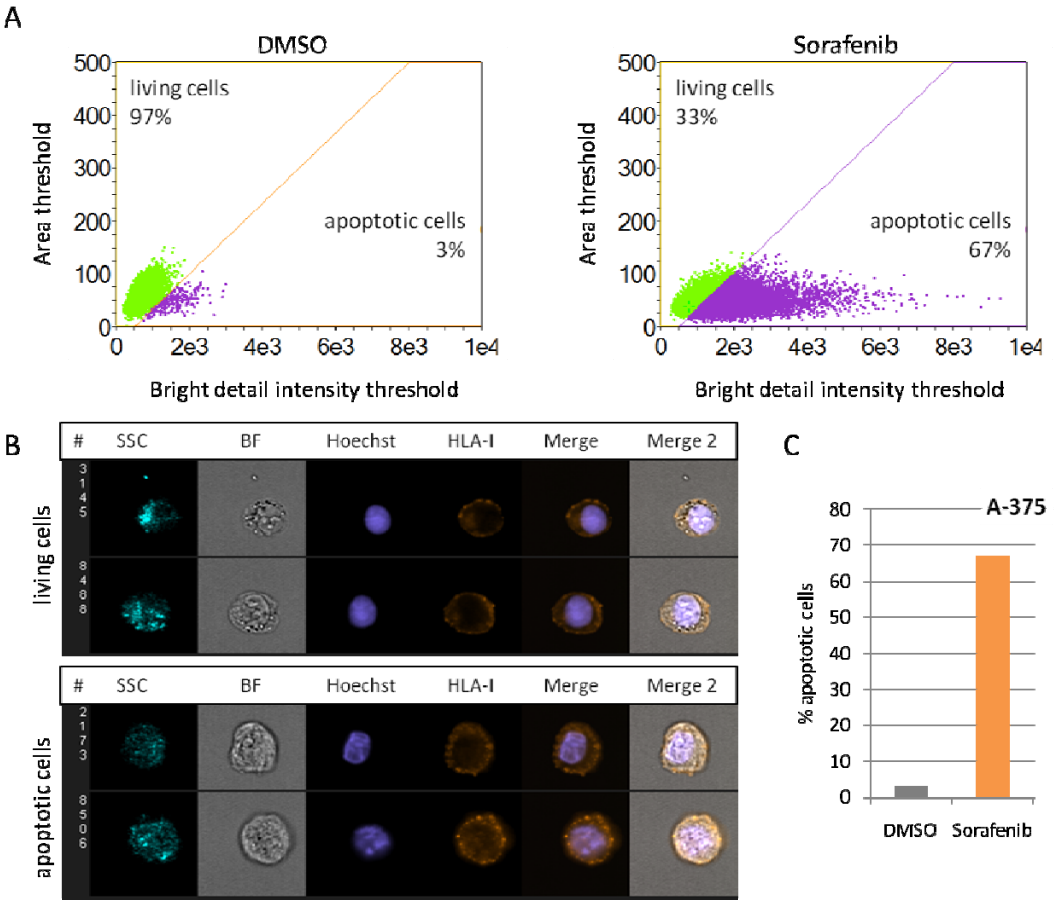

Figure R-19 - Identification of apoptotic cells based on nuclear condensation and nuclear fragmentation with the ImageStream. A total of 20000 cells have been collected per sample. Apoptosis was induced through Sorafenib (20µM) treatment for 24 hours. **A** Quantification of apoptotic cells based upon DNA staining with Hoecht 55432, and the detection of fragmented DNA and nuclear condensation. **B** Example pictures for living and apoptotic cells. Note the occoring DNA fragmentation in the Hoechst channel. Additionally to Hoechst, we have staind HLA class I. SSC= Side-ward scatter, BF= brightfield, Merge and Merge2 contain merges of Hoechst, BF and HLA class I channels. **C** Quantification of apoptotic cells upon treatment with Sorafenib (20µM) for 24 hours.

Corresponding pictures for living and apoptotic cells are shown in Figure R-19B, which clearly shows the extent of nuclear fragmentation in Hoechst-channel images. Also displayed are side scatter (SSC), brightfield (BF), HLA class I staining (HLA-I) as homogeneous surface staining, and merges of these channels. Figure R-19C shows a quantification of gated apoptotic cells for DMSO and Sorafenib treatment, showing more than 60% of apoptotic cells for Sorafenib treatment, and less than 5% for DMSO.

***In conclusion**, the ImageStream provides a new and improved method to identify apoptotic cells based on single cell analysis, but for large populations of cells*.

R.3.2 Monitoring autophagy with the ImageStream

Autophagy is a well-conserved response of eukaryotic cells to degrade portions of the cytosol and cytoplasmic organelles. During autophagy, they are sequestered in characteristic autophagosomes and delivered to lysosomes, where they are degraded by proteases, for the recycling of amino acids for instance.

Monitoring autophagy depends on the autophagosome-specific marker LC3 [59]. LC3 exists in two forms, the cytosolic LC3 I, and LC3-II, bound to autophagosome membranes. Upon induction of autophagy, LC3 I is converted to LC3 II by the attachment of Phosphatidylethanolamin (PE) and is then recruited to autophagosome membranes by the atg5-atg12 complex [89]. LC3 II remains attached to the membrane of autophagosomes until its degradation in the lysosome.

Commonly used methods to monitor autophagy are (i) Western blot experiments, which detect conversion of LC3I to LC3II; (ii) FACS which uses mean fluorescence of GFP-LC3 signals as a read-out of autophagic activity, and (iii) fluorescence microscopy through detection of GFP-labeled autophagosomes. These established methods all are insufficient in terms of either lack of specificity and quantification, or lack of statistical significance: Western Blot analysis is relatively unspecific in detection of the conversion of LC3, and hard to quantify [90] as shown in Figure R-20A. The addition of BafA1 leads to enhanced conversion of LC3-I to LC3-II, as seen in both, full medium as well as starvation medium. Under cumulative conditions in starvation medium we observed the strongest expression of LC3-II.

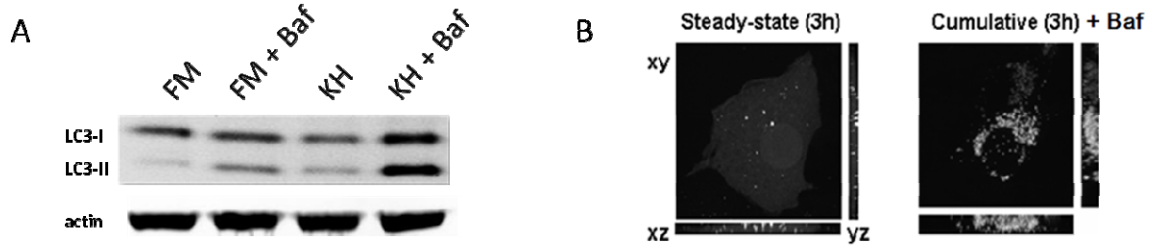

Figure R-20 - Comparison of established methodologies for autophagy monitoring. A Western Blotting shows the increased capture of LC3II under cumulative conditions (with Bafilomycin A1) after 3h, in full medium (FM) as well as starvation medium (KH). **B** High resolution fluorescence microscopy visualizes GFP-LC3 under starvation conditions for 3h. Notice the large increase of LC3-GFP dots under cumulative conditions. Western Blots and fluorescence microscopy were performed in the lab of N.R. Brady (Bioquant, Heidelberg).

FACS analysis provides statistical significance due to the large number of analysed cells but lacks specificity, because it does not provide any spatial information in the cellular distribution of the GFP-LC3 signal. In addition, both methods suffer from the finding that population average analysis is unable to account for occurring heterogeneity within cell populations in autophagic responses. Fluorescence microscopy provides the required sensitivity for specific detection of autophagosomes (Figure R-20B), but lacks statistical significance due to the limited number of

cells that can be analysed per sample and simultaneously. Analysis of fluorescence micrscopy involves manual inspection of acquired images and is therefore prone to subjectivity. In monitoring of autophagy, the challenge then was to develop a method which combines both needs: an integration of high-content analysis, and highly specific analysis on single-cell levels. We hypothesized that the ImageStream provides the possibility to establish such a new and improved method to quantify autophagy under different conditions with statistical significance.

In order to establish the method, the breast cancer cell line MCF7 was stably transfected with a vector encoding the GFP-LC3 fusion proteins. MCF7 cells do not carry activating Ras or Raf mutations, but possess a ^{E545K}PI3K mutation and are caspase-3 deficient. The activating PI3K mutation was confirmed in phosphoplex analysis, displaying constitutively high phosphorylated levels of Akt (Appendix figure 1). As in fluorescence microscopy, images acquired with the ImageStream show a cytosolic distribution of GFP-LC3 in non-autophagic cells, because under these conditions, LC3 is in its cytosolic LC3-I form. Upon induction of autophagy, for instance by starvation, LC3-II is recruited to autophagosomal membranes and then appears punctuated (compare Figure R-21). The amount of LC3-II is closely related to the number of autophagosomes, serving as a good indicator of autophagosome formation. Following fusion of autophagosomes with lysosomes, LC3-II is degraded and additionally, acidification in autolysosomes leads to an early quenching of the GFP signal, so the interpretation of results can be difficult [90]. Lysosomal inhibitors, e.g. Bafilomycin A1, inhibit the degradation of autophagosomes and therefore the loss of the GFP-LC3-II signal, but leaves LC3-I unaffected. The comparison of steady-state conditions (without lysosomal inhibition) and cumulative conditions (addition of Bafilomycin A1) is widely accepted as necessary for the quantification of true autophagic flux [60].

We analysed MCF7 GFP-LC3 cells under steady-state and cumulative conditions in full medium, as well as starvation medium in order to set up an automated detection of GFP-LC3 spots within cells. For each sample, we collected 10000 cells. Based on the manual inspection of cells with GFP-labeled autophagosomes, we created a “spot mask” to objectively detect autophagosomes. Based on our settings, measurements of 0 to 40 spots per cell, for full medium and starvation medium, under steady-state and cumulative conditions were obtained. Example pictures of cells and the application of the spot mask are shown in Figure R-21A. These findings underline the heterogeneity of autophagic responses within a population of cells, which is ignored using population average analyses like Western Blots and simple FACS analysis. In order to account for this heterogeneity, subpopulations of autophagic activity were defined: First, we gated on cells with 0-4 spots which show a rather cytosolic distribution of GFP-LC3 and therefore LOW autophagic activity. Second, we gated on cells with 5-12 spots, which show increased spot formation alongside a large decrease in cytosolic GFP-LC3 expression and therefore MEDIUM autophagic activity. Third, we defined a population of cells with HIGH levels of autophagic activity,

comprising cells with more than 12 spots, which show no more cytosolic GFP-LC3 expression. Figure R-21A shows respective pictures for each subpopulation, and Figure R-21B shows the gating of the respective populations.

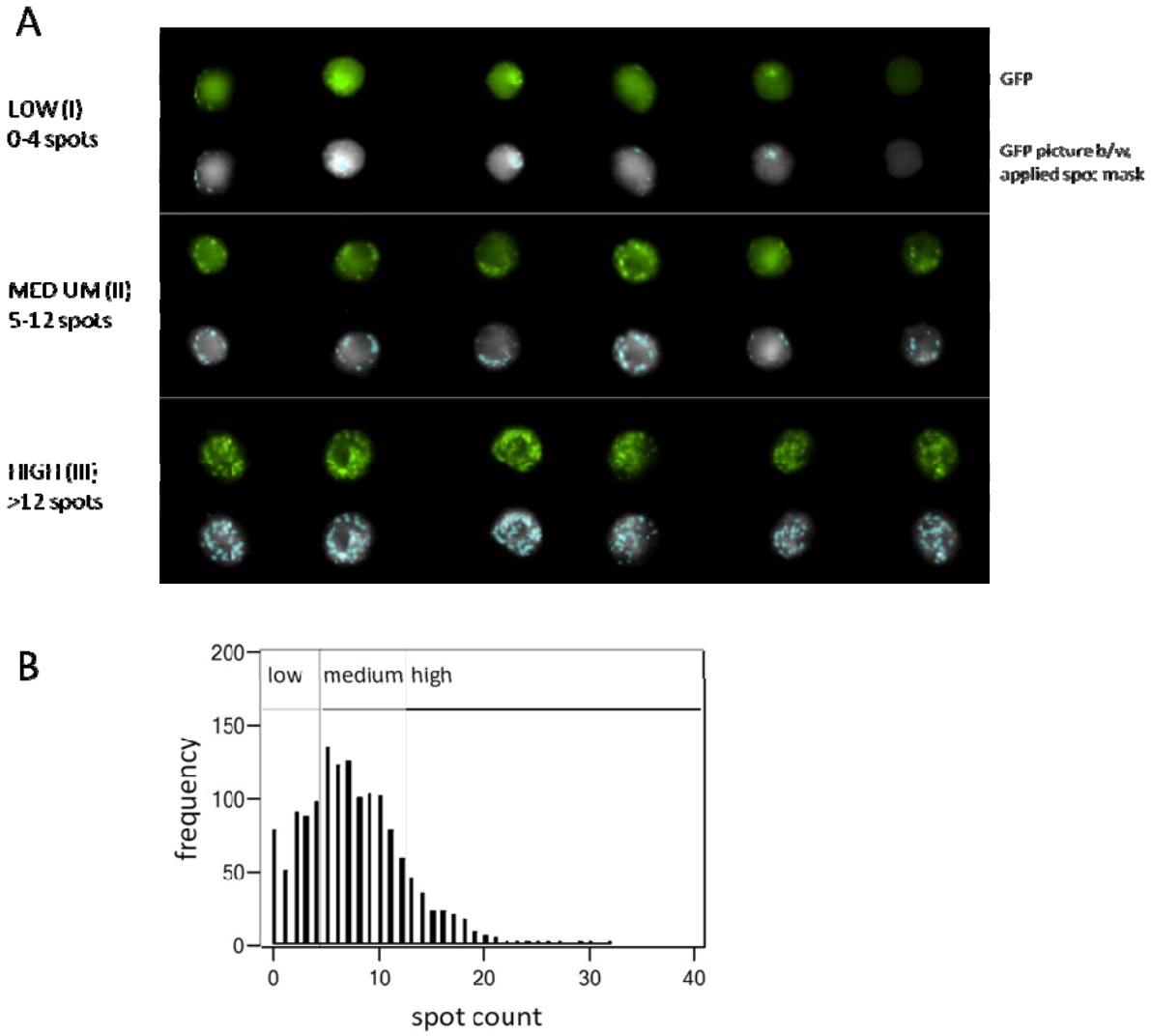

Figure R-21 - Example pictures of MCF7 GFP-LC3 cells showing LOW, MEDIUM and HIGH autophagic activity. A Shows MCF7 GFP-LC3 fluorescent cells, after 3h starvation under cumulative conditions. The response is heterogenic, and categorized in subpopulations of low, medium and high activity. **B** Definition of subpopulations, according to spot count numbers.

The defined subpopulations were used to further analyze the autophagic response of MCF7 GFP-LC3 cells, and introduce the metric of “autophagic flux”. After 3 hours in starvation medium and steady-state conditions (w/o BafA1), 73% of cells belong to the population of low activity, 26% to medium, and 1% to high autophagic activity (Figure R-22A). With the addition of BafA1, which inhibits the degradation of newly formed autophagosomes, the subpopulation distribution shifts accordingly: Only 22% of cells show low activity, 63% of cells show medium activity and 15% of

cells fall into the gate of high activity. The corresponding results for full medium are displayed in Figure R-22C.

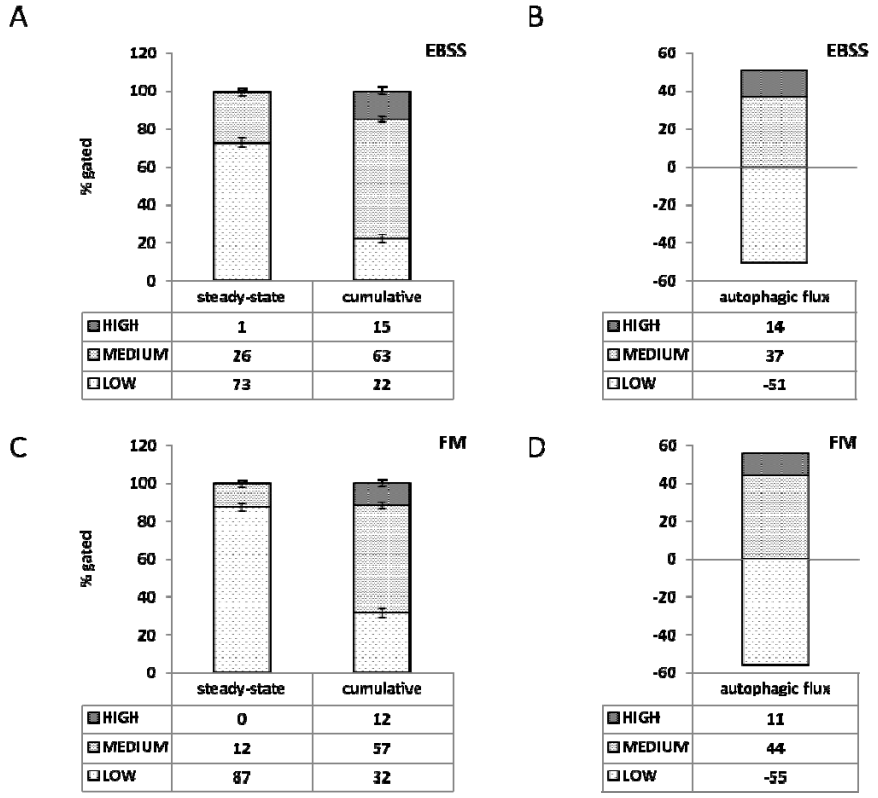

Figure R-22 - Subpopulations of autophagic activity shift under cumulative and steady-state conditions. MCF7 cells were cultured for three hours in starvation medium (A and B) or full medium (C and D) under steady-state and cumulative conditions. Autophagic flux was calculated from the substration of steady-state levels from cumulative levels for each subpopulation, integrating both conditions (B and D).

With measurement of steady-state as well as cumulative conditions, autophagic flux can be calculated by substracting steady-state from cumulative conditions for each subpopulation (Figure R-22B and D). This integration of steady-state and cumulative conditions leads to values of -51, 37 and 14 (low, medium and high) for EBSS, and -55, 44 and 11 for full medium.

The resolution of the first-generation ImageStream is 0.5µm^2 per pixel. The size of autophagosomes varies between different cells, with values ranging from 150nm to 1µm [91]. Therefore it is possible, that the software detects clusters of autophagosomes as single spots, because of insufficient resolution. Our method was further improved by taking into account the size and intensity of detected spots through the introduction of the secondary metrics “normalized spot intensity” and “normalized spot area”. They are normalized at the single cell level, by calculating the ratio of “spot area/intensity” and “cell area/intensity”. I created a tight object mask, based on the brightfield signal of the whole cell, to comprise the size of the cell. The GFP intensity and the area of this mask was calculated as “area object” and “intensity object”. The same was calculated for the spots within a cell, named “area spots” and “intensity of spots”.

"Normalized spot area" is the area of spots divided by the area of the object, and "normalized spot intensity" calculates as the intensity of spots divided by the intensity of the object. These secondary metrics can be additionally used to describe and analyze autophagic responses for each subpopulation, as shown in Figure R-23.

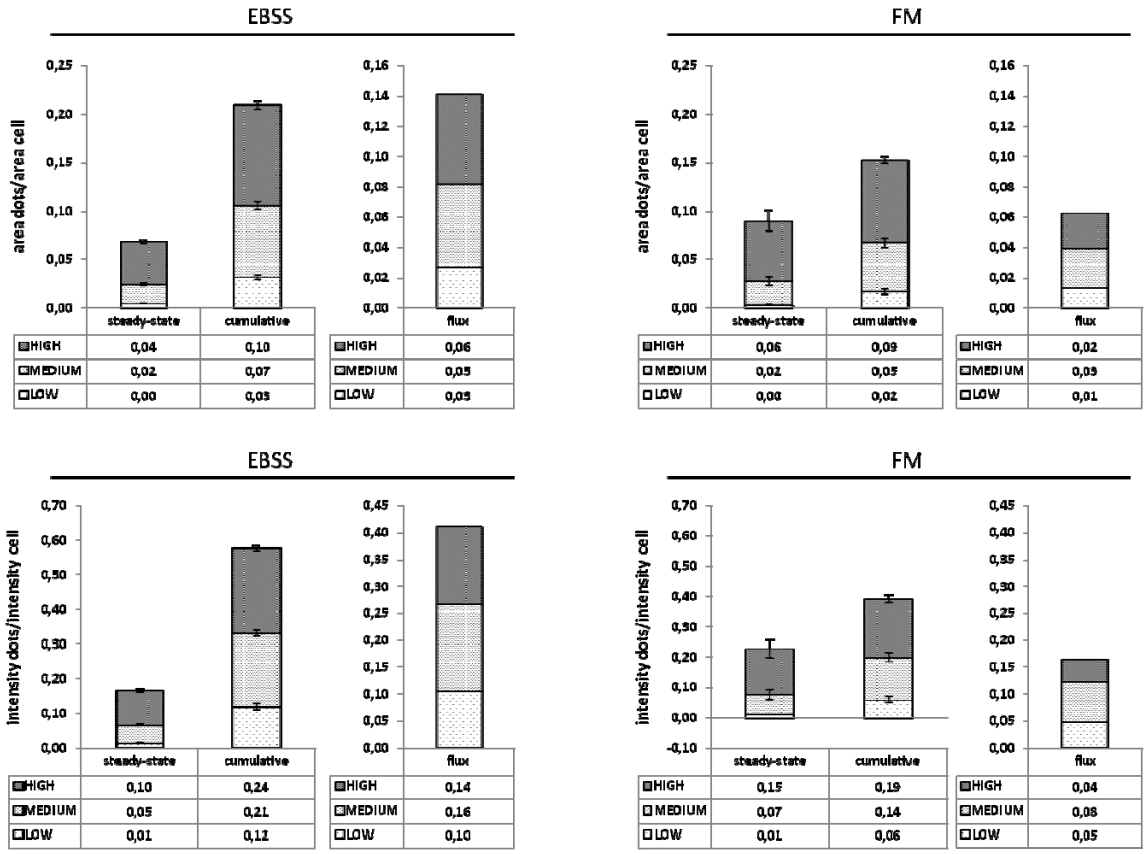

Figure R-23 - Normalized area and intensity support spot detection analysis. Secondary metrics account for the relative size and intensity of detected GFP-LC3 spots, to further characterize the autophagic response.

"Normalized spot area" shows large increases from steady-state to cumulative conditions, for EBSS as well as FM. (Figure R-23, A). The difference between basal autophagy (FM) and starvation-induced autophagy (EBSS) displays as a 2-fold increase in total normalized area, best seen with the comparison of flux between EBSS (0,03 – 0,05 – 0,06) and FM (0,01 – 0,03 – 0,02). "Normalized spot intensity"-analysis underlines these findings. (Figure R-23, B)

Valid detection of autophagosomes depends on the specificity of the GFP signal to LC3, because unspecific GFP fluorescence could lead to false-positive detections of autophagosomes. In order to validate my analysis of autophagic activity, MCF7 GFP-LC3 cells were treated with the PI3K inhibitor Wortmannin [92]. Wortmannin-mediated inhibition of PI3K has been shown to inhibit autophagy [93] and should therefore decrease spot numbers and lower the values of normalized

spot area and intensitiy. Respective cells were treated for 3h in full medium and starvation medium, under steady-state and cumulative conditions with Wortmannin [50µM] (Figure R-24).

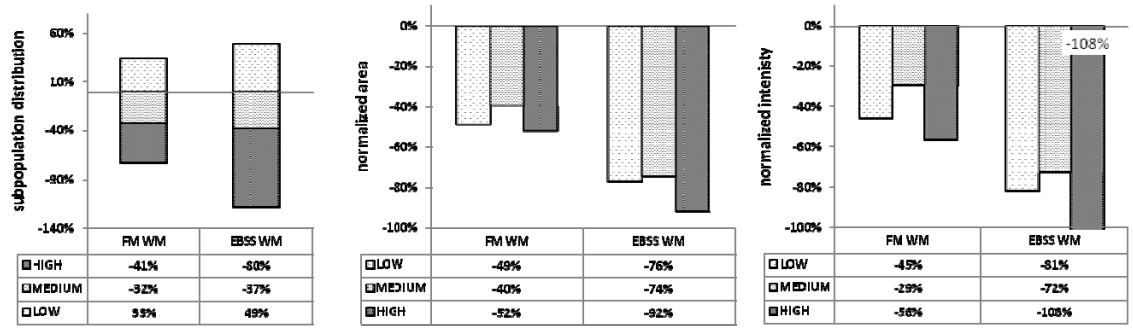

Figure R-24 - ImageStream analysis shows inhibition of autophagy following Wortmannin treatment. The data is summarized with the depiction of % changes between autophagic flux values of Wortmannin-treated MCF7 cells and control samples. From left to right, quantifications of spot count analysis, normalized area and normalized intensity. All conditions and metrics show large inhibiting effects of Wortmannin treatment.

The effects of PI3K-inhibition are depicted as percent changes. The percent changes are based on autophagic flux measurements to integrate cumulative and steady-state conditions, and the change of Wortmannin treatment is calculated relative to control treatment (same conditions without Wortmannin). Subpopulation distribution shows substantial decreases in the medium and high subpopulations and a strong increase in the low subpopulation in starvation medium (EBSS) as well as in full medium (Figure R-24). Wortmannin treatment shifted subpopulation distributions towards low and medium, showing a strong inhibition of autophagic activity. Normalized area and normalized intensity emphasize this inhibition, by displaying large decreases for all subpopulations and treatments.

***In conclusion**, we have established a new ImageStream-based method to monitor autophagy. It combines large sample sizes with the identification of autophagic activity on single-cell levels. After manual inspection of cells, we were able to set up an objective automated analysis of autophagic activity, using the definition of spot masks to identify autophagosomes and a count feature. The definition of subpopulations for low, medium and high autophagic activity based on autophagosome numbers, captures the observed amount of heterogeneity in autophagic responses. Measurements of steady-state and cumulative conditions allow for the calculation of autophagic flux. This integrated metric is a valuable read-out for true autophagic activity*.

R.3.2.1 Identification of JNK and NFkB as key regulators of autophagy

The ImageStream-based method is superior to common methods of autophagy monitoring. Therefore one of the goals of my thesis was to define the roles of JNK, NFkB, Bcl-2 and TNFα in the regulation of autophagy by using this technology. These proteins are controversely discussed in autophagy research. Therefore, small molecule inhibitors were selected to target JNK (SP600125), NFκB (QNZ) and Bcl-2 (HA141), or to activate TNFRI signaling through the addition of TNFα. To focus on starvation-induced autophagy, and immediate effects of pathway perturbations, MCF7 GFP-LC3 were cultured cells for 3h in starvation medium in the presence of the respective drugs. Surprisingly, addition of TNFα had no effect on subpopulations distributions, indicating that the TNFRI signal alone, in not one of the driving forces in autophagy induction of these cells. In contrast, inhibition of JNK or NFκB resulted in striking shifts in subpopulation distributions, that were clearly detectable under cumulative conditions of starvation-induced autophagy: Inhibition of JNK by SP600125 leads to an increase in the high activity spot count population (16%→25%), and a corresponding decrease in the low activity spot count population (22%→15%; both Figure R-25 - cumulative). Medium populations remain at ~60%. In contrast to JNK inhibition, NFkB inhibition has a strong inhibitory effect on autophagy, that becomes nicely visible under cumulative conditions. The low spot count activity population increases to 52%, from 22% under control conditions, which is accompanied by decreases in medium and high activity populations. Similar to TNFα treatment, Bcl-2 inhibiton had only minor effects.

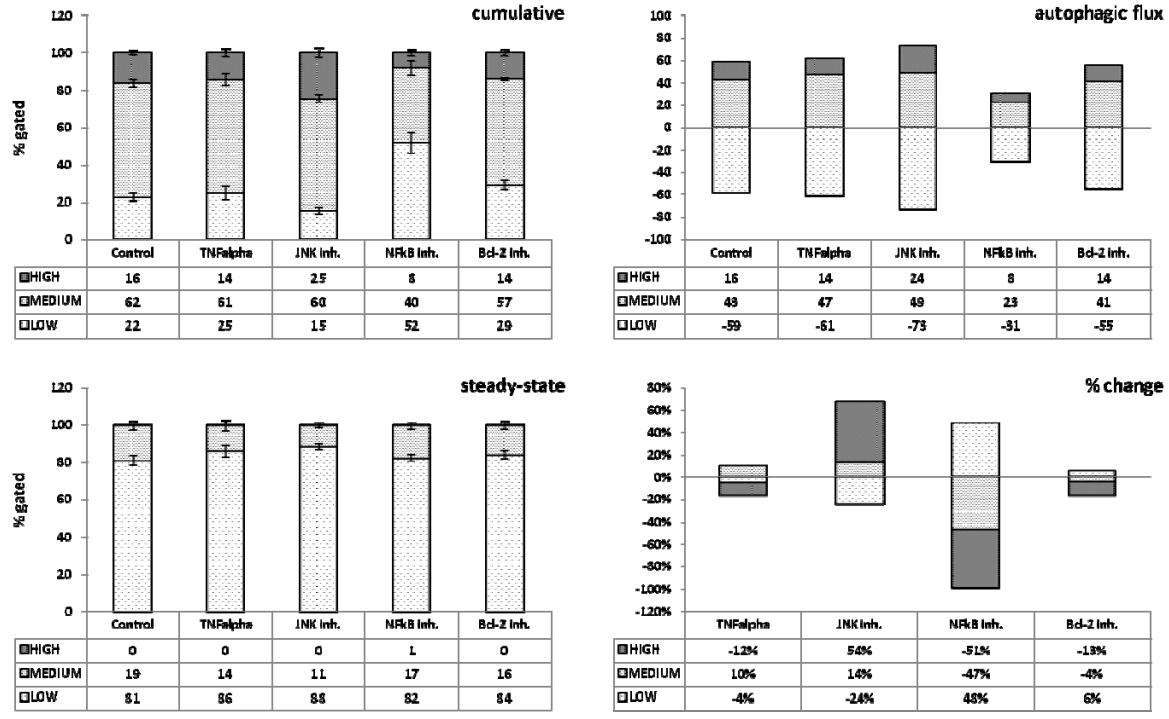

Figure R-25 - Pathway perturbation reveals autophagy regulation under starvation conditions. The regulative potential of TNFR, JNK, NFκB and Bcl-2 was evaluated in MCF7 GFP-LC3 cells, during 3h treatment periods in starvation medium. The data summarizes at least 5 experiments for each condition. NFκB inhibition leads to strong inhibition of autophagy, JNK inhibition induced autophagy above control conditions.

Steady-state conditions (w/o BafA1) show only minor changes in subpopulation distributions for all treatment conditions, underlining the need for careful evaluation of cumulative and steady-state conditions to assess regulated autophagic activity. The high amount of “low” detected activity in steady-state conditions, also assures, that increased numbers of spots under cumulative conditions are not due to a block in the degradation of autophagosomes, as this would be also visible in steady-state conditions. Because of the constant levels in steady-state measurements, the calculation of autophagic flux and corresponding percent changes of treatment analysis primarily reflects the changes observed under cumulative conditions: It shows a 54% increase in the high spotcount subpopulation with the JNK inhibitor, and a 48% increase in the low spotcount subpopulation with inhibited NFkB.

In conclusion *the ImageStream-based method was useful to clarify the role of JNK, NFκB, TNFRI and Bcl-2 in autophagy in MCF7 breast cancer cells. Surprisingly, neither TNFRI nor Bcl-2 seem to play a major role in the regulation of starvation induced autophagy, since addition of TNFα, or inhibition of Bcl-2 had no significant effect on the subpopulation distribution. In sharp contrast, JNK was identified as a negative regulator of autophagy, because JNK-inhibition increased autophagic activity under starvation conditions. Remarkably, NFκB seems to be required for the induction of autophagy since addition of an NFκ inhibitor suppressed autophagy substantially*.

R.3.2.2 Sorafenib inhibits autophagy in MCF7 GFP-LC3 cells

The MAPK pathway has been proposed to be tightly connected to autophagy regulation. Highly active ERK signaling has been reported to disrupt autophagosome formation [94]. On the contrary, it was recently shown that hyperactivated ERK signaling, as a consequence of BRaf mutation, leads to induction of autophagy and inhibition of melanoma growth. [77]. To clarify whether these discrepancies arise from the different mutation status in tumor cells, the ^{V600E}BRaf-mutated A-375 melanoma cells were compared to PI3K-mutated MCF7 cells. Therefore, a stably GFP-LC3 transfectant of A-375 was established and analyzed with the ImageStream-based approach.

As seen in Phosphoplex analysis with BRaf-mutated melanoma cells, BRaf or MEK perturbations also led to changes in phosphorylation of Akt, p53 and JNK pathways which are all involved in the regulation of autophagy as well as apoptosis. In order to see whether PI3K-mutated MCF7 cells are sensitive to BRaf or MEK inhibition with respect to autophagy induction, these cells were treated with Sorafenib, U0126 and AZD6244 and analyzed with the ImageStream. The effects on phosphorylation status of MEK, ERK, Akt and p53 were analyzed by phosphoplex experiments that confirmed the constitutively active phospho-Akt status and inhibition of MEK/ERK phosphorylation following treatment with MAPK inhibitors in MCF7 cells (Appendix figure 1).

MCF7 GFP-LC3 cells are caspase-deficient and were therefore analysed for autophagy only, not for the induction of apoptosis. To analyze the effects of MAPK treatment on autophagic activity, MCF7 GFP-LC3 cells were treated for 24 hours with MAPK inhibitors and controls in full medium. The evaluation of steady-state conditions in Figure R-26 shows no autophagic activity for all treatments, indicating that MAPK inhibition does not affect the process of autophagy. Under cumulative conditions however, a substantial increase in the low activity spotcount population of Sorafenib-treated cells became visible. Compared to full medium only, the low population increases from 63% to 95% gated cells, and accordingly the high spotcount population virtually disappears.

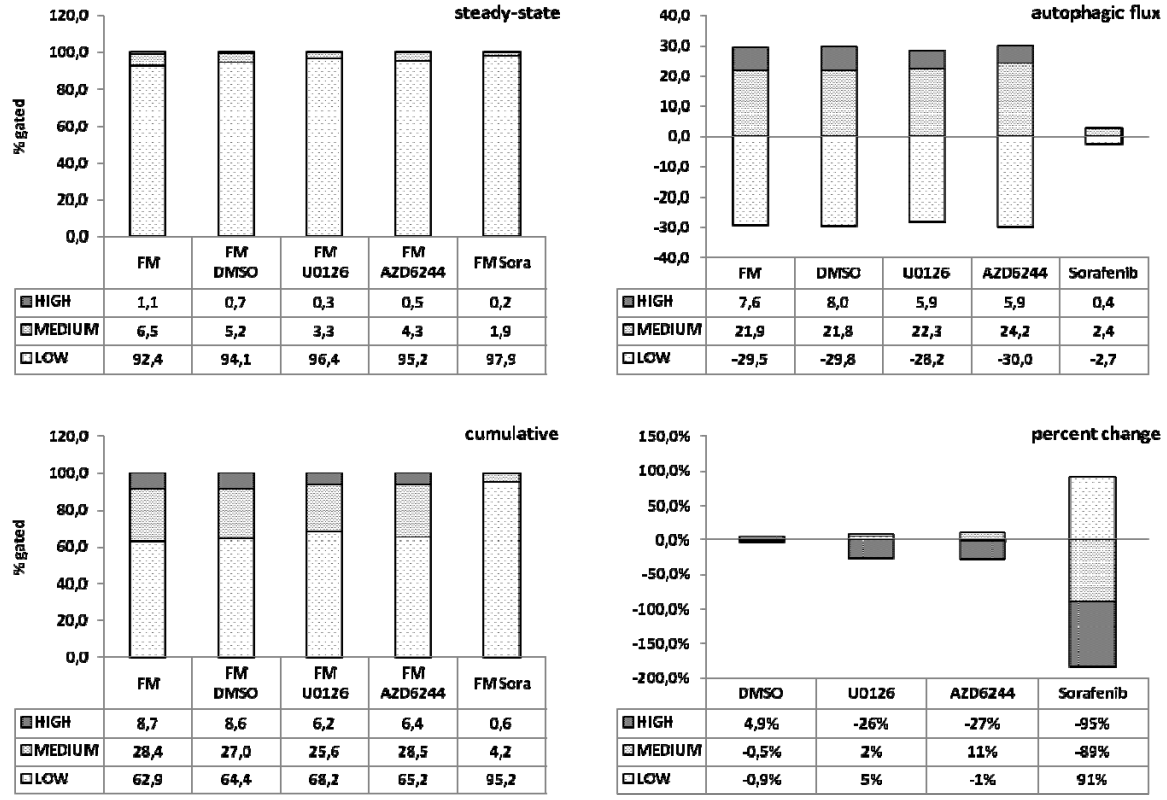

Figure R-26 - Sorafenib inhibits autophagy, unlike U0126 and AZD6244. MCF7 GFP-LC3 cells were treated for 24 hours in full medium with the MAPK inhibitors U0126 [10µM], AZD6244 [3µM] and Sorafenib [5µM]. The analysis reveals strongly inhibiting effects of Sorafenib on the induction of autophagy.

While U0126 and AZD6244 had no effect on autophagic flux, Sorafenib suppressed autophagy completely. Along this line, the calculated percent change analysis shows a 91% increase in the low subpopulation of Sorafenib-treated cells, accompanied by 89% and 95% decreases in medium and high subpopulations respectively. This strong inhibiting effect of Sorafenib on autophagy by far exceeds the effects of NFkB inhibition observed before.

In conclusion *– U0126 and AZD6244 had no significant effects on subpopulation distribution of autophagic activity. In contrast, Sorafenib completely inhibited the formation of autophagosomes, exceeding levels of inhibition we observed before with NFκB inhibitors.*

R.3.2.3 MAPK inhibition in melanoma cells shifts the balance between apoptosis and autophagy

One of the most important differences to the MCF7 system is the constitutively active MAPK pathway in BRaf-mutated melanoma A-375 cells. In an effort to simultaneously quantify apoptosis and autophagy, I combined the ImageStream-based approaches to monitor autophagy and apoptosis. First, the responsiveness of stably transfected A-375 GFP-LC3 to starvation-incuced autophagy and specificity of GFP-LC3 were tested, and the achieved results of subpopulation distributions showed to be comparable to MCF7 GFP-LC3 cells (data not shown).

In order to evaluate the immediate effects of MAPK-inhibitor treatment, A-375 GFP LC3 cells were cultured for 3h in full medium and starvation medium, under steady-state and cumulative conditions and in the presence of MAPK inhibitors. Figure R-27 shows the impact of MAPK inhibitor treatment on the regulation of autophagy. Steady-state conditions of starvation-induced autophagy (EBSS) show slight increases in the medium population of U0126 (22%), AZD6244 (27%) and Sorafenib (31%) compared to DMSO treatment (17%). In cumulative conditions and starvation medium, we observe an increase in the low population of cells with Sorafenib treatment (26,6%) compared to DMSO (20,2%), along with a decrease of the high population.

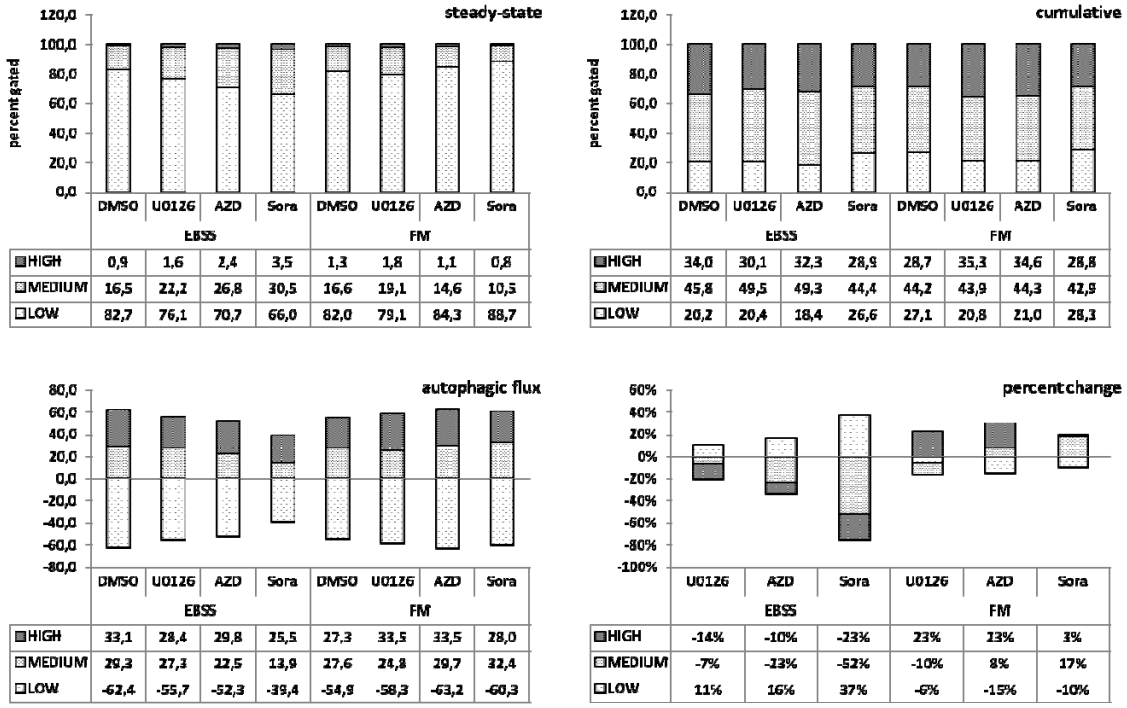

Figure R-27 - In A-375 GFP-LC3 cells, Sorafenib shows inhibiting effects on autophagy under starvation conditions within 3 hours. Analysis of MAPK inhibition on the induction of autophagy in A-375 GFP-LC3 cells, in full medium as well as in starvation medium. Cells have been treated for 3h with U0126 [10μM], AZD6244 [3μM] and Sorafenib [5μM].

The calculation of autophagic flux and the corresponding calculation of percent change of treatment shows that in starvation medium, Sorafenib has the strongest impact on autophagy regulation. The low population increased by 37%, while the medium population decreased by 52%, and the amount of high cells was recuced by 23%. Notably, under full medium conditions, 3 hours of treatment with MAPK inhibitors did not result in any immediate effects on autophagy regulation.

Simultaneously to the analysis of autophagy, the amount of apoptotic cells in response to MAPK treatment was quantified by DNA staining with Hoechst, and occurring DNA fragmentation and nuclear condensation. Figure R-28A shows that under steady-state levels (fully functional autophagy), starvation for 3 hours induced apoptosis to a limited extent in all samples. Among all inhibitors, Sorafenib showed the highest amount of apoptotic cells (14%). In full medium under steady-state conditions, we observed only background levels of apoptotic cells, indicating that in full medium the cells protected against the immediate toxic effects of MAPK inhibition.

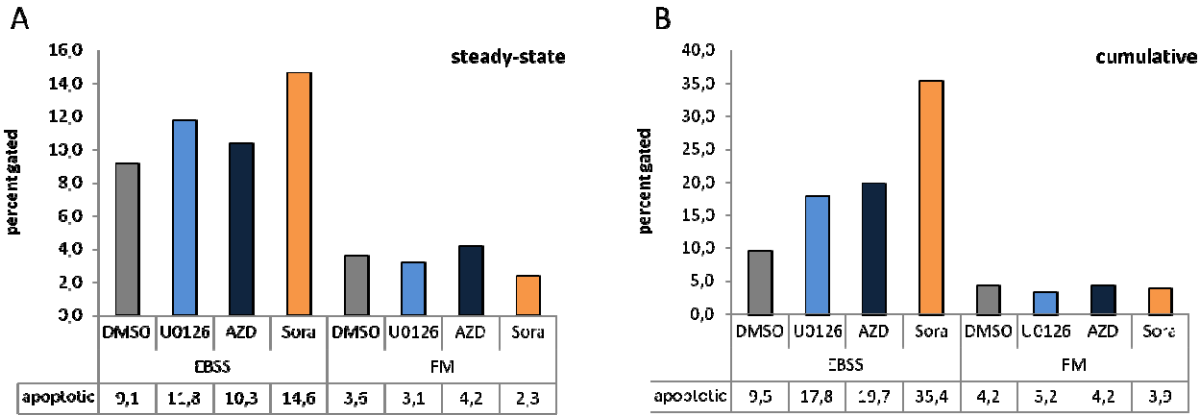

Figure R-28 - Sorafenib treatment induces apoptosis after 3 hours, esspecially under cumulative conditions. Simultaneous to the analysis of autophagy, A-375 GFP-LC3 cells were analyzed for the induction of apoptosis with the ImageStream. In starvation medium, under steady-state conditions we detected 14% apoptotic cells in Sorafenib samples. Under cumulative conditions, this amount increased to 35%. In full medium, we observed less than 5% apoptotic cells in steady-state as well as cumulative conditions.

However, in starvation medium under cumulative conditions (Figure R-28B), an increase in apoptosis induction was observed. While DMSO treated samples showed comparable amounts of apoptotic cells, U0126 and AZD6244 treated samples showed somewhat increased amounts of 17,8% and 19,7% respectively. Sorafenib treated cells, showed an even stronger induction of apoptosis with 35,4% apoptotic cells, compared to 9,5% in DMSO-treated control cells. In full medium samples, only background amounts of apoptotic cells were detectable, similar to steady-state conditions. For the analysis of long-term effects of MAPK inhibition, I focused on full medium conditions only, because most cells died from starvation conditions within 24 hours. Additionally, Sorafenib was selected for this analysis, because it was implicated twice as a strong

regulatior of autophagy. As a positive control for autophagic activity, the DMSO- and Sorafenib-treated cells (24 hours), were compared with a 3 hour starvation medium control sample.

As seen in Figure R-29A, after 24 hours of treatment, Sorafenib in full medium achieves complete inhibition of autophagic activity in A-375 GFP-LC3 cells, whereby under cumulative conditions, the low population comprises 99,7% of cells. Since DMSO-treated cells show normal, basal levels of autophagic acitivty, the integration of steady-state and cumulative conditions reveals substantial differences between DMSO control and Sorafenib-treated cells, that are reflected in 100% changes for all subpopulations.

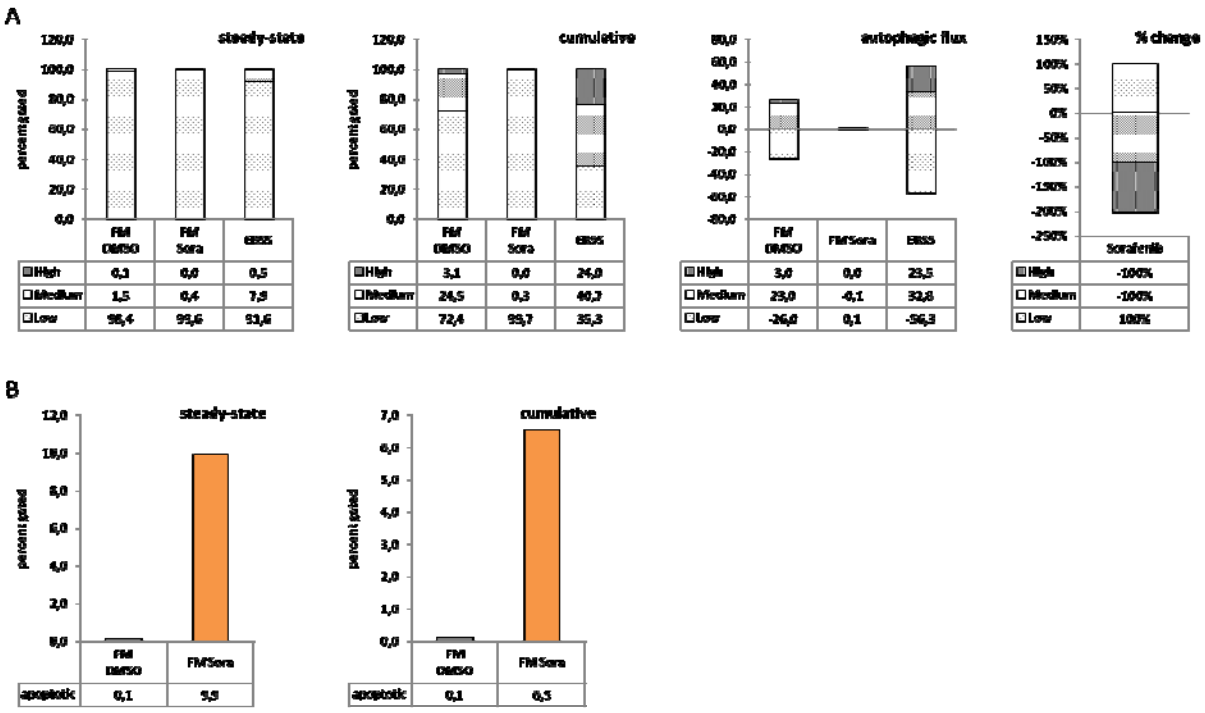

Figure R-29 - Within 24 hours of treatment Sorafenib achieves full inhibition of autophagic activity in A-375 GFP-LC3 cells in full medium. A-375 GFP-LC3 cells have been treated for 24h Sorafenib [5µM] and DMSO as a solvent control. EBSS samples were starved for only 3 hours as a positive control for autophagy induction. **A** Quantification of autophagy, reveals that Sorafenib completely inhibited autophagic activity upon 24h of treatment with Sorafenib. **B** Simultaneous quantification of apoptotic cells, shows largely increased amounts of apoptotic cells in comparison to DMSO-treated samples.

As shown in Figure R-29B, the parallel quantification of apoptosis by Hoechst staining revealed a strong induction of apoptosis following treatment with Sorafenib, in steady-state as well as cumulative levels. DMSO treatment showed only 0,1% of apoptotic cells in both conditions, which increased in response to Sorafenib treatment to 9,9% and 6,5% respectively.

***In conclusion**, we have identified Sorafenib as a strong inhibitor of autophagy, in MCF7 GFP-LC3 cells as well as in A-375 GFP-LC3 cells. In addition, Sorafenib treatment, induced a simultaneous strong induction of apoptosis in A-375 GFP-LC3 cells. Possibly, this underlines the cytoprotective function of autophagy. It seems that through inhibition of autophagy, the cells are more prone to undergo apoptosis. The dysregulation of autophagy and apoptosis implicates*

strong effects on cell fate in response to Sorafenib treatment. In contrast to Sorafenib, neither U0126 nor AZD6244 showed significant effects on the regulation of autophagy or induction of apoptosis.

D.Discussion

The frequently-mutated MAPK pathway in melanoma is a main focus in the search of therapeutic possibilities for metastatic melanoma patients. Several small molecule inhibitors have been developed to inhibit the MAPK pathway through inhibition of Raf or MEK. In an attempt to comprehensively analyze the effects of MAPK inhibition on melanoma cells, we have used U0126, AZD6244 (both MEK inhibitors) and Sorafenib (multi-kinase inhibitor with BRaf activity) for the treatment of melanoma cell lines. The major focus was on (I) cell surface molecule expression of melanoma cells involved in NK cell recognition, (II) the effects of treatment on cytokine/chemokine and growth factor secretion, (III) comprehensive analyses of cell signaling, and (IV) evaluation of the effects of MAPK inhibition on cell fate decisions regarding induction of apoptosis and autophagy.

D.1 Modulation of immune cell recognition following MAPK inhibition

The development of new inhibitors for MAPK inhibition usually involves tests in melanoma cell lines, as well as in preclinical mouse models. A commonly featured melanoma cell line is A-375, which carries the most frequent ^{V600E}BRaf activating mutation, and was therefore included in our set of melanoma cell lines. In contrast to A-375 cells, I included three primary melanoma lines, Ma-Mel-48a-c, which have been established from one patient over a timeperiod of one year, from different tumor sites. Ma-Mel-48a was established from a skin lesion, Ma-Mel-48b and -48c are both established from lymph node metastases. All three Ma-Mel-48 cells heterozygously carry the ^{G469R}BRaf mutation, which affects a region closest to the gate keeper domain in exon 11 of the BRaf gene.

The evaluation of these melanoma lines revealed a loss of HLA class I expression in Ma-Mel-48c cells in FACS and WB characterization, comfirmed through the detection of a mutation in β2-microglobulin in RT PCR (Figure R-1, and personal communication Annette Paschen, University Hospital Essen). In light of the evaluation of NK cell recognition of melanoma cells, Ma-Mel-48 cells provide three different cell lines with the same mutation of BRaf, identical genetic background, but different levels of HLA class I expression. Since HLA class I expression on target cells is the main mechanism of NK cell inhibition in theory, the loss of HLA class I expression in Ma-Mel-48c cells should render them more susceptible for NK cell recognition and killing. I have therefore been surprised by the finding that Ma-Mel-48c cells are not killed more efficiently by the highly cytotoxic NK cell line NK92 than Ma-Mel-48b cells (Figure R-2). Interestingly, highly HLA class I positive Ma-Mel-48a cells seemed to be the most resistant cells to NK92-cytotoxicity. This experiment underlined that loss of HLA class I alone does not guarantee increased NK cell cytotoxicity against melanoma cells. This observation was confirmed by independent experiments

and melanoma lines by Annette Paschen (University Hospital Essen). Besides inhibition, NK cell activation also depends on the expression of ligands for activating receptors. Since this set of melanoma cell lines has been killed with different kinetics and to different extents by NK92 cells, this suggests that they activate NK cells to different levels, which could be related to individual expression of NK ligands. It has to be considered however, that the NK cell kill measured with the xCELLigence system included a time frame of 30 hours, in contrast to immediate kill assays like chromium release assays or CD107a degranulation assays. Thus, killing of melanoma cells by NK92 cells is an evaluation of rather slow and late effects of NK cell recognition. Nevertheless, the analysis led to the hypothesis, that Ma-Mel-48 cells may have low levels of ligands for the activating NK cell receptors NKG2D and DNAM-1, the two most relevant NK receptors in melanoma [51]. This was indeed shown to be the case and will be discussed in the context of the MAPK-inhibition-mediated alteration of the DNAM-1 ligand CD155 in particular.

In order to visualize the effects of different MAPK inhibitiors on melanoma cell growth, we have made use of the xCELLigence system, which provides real-time quantification of tumor cell proliferation over time periods of several days. In these long-term proliferation tests, the four melanoma lines showed different susceptibility to MAPK-inhibition. I have detected reduced levels of proliferation in the presence of inhibitors in all cell lines, but A-375 cells were more susceptible to the treatment with U0126, AZD6244 and Sorafenib than Ma-Mel-48 cells (Figure R-3). This difference may be due to the different mutations of BRaf in A-375 and Ma-Mel-48 cells. A-375 cells carry the strongly activating ^{V600E}BRaf mutation, which has been shown to enhance BRaf activity 500-fold compared to wild-type [16]. The “gate-keeper-like” mutation ^{G469R}BRaf in Ma-Mel-48 cells in contrast, does not result in a comparably activated state of BRaf, which became visible by the lower starting levels of phospho-MEK (Figure R-10). This renders A-375 cells more sensitive to inhibition of MAPK signaling, as many studies have previously shown [95, 96].

Previous findings [24] as well as initial experiments have shown the need for short-term as well as long-term analyses of MAPK inhibition effects. Immediate events (30min-12h) primarily affect phosphorylation and stabilization of kinases, early events (12h-24h) rather affect cell cycle progression, and late events (>24h) affect surface expression of HLA and NK ligands. Hence, inhibition of the MAPK pathway in colon cancer cell lines revealed modulated cell surface molecule expression in response to treatment after 24 hours, depending on protein synthesis and transcriptional effects. Besides real-time monitored xCELLigence assays, I have therefore decided to analyze a defined kinetic, at the timepoints of 0’, 30’, 6h, 12h, 24h, 48h, 72h and 96 hours in an effort to comprehensively capture different effects of treatment.

The examination of various surface molecules on melanoma lines showed that CD155 was affected the most. The ligand for the activating NK cell receptor DNAM-1 was opposedly regulated: On the one hand by U0126 and AZD6244, which inhibited CD155 expression, and on the other hand by Sorafenib, which enhanced CD155 expression in Ma-Mel-48a and A-375 cells, and to a limited extent in Ma-Mel-48b cells (Figure R-4). This opposing alteration in CD155

expression became detectable at 24 hours with a further increased effect at 48, 72 and 96 hours, indicating that these changes are not directly connected to the immediate MAPK pathway inhibition. The occurrence of this effect in Ma-Mel-48a cells and A-375 cells hints that this effect is independent of the BRaf mutation. With MEK inhibitors going in one, and Raf inhibition going in the other direction, it seems more likely that the point of inhibition in the MAPK signaling cascade is critical for this effect. Additionally, Sorafenib, as a multi-kinase inhibitor, inhibits other targets besides Raf, which might be involved in expression of CD155. HLA class I expression is also affected in response to MAPK inhibition but in the opposite direction (Figure R-5). This modulation did not show to be important in the regulation of NK cell function. In addition, MICA/B and ULBP1-4, all ligands for the activating NK receptor NKG2D, showed very low expression levels in all melanoma lines, and have not been modulated in response to treatment.

Functional consequences of this CD155 and HLA regulation in response to MAPK inhibition were examined in CD107a degranulation asssays (Figure R-6). The over-expression of CD155 following Sorafenib treatment did not prove to further enhance NK cell activation, and showed levels of NK cell activation similar to DMSO control samples. But downregulation of CD155 led to reduced levels of NK cell degranulation, which implies the dependence of NK cell activation on the activating interaction between CD155 and the DNAM-1 receptor. The interaction of CD155 ligand expression on tumor cells and activation of NK cells through DNAM-1 signaling has been described before. A challenge of DNAM-1 deficient mice with transplantation of CD155-positive sarcoma cells, showed increased tumor development and metastasis in these deficient mouse-models, and increased occurrence of CD155 positive tumor cells. [97]. Further evaluation described the dependence of NK cells on activation through DNAM-1 for natural or cytokine suppression of tumor metastases, in the absence of NKG2D, or NKG2D ligands respectively. However, DNAM-1 was shown to be dispensable, if the tumor cells expressed ligands for NKG2D. [51]. Tumor cells have also been shown to downregulate DNAM-1 expression through chronic ligation [52]. In light of the importance of CD155 epxression for NK cell targeting of tumor cells, our results provide new insights with the modulation of CD155 by MAPK inhibition, which results in impaired NK cell-targeting of A-375 cells in the case of CD155 downregulation.

Taken together, our results reveal a special role of CD155 in the context of MAPK inhibition in melanoma cell lines, resulting in differential modulation of CD155, and the implications for NK cell cytotoxicity. This raised several questions: Why is CD155 in this context more crucial than HLA class I or NKG2D-ligand expression for NK cell cytotoxicity regulation? Why do the MEK inhibitors have opposing effects on the expression of CD155 compared to the BRaf inhibitor Sorafenib? CD155 (PVR) is an immunoglobulin-like molecule, and was first described as the cellular receptor for poliovirus [98]. CD155 has been reported to be involved in cell-cell adhesion via a heterophilic trans-interaction with nectin-3 and stimulation of this receptor has been shown to inhibit cell adhesion and enhance cell migration [99, 100]. CD155 is also over-expressed in many human cancers [100-102]. The cytoplasmic domain of human CD155α contains a conserved immunoreceptor tyrosine-based inhibitory motif (ITIM), which is tyrosine-phosphorylated by Src

kinase family members (SrcK), and recruits SH2-containing tyrosine phosphatase-1 (SHP-1) and SHP-2. SHP-2 is a likely mediator of the cellular functions of CD155, since dominant negative SHP-2 inhibits cell migration and FAK dephosphorylation after stimulation of cellular CD155 in fibroblasts [103]. Furthermore, it has been reported in 2004, that mouse Necl-5 enhances cell proliferation by serum- or PDGF-stimulation through the MAPK signaling pathway [104]. Prompted by the structural and functional similarities of Necl-5 with human CD155, Tokuyuki et al have shown that CD155 also signals to enhace the proliferation of Ras-mutated cells [105]. They demonstrated that expression of a truncated version of CD155, lacking the cytoplasmic domain (CD155ΔCP), resulted in decreased levels of serum responsiveness in ras3T3 and DLD-1 carcinoma cells, compared to wild-type CD155 expression. This suggests, that the cytoplasmic domain of CD155 containing an ITIM has a pivotal role in the growth support by CD155. Additionally, a dominant-negative effect of CD155ΔCP expression on cell proliferation in ras-mutated DLD-1 cells was observed and hence, they speculate that CD155 expression might enhance the recruitment of SHP-2, which may then somehow activate the MAPK cascade, to facilitate the enhancement of serum-stimulated cell growth (compare Figure D-1).

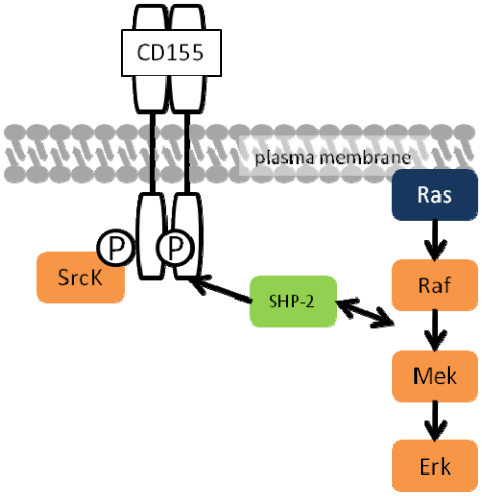

Figure D-1 - **A model of the signal transduction from CD155 upon ligation.** CD155 is tyrosine phosphorylated by members of the Src kinase family (SrcK) and recruits SHP-2 to the plasma membrane. In Ras-mutated cells, SHP-2 leads to enhanced cell proliferation through activation of the MAPK pathway.

On the basis of this model, I hypothesize that the connection of CD155 with MAPK signaling is the main reason for the divergent effects on CD155 expression patterns. Additionally, I suggest that the link between SHP-2 recruitment and MAPK signaling probably can be postulated to lie between Raf and MEK, since inhibition of these kinases results in opposing effects. The situation in Ras-mutated cells furthermore implies an important role for CD155 in the regulation of proliferation in melanoma cells. We are planning to further study the role of CD155 in cell growth in an extended set of melanoma cell lines, to further elucidate this situation.

Nevertheless, NK cell recognition of Ma-Mel-48 cells showed to be very low, probably due to the low expression of NKG2D and natural cytotoxicity receptor (NCRs) ligands in particular. Even fresh pre-activated NK cells showed only low CD107a subpopulations in corresponding degranulation assays (Figure R-7). These findings suggest, that the relatively frequent loss of HLA class I molecules can be covered by NK cell because of their higher anti-tumor activity in the absence of HLA class I. However simultaneous downregulation of NK ligands via several mechanisms may counteract this opportunity.

D.2 MAPK inhibition leads to changes in tumor microenvironment

In an effort to comprehensively identify downstream targets of oncogenic BRaf V600E/MEK signaling, Marais et al found CXCL1 and CXCL8 (IL-8) downregulated in response to inhibition with the ^{V600E}BRaf-specific inhibitor PLX4720 [106]. Our analysis of cell culture supernatants of melanoma cell lines underlined and expanded these findings to more chemokines and growth factors. CXCL8 is produced by Ma-Mel-48a cells, but after 48 hours, MAPK treatment resulted in efficient downregulation. Since IL-8 (CXCL8) expression is driven by an AP-1 site, among other promotor sites, the suppression of c-Jun phosphorylation after 24 hours of MAPK inhibitor treatment could be involved in the suppression of IL-8 secretion in Ma-Mel-48 cells. Accordingly, Marais et al showed that the downregulation of IL-8 is mediated transcriptionally. Loss of IL-8 secretion of Ma-Mel-48 cells could provide a survival benefit for disseminating cells, because this chemokine usually attracts granulocytes, T and NK cells. However, IL-8 is a double-edged sword in tumor biology, since it has also been shown to act as a growth promoter in tumor cells [107]. Similar to IL-8 - HGF, SDF-1α (CXCL12) and M-CSF have only been strongly secreted by Ma-Mel-48a cells, and secretion was effectively down-regulated with all three inhibitors. This implies that their expression is at least in part driven by MAPK signaling. In addition, the chemokines IL-8 and SDF-1α share with growth factors like VEGF, HGF, and M-CSF the transcriptional regulation by AP-1 sites in cooperation with NFκB and/or SP-1 and p53 sites. Therefore, this concerted action of MAPK inhibition of these factors may be due to the suppression of c-Jun and subsequent missing AP-1 dependent transcription of these genes. HGF, also known as scatter factor, is a pleiothrophic growth factor, stimulating motility and invasion of several cancer types via its receptor c-Met, and has also been shown to induce angiogenesis. Downregulation of HGF should therefore be desirable in tumor treatment. SDF-1α belongs to the CXCL chemokine family and acts as a strong attractant for T, B, and NK lymphocytes. Macrophage colony-stimulating factor (M-CSF) is a cytokine that primarily acts in hematopoiesis by controlling the production, differentiation and function of granulocytes and macrophages. The downregulation of these factors therefore provides beneficial as well as counterproductive effects of MAPK inhibition regarding tumor treatment.

Vascular endothelial growth factor (VEGF) has been shown to play an important role in angiogenesis. Secretion of VEGF was detected in all three Ma-Mel-48 cell lines, and was almost completely down-regulated following MAPK inhibition. In contrast to early reports of VEGF expression in melanoma [108], VEGF expression has recently been repeatedly related to melanoma progression serving as a negative prognostic factor for melanoma therapy responses [109-111]. Our findings suggest, that inhibition of MAPK signaling can lead to reduced expression levels of VEGF in melanoma patients and this is currently analyzed in a melanoma phase I clinical trial (personal communication D. Schadendorf, University Hospital Essen).

In light of several changes in tumor immunology in response to MAPK inhibition, and NK cell recognition of treated melanoma cell lines, the secretion of macrophage migration inhibitory factor (MIF) was of special interest to us. In tumor biology, MIF has been proposed as a biomarker for prostate cancer [112]. Furthermore, MIF plays a critical role for angiogenesis, stimulates tumor cell migration, and suppresses p53 activity [113, 114]. Wischhusen et al showed that MIF may contribute to the immune escape of ovarian carcinoma by transcriptionally down-regulating NKG2D in vitro and in vivo which impairs NK cell cytotoxicity towards tumor cells [115]. Due to its potent tumor-promoting and escape properties, it would be very interesting to unravel the role of MIF expression in melanoma. As a known counterpart to p53, it might inhibit induction of apoptosis, and additionally influence NK cell recognition of melanoma cells. If MIF presents an important escape mechanism for melanoma cells, a correlation of responders and non-responders with MIF expression levels in clinical studies, e.g. of Sorafenib treatment in metastatic melanoma, could provide an early opportunity to identify the potential benefit of treatment. Our data shows that MIF is only secreted by Ma-Mel-48b cells, and is strongly upregulated with Sorafenib, in contrast to all other factors that are downregulated. Through this sole role of Ma-Mel-48b cells, and the strong impact of Sorafenib treatment, we hold a unique situation in our hands, to further elucidate the effects of MIF expression and over-expression with Sorafenib in context of melanoma immunology, and NK cell recognition. The possible escape mechanism via MIF will also be further investigated in our lab.

Finally, SCGF-β turned out to be the only growth factor which was secreted from all Ma-Mel-48 cell lines, but was not affected by MAPK inhibition. For the evaluation of chemokine and growth factor secretion profiles, this non-modulated expression pattern of SCGF-β is very important, because it shows that the observed inhibiting or increasing effects of MAPK treatment are specific and not due to some general impairment in protein synthesis. In addition, SCGF-β itself may act as an autocrine growth factor through its binding to the c-Kit receptor that is mutated often in non-sun-exposed mucosal melanoma. Therefore, the inability of Sorafenib to suppress SCGF-β secretion may also contribute to the poor, non-existing effectiveness of this drug in melanoma. Taken together, the analysis of melanoma cell culture supernatants reveals strong effects of MAPK inhibition on the composition of the tumor microenvironment, which could have strong and far-reaching effects on tumor metastasis and tumor escape mechanisms.

Without accounting for our specific findings, Figure D-2 tries to give an overview of MAPK signaling, and its connections to surface molecule expression, chemokine and growth factor secretion, surrounding pathways and the induction of apoptosis and autophagy. The various effects of MAPK inhibition occur in a time-dependent manner. Surface molecule expression and the tumor microenvironment are longterm effects of treatment, whereas signaling events and the corresponding impact of pathway perturbations can occur immediately.

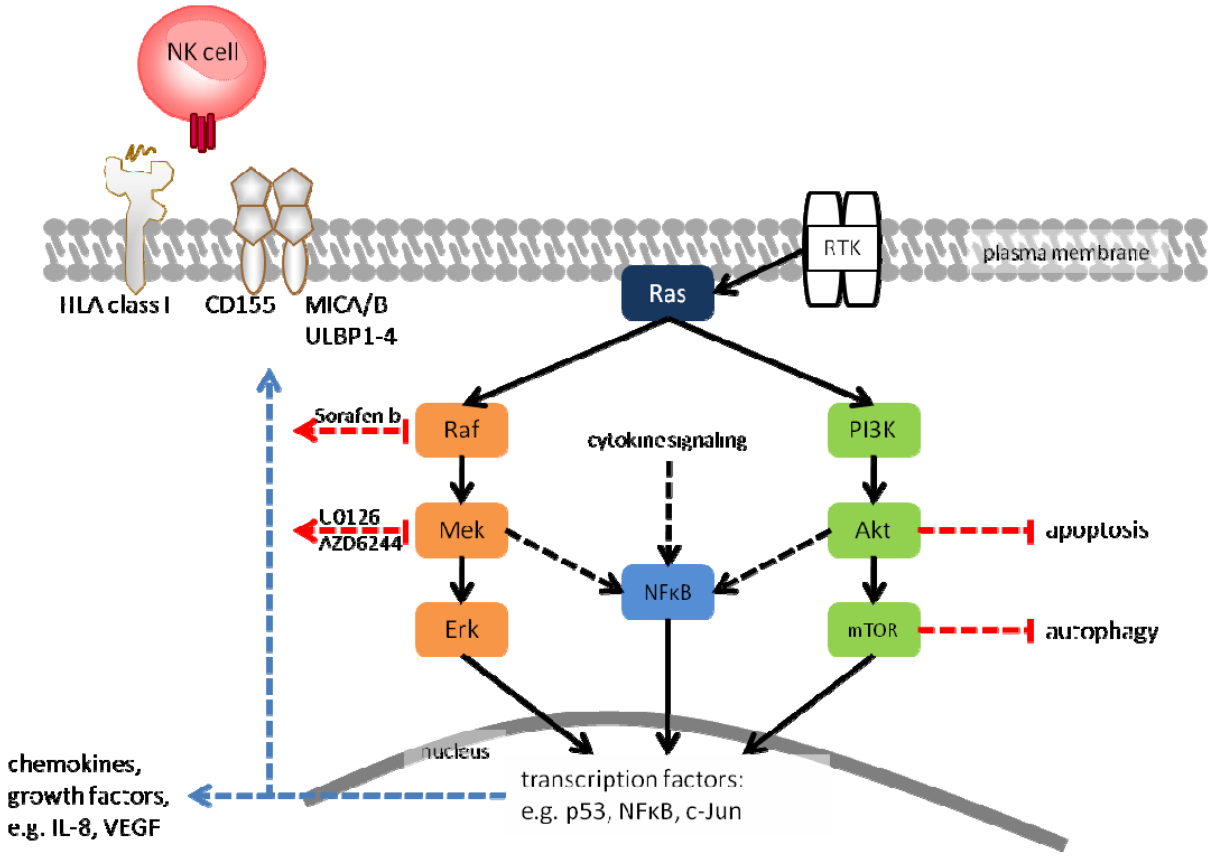

Figure D-2 - Summarizing scheme of the multiple impacts of MAPK inhibition. Due to the interconnectivity of the MAPK pathway, inhibition has far-reaching effects on cell signaling, surface molecule expression, micrenvironment and the induction of apoptosis and/or autophagy.

D.3 Surrounding effects of MAPK inhibition on other critical cell signaling pathways

It is becoming increasingly clear that cell fate decisions in most mammalian cells are not regulated by one pathway alone. Rather, the combinatorial and quantitatively regulated activation of signalling pathways seems to determine the cellular response. The MAPK pathway is one of the most and best studied pathways in human normal and oncogenic cell signaling. Still, the systemic effects of MAPK inhibition in malignant and non-malignant cells are poorly understood. It is currently unclear, what the best method to study the widespread effects of MAPK inhibition

would be. We have applied Phosphoplex analyses to investigate the directly and indirectly connected pathways in regulation of cell fate decisions, which included JNK and c-Jun signaling, p53 activation and stabilization and Akt signaling, amongst others I did not report on in this work. As expected I have shown, that the three inhibitors show downstream inhibition of phospho-ERK within 30 minutes of treatment, and inhibition was sustained constantly for up to 96 hours. A-375 cells have only been partially inhibited with Sorafenib (Figure R-9).
ERK inhibition is achieved over different mechanisms of action. Sorafenib inhibits BRaf, upstream of MEK and ERK, and therefore achieves dephosphorylation of both, MEK and ERK. U0126 binds to MEK, and inhibits phosphorylation of the kinase itself. AZD6244, in contrast, inhibits MEK function effectively, as we have shown complete inhibition of ERK phosphorylation, but surprisingly leads to a stabilized or even increased phosphorylation of MEK (Figure R-10). Presumably, it binds to MEK independent of its phosphorylation state, and thereby prevents dephosphorylation. Besides the different effects of U0126, AZD6244 and Sorafenib on MEK phosphorylation, our analyses also revealed a large difference between Ma-Mel-48 cells and A-375 cells. All Ma-Mel-48 cells show relatively low amounts of p-MEK at starting points. In contrast, A-375 cells have large amounts of p-MEK at the start of treatment. This allows for some conclusions about the involvement of the different BRaf mutations. The ^{G469R}BRaf mutation, which is closely located to gate-keeper mutations, obviously does not lead to constitutively active MAPK signaling, because the downstream target of mutated Raf shows relatively low phosphorylation levels. In contrast, ^{V600E}BRaf leads to a strong constitutive MEK-activation as proposed before. This observation might contribute to the different susceptibility of Ma-Mel-48 cells and A-375 cells to MAPK treatment, as I have shown in xCELLigence analyses. The perturbation of constitutively active oncogenic ^{V600E}BRaf signaling through MAPK inhibitors in A-375 cells probably showed the largest impact, because oncogenic MAPK signaling plays a major part in transformation of these cells. Ma-Mel-48 cells instead, carry a gate-keeper-like mutation, and have probably acquired other mutations to drive transformation of these cells forward, which explains the smaller dependence on oncogenic BRaf signaling. These co-existing mutations possibly target PTEN, since a strong correlation of PTEN with BRaf and p53 with N-Ras has been described previously [116, 117]

The analysis of phosphorylation proves ERK to be a good read-out for inhibitor activity. Surprisingly, not only phosphorylation of ERK and MEK was changed in response to MAPK inhibitors, but in addition, total protein amounts have been modulated. Total ERK levels showed little variation in Ma-Mel-48 cells. In A375 cells though, I have observed stable total ERK levels in MAPK inhibitor treated samples, but DMSO control lysates showed increasing total ERK levels (Figure R-11). Examination of total MEK levels again proved the different mechanisms of action of AZD6244 and U0126, since AZD6244 treatment led to the degradation of total MEK, whereas U0126 did not (Figure R-12). Such decreased total kinase levels become more visible in Phosphoplex assays, due to the more sensitive quantification in terms of MFI of more than 50

beads per sample and analyte, instead of density evaluation in Western Blots, where degradation of proteins can easily be mistaken as variations in loaded protein, or overlooked due to longer exposure times of the WB membrane. This technical reason may be responsible for the underestimation of total kinase changes in control samples and during MAPK inhibition. Therefore, direct comparisons between Phosphoplex and WB were performed for p53. These analyses used the same lysate and reveased an almost perfect correlation of phosphoplex analysis with Western Blot analysis, but higher sensitivity of the phosphoplex technique (Figure R-18).

In light of our findings in the linear MAPK pathway, I decided to concentrate on JNK, p53 and Akt signaling to evaluate the effects of MAPK inhibition on other pathways involved in cell fate decisions. The JNK signaling pathway belongs to the superfamily of MAPK pathways and was originally described to be activated by stress signals like UV and gamma radiation, chemokines and interleukins. JNKs are also called stress activated phospho kinases (SAPK), and got their original name of “c-Jun n-terminal activating kinases” through their ability to activate and phosphorylate c-Jun. C-Jun regulates gene expression in combination with c-fos as the AP-1 complex in the nucleus, and targets proteins involved in cytosceletal function, microenvironment and chemokines and regulates proteins of the BH3-only family involved in apoptosis.
The anti-apoptotic Bcl-2 protein is inhibited through phosphorylation of JNK, while pro-apoptotic Bax is activated. Therefore JNK signaling is regarded as a pro-apoptotic pathway. Recently the view on JNK signaling has changed quite substantially, since Alexaki et al have provided evidence that JNK, in particular JNK1, supports the growth of melanoma cells, acting either through the control of cell cycle by regulating the expression of p21Cip1/Waf1, or by controlling apoptosis [118]. The controversial involvement in the regulation of autophagy will be discussed in the next section. In our melanoma lines, little influence of MAPK inhibiton on phosphorylated levels of JNK was shown, in fact phosphorylation levels of JNK are constantly very low (Figure R-13). The antibody used in phosphoplex analysis is supposed to recognize JNK1 and JNK2, yet in total there are ten isoforms of JNK existing in humans. The abundance of these isoforms might explain the low phosphorylation levels of JNK, because not all JNK isoforms are detected in this assay. Phosphorylation of c-Jun, which is directly regulated through JNK was strongly suppressed in the presence of MAPK inhibitors in Ma-Mel-48a and-48b (Figure R-13). In contrast, Ma-Mel-48c cells show increased levels of c-Jun phosphorylation at Serine 63 by Sorafenib treatment. This difference is very interesting based on the fact, that the Ma-Mel-48c cells, which are so closely related to Ma-Mel-48a and -48b, show different phosphorylation patterns. Along this line, A-375 cells show a JNK/c-Jun regulation again different from all Ma-Mel-48 cells. In inhibitor-treated samples an increase in c-Jun phosphorylation was observed, indicating that in A-375 cells, AP-1 complex dependent transcription could be induced upon MAPK inhibition, which is further inverstigated.

The PI3K pathway is linked to the MAPK pathway via several signaling nodes, e.g. PI3K p110α [119]. Therefore, it was of interest to determine possible consequences of MAPK inhibition for Akt signaling. Phosphorylation of Akt at Serine 473 has previously been suggested to be regulated by Akt autophosphorylation in a PI3 kinase dependent kinase 1(PDK-1) dependent manner. Additionally, it has been shown that integrin-linked kinase (ILK) is also involved in phosphorylation of this site, and critical for kinase activity [120]. Recently, Akt Ser 473 has also been shown to be regulated through mTOR complexes 1 and 2 [121], leading to autophagy activation and other cellular responses. Its pleiotropic functions render Akt a critical player in autophagy and apoptosis activation which is discussed in detail in the next chapter.
PI3K signaling can be dependent on Ras activation and since Ras is upstream of the inhibitors I used, it can only be altered as a result of feedback loops in Ras-Raf-MEK-ERK signaling. Our results implicate such feedback loops by showing that Akt phosphorylation, similar to c-Jun, is reduced in MAPK inhibitor treated samples in Ma-Mel-48a, -48b and -48c cells (Figure R-16). Again, A-375 cells show a different pattern of Akt regulation, especially because treatment with Sorafenib led to increased phosphorylation of Akt at Serine 473. Analogously to t-JNK, total levels of Akt are low in our analyses, and of special note, lower than phosphorylated levels. As the antibody for total protein should recognize phosphorylated as well as unphosphorylated protein, this appeared unlikely and I therefore assumed, that the effect is probably due to different specificity of Akt antibodies. Indeed, it turned out that the phospho-Akt antibody recognizes Akt 1-3, whereas the total protein antibody only recognizes Akt1. The data suggests, that Ma-Mel-48 cells express all three Akt isoforms, whereas A-375 cells, which show surprisingly low levels of total Akt, assumingly possess Akt2 and/or Akt3, a feature described for many melanoma lines [122]. Our analyses of components of the JNK/c-Jun and PI3K/Akt pathways revealed that BRaf as well as MEK inhibition, also affects other pathways, in part by a cell-specific manner. Thus, MAPK inhibition should be addressed in the future in the context of the JNK/c-Jun and PI3K pathway to get a more comprehensive view on possible links between signaling cascades.

p53 functions primarily as a transcription factor, where cellular stress serves to activate and target p53 to genes that initiate accelerated DNA repair, inhibit cell cycle progression, or lead to senescence or apoptosis [123]. Since p53 plays a vital role in preserving the genetic integrity of a cell, it is not surprising that regulation of its activity is complex [124], by integrating several positive and negative feedback loops that either promote or reverse the stress response. One of these negative regulators, MDM2, binds to Serine15-non-phosphorylated p53, blocking its transcriptional activity and targeting it for ubiquitin-mediated proteasome degradation. P53 itself positively regulates MDM2 transcription, thus creating a negative autoregulatory feedback loop. In Ma-Mel-48 cells we observed reduced levels of phosphorylated and total amounts of p53 in MAPK-inhibitor-treated samples compared to DMSO (Figure R-17). In DMSO controls, p53 was obviously stabilized, which was detectable by increasing amounts of phosphorylated and total protein, whereas in U0126, AZD6244 and Sorafenib samples, the levels remained low. The

kinetics of Ma-Mel-48 cells display a biphasic curve with peaks at 6-12 hours and 72 hours respectively, and a valley at 24 hours. This time-dependent distribution of p53 indicates a close link to cell cycle and proliferation. In contrast to Ma-Mel-48 cells, A-375 cells show late p53 stabilization in response to Sorafenib treatment only, preceeded by an early peak at 12 hours that was supported by MEK inhibition. The strong correlation of phosphorylated and total amounts of p53 underlines the strict regulation of active p53 via Serine 15 phosphorylation, which protects p53 from immediate degradation. The modulation of this regulation in Sorafenib treated A-375 cells is of great interest, and could account for enhanced levels of apoptosis in A-375 cells, compared to Ma-Mel-48 cells.

Altogether, the analysis of this phosphoplex data set is not intuitive, first of all due to the huge amount of data. Four phosphorylation profiles over 8 timepoints for 12 proteins, the same for total protein levels, and that across 4 cell lines, makes up for a total of 3072 datapoints. Secondly, the data is quite complex in terms of interactions and non-linear effects. We have therefore decided to use a systems biology approach, in order to establish off-target effects, interactions that contribute to the cellular response and to select the best procedure to inhibit tumor proliferation. Our computational modeling approach uses a data-driven “fuzzy logic” approach. Once we have established this analysis in cooperation with Nathan Brady and Marti Bernardo Faura (Bioquant, Heidelberg), it will hopefully enable us to comprehensively compare the response of our melanoma cells to MAPK inhibition, and unravel differences between the inhibitors themselves, as well as between cell lines. The model system will also be connected to functional responses, in order to identify protein kinases that are most likely responsible for variations in cellular reactions at the surface. The first response we are going to add is the modulated expression of CD155 on melanoma cells during MAPK inhibitor treatment. Subsequently, we can also relate it to induction of autophagy or apoptosis, which could help to further understand the observed variations in patient response to MAPK inhibitor treatment. In the future, such approaches could pave the way to predictions of patient responses, depending on the phosphorylation profile of the patient.

D.4 MAPK inhibition modulates the balance between apoptosis and autophagy

As our phosphoplex analysis has shown, even the specific inhibiton of a single protein kinase (MEK, U0126, AZD6244) can lead to cellular reactions apart from the linear signaling cascade. Therefore, I focused on pathways which are involved in the regulation of apoptosis and autophagy.

D.4.1 ImageStream-based approach for the quantification of autophagy

Even though autophagy is a tremendeously expanding research field, it lacks an elegant and practical “go-to” method for correct quantification of autophagic activity. Common measurements of autophagic activity report an average or a typical response of a population, or changes to a pre-defined population, yet do not account for cell-to-cell variation. This is particularly relevant in the context of autophagy measurements using the macroautophagy-specific marker LC3 [59]. Typically GFP-LC3 is used to determine the number of cells displaying autophagosomes, or numbers of autophagosomes per cell based on manual counting. While fluorescence microscopy provides the necessary resolution for the detection of single autophagosomes per cell, classification is neither standardized, nor fully quantitative and objective. Moreover, steady-state autophagosome numbers, the most commonly reported autophagy metric, are not indicative for autophagic activity and can therefore not be considered a reliable indicator of autophagic flux [125].

I hypothesized, that an ImageStream-based method could provide a new and improved approach to address the methodological constraints in detecting autophagy by integrating high resolution imaging, the high-sampling capacity of flow cytometry and rich feature extraction for population-level statistical analyses. In order to establish the new method for autophagy quantification, I have used MCF7 GFP-LC3 cells, which are commonly used in autophagy research. First steps in establishing the method were performed in starvation medium to induce autophagy, and imaged under steady-state versus cumulative conditions. This comparison is necessary, because the full process of autophagy involves the turnover of formation and degradation of autophagosomes, giving rise to punctuated as well as non-punctuated cells. Under cumulative conditions, I use the lysosomal inhibitor Bafilomycin A1, which inhibits fusion of autophagosomes to lysosomes, and therefore inhibits degradation of newly-formed autophagosomes, and the acid-induced quenching of GFP fluorescence. For a correct analysis of autophagic activity, it is necessary to compare steady-state levels to cumulative levels. The integrating metric “autophagic flux” is calculated by the substraction of steady-state levels from cumulative levels. First evaluations of autophagic activity in response to starvation supported the assumption of heterogenic responses within populations of cells. Thus, I observed non-spotted as well as spotted cells (Figure R-21), and sought to capture this heterogenic response with the definition of subpopulations of autopagic activity according to the spot count per cell. We have clustered cells with 0-4 spots as “low” autophagic activity, 5-12 spots as “medium” and more than 12 spots as “high” autophagic activity. The subpopulation distribution shifts significantly between steady-state and cumulative levels (Figure R-22). Of note, even after a 3 hour starvation period, which strongly induces autophagy, subpopulation distributions of around 20% low, 65% medium and 15% high autophagic activity were found under cumulative conditions. In this situation, without the degradation of autophagosomes, the high cell-to-cell variability in autophagic responses becomes visible, which

can not be evaluated by other methods based on population-average analyses. Besides the quantification of autophagy by the number of detected spots, I introduced the secondary metrics of normalized spot area and intensity to further characterize the cellular reactions. These metrics are secondary, because *a priori*, they depend on the identification of spots. Both metrics supported our findings based on spot count analysis, and proved to be valuable additional metrics to characterize the autophagic response (Figure R-23).

D.4.2 Modulation of autophagy by TNFR, JNK, Bcl-2 and NFκB signaling

Although I have not reported extensively on our findings regarding the regulation of autophagy in MCF7 cells in this thesis, they show that the autophagic response is highly tunable, und critically dependent on JNK and NFκB [Maßen et al, in preparation. Compare Figure D-3]: TNFα has been implicated in activation of autophagy in T-lymphoblastic cells [126], and has been used to induce autophagy in rat Ewing sarcoma cells [69]. We have therefore added TNFα to study the regulatory effects of TNF receptor I activation on autophagy. Our results reveal that TNFα treatment under starvation conditions showed only minor effects on induction of autophagy (Figure R-25), and full medium experiments did not show any significant activation of autophagy (data not shown), contradiciting previous findings. On the one hand, this might be due to the analysis of only steady-state levels in previous studies, and on the other hand on differences between cell systems.

Moreover, direct inhibition of Bcl-2 using the BH3 mimetic HA14-1 protein tended to decrease autophagic activity (Figure R-25). Although these results are not consistent with the proposed paradigm of a Bcl-2 mediated inhibition of Beclin 1, they suggest the co-existence of pro-survival activities of both Bcl-2 and autophagy [127]. Furthermore, these results are consistent with earlier flux measurements of Beclin 1 lacking the Bcl-2 domain, which indicated a decreased Beclin 1 activity in the absence of Bcl-2 binding [128] and further supports a more complex relationship between Beclin 1 and Bcl-2 [129, 130].

During nutrient deprivation-induced autophagy the pharmacological inhibition of the NFκB pathway reduced levels of autophagy in my experiments (Figure R-25). This is in contrast to previous findings [69], which established that NFκB activation, associated with TNF and nutrient deprivation, blocks the autophagic response. However, our findings are consistent with a recent report that NFκB directly activates autophagy by increasing Beclin 1 expression [131], as well as consistent with the survival role of autophagy in nutrient deprivation, as NFκB inhibition has been shown to enhance starvation-induced cell death [132].

Importantly, results from pharmacological perturbations indicated that in our model system, autophagy is negatively regulated by JNK (Figure R-25). JNK inhibition during nutrient deprivation-induced autophagy further increased autophagic activity above nutrient deprivation

levels. Importantly, the sensitivity of the autophagy detection method described here evidenced an increase from “medium” to “high” cumulative autophagosome levels, demonstrating that a large percentage of cells up-regulated autophagy, and thus had maintained an extra capacity in terms of both autophagosome formation and degradation which is pharmacologically responsive. These results strongly suggest that JNK acts in our experimental model to inhibit autophagy, which is in contrast to other reports that state that inhibition of JNK with SP600125 inhibited the induction of autophagy [133-137].

Building on our findings, I have further elucidated the mechanism of action behind the inhibiting role of JNK, and activating role of NFκB in cooperation with Nathan Brady (Bioquant, Heidelberg). Using Western Blots experiments, transfection of dominant-negative JNK, and TAT-delivered JNK inhibitor peptide, it was possible to identify JNK as a critical negative regulator of autophagy induction. JNK was phosphorylated upon induction of autophagy and with addition of Bafilomycin A1, and inhibition of NFκB lead to increased phosphorylation of JNK. Together with the confirmation of JNK inhibition leading to increased autophagy, this implicates that JNK acts as a “brake” in autophagy regulation in MCF7 cells, and that NFκB regulates autophagy via phosphorylation of JNK [Massen et al, manuscript in preparation]

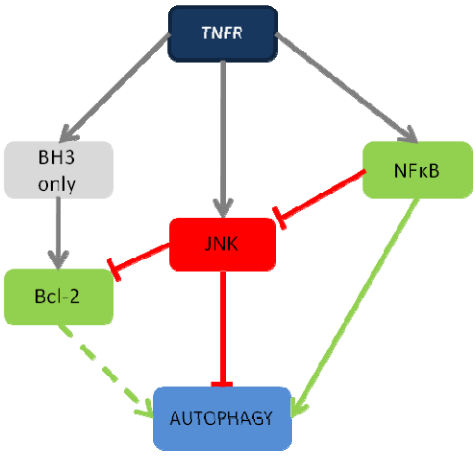

Figure D-3 - Expansion of a literature-derived autophagy regulation scheme, with our experimental findings. In contrast to previous studies, TNFR activation did not lead to induced autophagy, presumably because of the simultaneous activation of activating and inhibiting pathways. Bcl-2 seemed to play a minor activating role in the regulation of MCF7 starvation induced autophagy. In contrary, we have identified the pro-apoptotic JNK as a major critical brake in the regulation of autophagy. NFκB showed to be necessary for autophagy induction, presumably through inhibition of JNK activation.

The dynamic balance between death and survival signals showed to be even more complex, calling into question how well we understand the balance between pro-survival and pro-death signaling events. Overall, our results indicate that pro-survival NFκB pathways can also positively regulate autophagy, a potent cytoprotective mechanism [138], and pro-death JNK pathways are inhibiting autophagy. However, JNK-associated promotion of autophagic cell death (PCD II) [139], likely involves the participation of additional pathways, including DAPK [140], which is presumably absent in our MCF7 model [141].

This work clearly illustrates the need for a methodical re-evaluation of early versus late signaling events pertaining to autophagy. Future work, integrating new perturbation strategies based on the topology established here with time-resolved measurements, will require the assistance of mathematical tools to integrate and predict solutions to non-intuitive results [142, 143]. Furthermore, such an approach outlined here indicates the possibility of standardizing autophagy measurements across model systems which would allow for a more direct comparison across laboratories.

D.4.3 Sorafenib inhibits autophagy induction and induces apoptosis in A-375 cells

With the establishment of a solid method for the quantification of autophagy, the intention was to clarifiy the impact of MAPK inhibition on the induction of autophagy. Upon treatment for 24 hours with the MAPK inhibitors U0126, AZD6244 and Sorafenib, the autophagic response in MCF7-GFP LC3 cells was evaluated in a first step (Figure R-26). In full medium, I could not detect an impact of the MEK inhibitors U0126 and AZD6244, but Sorafenib, in contrast, mediated strong inhibiton of autophagy: Under cumulative conditions, i.e. in presence of BafA1, in Sorafenib-treated cells, we did not observe a subpopulation shift towards medium and high spot counts as usually seen - instead, cumulative levels almost perfectly matched steady-state conditions. This becomes clearly visible by calculating the % change for Sorafenib-treated cells, and identifies Sorafenib as a strong inhibitor of autophagy induction in MCF7 GFP-LC3 cells. The analysis of the corresponding phosphorylation states regarding ERK1/2, MEK1 and Akt revealed most importantly, that Sorafenib treatment did not result in inhibition of p-ERK1/2 in contrast to both MEK inhibitors (Appendix Figure 1). This observation suggests that the phosphorylation status of ERK1/2 may be relevant for autophagy induction in MCF7 cells. This striking difference to the inhibition of p-ERK1/2 in melanoma lines prompted us to analyze the situation in melanoma.

We have made use of stably transfected A-375 GFP-LC3 cells to evaluate the effects on autophagy and apoptosis in a MAPK-driven melanoma cell system. Our findings of phosphoplex analysis concerning the modulation of p53, JNK and Akt, already suggest a possible shift in the “balance” between autophagy and apoptosis. Along these lines we sought to combine an ImageStream based approach for the quantification of apoptosis with our approach of autophagy quantification. Detection of apoptotic cells with the ImageStream is based on occurring nuclear fragmentation that can be visualized by Hoechst DNA staining [84]. The simultaneous inspection of GFP-LC3 and Hoechst staining made it possible to evaluate both, apoptosis and autophagy on single cell levels simultaneously in A-375 GFP-LC3 cells. After 3 hours of starvation, with respect to autophagy, we have observed inhibiting effects of Sorafenib treatment in this model system too (Figure R-27). Careful evaluation of steady-state and cumulative levels, shows a modulated response in steady-state conditions. The “low” spot count population of cells decreased,

corresponding to an increase in the “medium” population of cells. Although an increase in the “low” cell population was also seen under cumulative conditions, the inhibiting effect of Sorafenib appeared to be most prominent under steady-state conditions. The increase in medium autophagic activity under steady-state conditions, leads to the assumption that Sorafenib may be able to block the degradation of newly formed autophagosomes, possibly interfering with the transport of cytoplasmic organelles or the fusion of autophagosomes to lysosomes. The inhibiting effect could only be observed in starvation medium, and was not visible in full medium conditions within 3 hours. This implicates, that it is probably due to the higher rate of autophagy in starvation medium.

The simultaneous quantification of apoptotic cells shows a corresponding picture (Figure R-28): In starvation conditions the same amount of apoptotic cells in DMSO treated samples in steady-state and cumulative conditions was observed, indicating that starvation for 3 hours alone does not induce apoptosis. In starvation medium under steady-state conditions, 8% apoptotic cells were detectable in DMSO samples, and 14% apoptotic cells in Sorafenib-treated cells. Sorafenib showed the highest levels of apoptosis-induction compared to the two MEK inhibitors. In starvation medium and under cumulative conditions, meaning disturbed autophagy, DMSO samples still show only 10% apoptotic cells. But of note, this was substantially increased to 35% in Sorafenib treated cells. This 3.5 fold increase of apoptotic cells compared to the corresponding DMSO control samples exceeds the effects of U0126 and AZD6244 substantially. Thus, Sorafenib treatment simultaneously reduced autophagy and increased apoptosis, i.e. shifts the balance towards apoptosis, but U0126 and AZD6244 did not. Even though this does not prove a direct connection between apoptosis and autophagy, it strongly implicates a cytoprotective role of autophagy under starvation conditions, and dysregulation of autophagy seems to promote apoptosis.

Several scenarios could provide an explanation for this increase in apoptotic cells. Possibly, starvation results in apoptosis, if autophagy is inhibited through Sorafenib, while in DMSO control cells, fully functional autophagy is able to counteract the induction of apoptosis. Another option would be the induction of apoptosis through Sorafenib, independently from inhibiting effects of Sorafenib on autophagy. This would imply a coincidental correlation of inhibited autophagy and increased amounts of apoptotic cells. Claerhout et al have shown for metastatic skin cancer, that chemoresistance to cisplatin depends on induction of autophagy, since inhibition of autophagy with 3-MA in addition to cisplatin significantly enhanced cytotoxicity of cisplatin treatment [144]. This, among other studies shows that it is more likely that inhibition of autophagy with Sorafenib induces higher levels of apoptosis in starvation medium.

We wanted to further characterize this Sorafenib specific behavior in longer treatment periods. 24 hours of starvation would be rather toxic, that is why we had to focus on full medium conditions. Similar to the effect previously shown for MCF7 GFP-LC3 cells, almost complete inhibition of autophagy in A-375 GFP-LC3 cells was observed (Figure R-29). The evaluation of apoptotic cells reveals enhanced levels of apoptotic cells in Sorafenib-treated A375 GFP-LC3 cells compared to

DMSO, even though cells were cultured in full medium. Of note, we could not detect any changes in induced apoptosis in full medium within 3 hours (Figure R-28). Even though the amount of 9% apoptotic cells might seem rather low, we suggest that this number is probably underestimating the amount of apoptotic cells, because cells that get detached within these 24 hours of treatment are not included in the measurement due to washing steps prior to DNA staining with Hoechst, which resembles a selection for attached, i.e. living cells. The high amount of apoptotic cells after 3 hours of starvation and Sorafenib treatment (Figure R-28), is probably unaffected by this "selection", because these early-apoptotic cells, have probably not yet detached from the plate. We possibly observe a multiplicative effect of Sorafenib treatment. On the one hand, it induces apoptosis within 24 hours of treatment, and on the other hand it inhibits the cytoprotective function of autophagy, to further enhance the effect of induced apoptosis. The amount of apoptotic cells after 24 hours of treatment corresponds well to the levels we have observed in full medium conditions after 3 hours.

Although this balance between autophagy and apoptosis is clearly modulated by Sorafenib in a similar fashion in different tumor cells (MCF7 and A-375) harbouring different constitutive signaling pathways, it is still puzzling to observe almost 100% non-autophagic cells but <50% apoptotic cells. This discrepancy suggests that non-autophagic cells do not automatically undergo apoptosis but rather additional events may drive them to the "point of no return" on their way to apoptosis. Before this point of no return, the direction seems to be "reversible". Taken together, the simultaneous quantification of autophagy and apoptosis at the single cell level allows a detailed view on the delicate balance between these two cellular reactions. Since several pathways are involved in the adjustment of this balance according to the nutrient conditions, it is not surprising that perturbation of these pathways can either inhibit or promote autophagy. However, the reaction of tumor cells to these perturbations may be determined by the individual oncogenic signaling that is driven in part by mutations in signaling nodes like BRaf, NRas and PI3K components. In consequence, this would argue for a detailed analysis of autophagy and apoptosis in the context of the "driver" mutations in order to understand how the oncogenic signaling pathways impact tumor cell survival and resistance to apoptosis. This novel conncetion between oncogenic signaling, depending on the mutational status of the tumor cell, microenvironment, immune recognition and balance between autophagy and apoptosis will be further investigated in the context of malignant melanoma. In a larger perspective, our data may be relevant, especially when deep-sequencing of tumors will generate comprehensive mutation patterns – because our studies provide a link to the functional consequences for tumor biology. Whithout this information, it will be fairly impossible to use the sequence information for the prediction of responder versus non-responder subgroups of patients.

Abbreviations

ADCC	antibody-dependent cellular cytotoxicity
AR	activating receptor
ATP	adenosine-triphosphate
Baf	Bafilomycin
BF	bright-field
CD107a, LAMP-1	lysosomal-associated protein 1
CI	cell index (xCELLigence)
CP	cytoplasmic part
DNAM-1	DNAX accessory molecule-1
EBSS	Earle’s balanced salt solution (starvation medium)
EGFR	epidermal growth factor receptor
ER	endoplasmatic reticulum
ERK	extracellular signal-regulated kinase
FACS	fluorescenceactivated cell sorting
FLT-3	fms-related tyrosine kinase-3
GDP	guanindiphosphate
GFP	green-fluorescent protein
GRB2	growth-factor-receptor bound-2
GTP	guanintriphosphate
HLA	human leukocyte antigen
IFN	Interferon
Ig	Immunoglobulin
IL	Interleukin
IR	inhibitory receptor
ITIM	immunoreceptor tyrosine-based inhibitory motif
LC3	rat microtubule-associated protein 1 light chain
MAPK	mitogen-activated protein kinase
MEK	MAPK ERK kinase
MFI	mean/median fluorescence intensity
MHC	major histocompatibility complex

mTOR	mammalian target of rapamycin
NEAA	non-essential amino acids
NK cell	natural killer cell
PAS	pre-autophagosomal structure
PBL	peripheral blood leukocytes
PBMC	peripheral blood mononuclear cells
PCD	programmed cell death
PDGFR	platelet-derived growth factor receptor
PFA	paraformaldehyde
PI3K	phophatidylinositol-3-kinase
PIP2(3)	Phosphatidylinositol-bi(tri)phosphate
p-protein	phosphorylated protein
RT	room temperature
RTCA	real-time cell analyzer
RTK	receptor tyrosine kinase
SAPE	Streptavidine-PE
SHP-2	SH2-containing tyrosine phosphatase-2
SOS	son-of-sevenless
SrcK	Src kinase family members
SSC	side scatter
TM	“tumor medium”
TNF	tumor necrosis factor
t-protein	total protein
V-EGFR	vascular endothelial growth factor receptor
WB	western blot
WM	Wortmannin
β2m	β2-microglobuline

Literature

1. Hanahan, D. and R.A. Weinberg, *The hallmarks of cancer.* Cell, 2000. **100**(1): p. 57-70.

2. Cummins, D.L., et al., *Cutaneous malignant melanoma.* Mayo Clin Proc, 2006. **81**(4): p. 500-7.

3. Seger, R. and E.G. Krebs, *The MAPK signaling cascade.* FASEB J, 1995. **9**(9): p. 726-35.

4. Barbacid, M., *ras genes.* Annu Rev Biochem, 1987. **56**: p. 779-827.

5. Lowy, D.R. and B.M. Willumsen, *Function and regulation of ras.* Annu Rev Biochem, 1993. **62**: p. 851-91.

6. Herrmann, C., *Ras-effector interactions: after one decade.* Curr Opin Struct Biol, 2003. **13**(1): p. 122-9.

7. Cully, M., et al., *Beyond PTEN mutations: the PI3K pathway as an integrator of multiple inputs during tumorigenesis.* Nat Rev Cancer, 2006. **6**(3): p. 184-92.

8. Hennessy, B.T., et al., *Exploiting the PI3K/AKT pathway for cancer drug discovery.* Nat Rev Drug Discov, 2005. **4**(12): p. 988-1004.

9. Wu, H., V. Goel, and F.G. Haluska, *PTEN signaling pathways in melanoma.* Oncogene, 2003. **22**(20): p. 3113-22.

10. Kolch, W., *Meaningful relationships: the regulation of the Ras/Raf/MEK/ERK pathway by protein interactions.* Biochem J, 2000. **351 Pt 2**: p. 289-305.

11. Marshall, C.J., *Specificity of receptor tyrosine kinase signaling: transient versus sustained extracellular signal-regulated kinase activation.* Cell, 1995. **80**(2): p. 179-85.

12. Davies, H., et al., *Mutations of the BRAF gene in human cancer.* Nature, 2002. **417**(6892): p. 949-54.

13. Gray-Schopfer, V., C. Wellbrock, and R. Marais, *Melanoma biology and new targeted therapy.* Nature, 2007. **445**(7130): p. 851-7.

14. Dhomen, N., et al., *Oncogenic Braf induces melanocyte senescence and melanoma in mice.* Cancer Cell, 2009. **15**(4): p. 294-303.

15. Dankort, D., et al., *Braf(V600E) cooperates with Pten loss to induce metastatic melanoma.* Nat Genet, 2009. **41**(5): p. 544-52.

16. Wan, P.T., et al., *Mechanism of activation of the RAF-ERK signaling pathway by oncogenic mutations of B-RAF.* Cell, 2004. **116**(6): p. 855-67.

17. Heidorn, S.J., et al., *Kinase-dead BRAF and oncogenic RAS cooperate to drive tumor progression through CRAF.* Cell, 2010. **140**(2): p. 209-21.

18. Poulikakos, P.I., et al., *RAF inhibitors transactivate RAF dimers and ERK signalling in cells with wild-type BRAF.* Nature, 2010. **464**(7287): p. 427-30.

19. Kortylewski, M., et al., *Mitogen-activated protein kinases control p27/Kip1 expression and growth of human melanoma cells.* Biochem J, 2001. **357**(Pt 1): p. 297-303.

20. Levy, C., M. Khaled, and D.E. Fisher, *MITF: master regulator of melanocyte development and melanoma oncogene.* Trends Mol Med, 2006. **12**(9): p. 406-14.

21. Wilson, D.J., A. Alessandrini, and R.C. Budd, *MEK1 activation rescues Jurkat T cells from Fas-induced apoptosis.* Cell Immunol, 1999. **194**(1): p. 67-77.

22. Smalley, K.S., *A pivotal role for ERK in the oncogenic behaviour of malignant melanoma?* Int J Cancer, 2003. **104**(5): p. 527-32.

23. Curry, J.M., et al., *M-CSF signals through the MAPK/ERK pathway via Sp1 to induce VEGF production and induces angiogenesis in vivo.* PLoS One, 2008. **3**(10): p. e3405.

24. Sers, C., et al., *Down-regulation of HLA Class I and NKG2D ligands through a concerted action of MAPK and DNA methyltransferases in colorectal cancer cells.* Int J Cancer, 2009. **125**(7): p. 1626-39.

25. Gogas, H.J., J.M. Kirkwood, and V.K. Sondak, *Chemotherapy for metastatic melanoma: time for a change?* Cancer, 2007. **109**(3): p. 455-64.

26. Wilhelm, S., et al., *Discovery and development of sorafenib: a multikinase inhibitor for treating cancer.* Nat Rev Drug Discov, 2006. **5**(10): p. 835-44.

27. Eisen, T., et al., *Sorafenib in advanced melanoma: a Phase II randomised discontinuation trial analysis.* Br J Cancer, 2006. **95**(5): p. 581-6.

28. Amaravadi, R.K., et al., *Phase II Trial of Temozolomide and Sorafenib in Advanced Melanoma Patients with or without Brain Metastases.* Clin Cancer Res, 2009. **15**(24): p. 7711-7718.

29. Flaherty, K.T., et al., *A phase I trial of the oral, multikinase inhibitor sorafenib in combination with carboplatin and paclitaxel.* Clin Cancer Res, 2008. **14**(15): p. 4836-42.

30. Jilaveanu, L., et al., *Expression of sorafenib targets in melanoma patients treated with carboplatin, paclitaxel and sorafenib.* Clin Cancer Res, 2009. **15**(3): p. 1076-85.

31. Escudier, B., et al., *Sorafenib in advanced clear-cell renal-cell carcinoma.* N Engl J Med, 2007. **356**(2): p. 125-34.

32. Zhang, T., et al., *Sorafenib improves the survival of patients with advanced hepatocellular carcinoma: a meta-analysis of randomized trials.* Anticancer Drugs, 2010. **21**(3): p. 326-32.

33. Yeh, T.C., et al., *Biological characterization of ARRY-142886 (AZD6244), a potent, highly selective mitogen-activated protein kinase kinase 1/2 inhibitor.* Clin Cancer Res, 2007. **13**(5): p. 1576-83.

34. Adjei, A.A., et al., *Phase I pharmacokinetic and pharmacodynamic study of the oral, small-molecule mitogen-activated protein kinase kinase 1/2 inhibitor AZD6244*

(ARRY-142886) in patients with advanced cancers. J Clin Oncol, 2008. **26**(13): p. 2139-46.

35. Tsai, J., et al., *Discovery of a selective inhibitor of oncogenic B-Raf kinase with potent antimelanoma activity.* Proc Natl Acad Sci U S A, 2008. **105**(8): p. 3041-6.

36. Halaban, R., et al., *PLX4032, a selective BRAF(V600E) kinase inhibitor, activates the ERK pathway and enhances cell migration and proliferation of BRAF melanoma cells.* Pigment Cell Melanoma Res, 2010. **23**(2): p. 190-200.

37. Sondergaard, J.N., et al., *Differential sensitivity of melanoma cell lines with BRAFV600E mutation to the specific raf inhibitor PLX4032.* J Transl Med, 2010. **8**(1): p. 39.

38. Emery, C.M., et al., *MEK1 mutations confer resistance to MEK and B-RAF inhibition.* Proc Natl Acad Sci U S A, 2009. **106**(48): p. 20411-6.

39. Houben, R., et al., *MAPK-independent impairment of T-cell responses by the multikinase inhibitor sorafenib.* Mol Cancer Ther, 2009. **8**(2): p. 433-40.

40. Krusch, M., et al., *The kinase inhibitors sunitinib and sorafenib differentially affect NK cell antitumor reactivity in vitro.* J Immunol, 2009. **183**(12): p. 8286-94.

41. Ljunggren, H.G. and K. Karre, *In search of the 'missing self': MHC molecules and NK cell recognition.* Immunol Today, 1990. **11**(7): p. 237-44.

42. Kumar, V. and M.E. McNerney, *A new self: MHC-class-I-independent natural-killer-cell self-tolerance.* Nat Rev Immunol, 2005. **5**(5): p. 363-74.

43. Raulet, D.H. and R.E. Vance, *Self-tolerance of natural killer cells.* Nat Rev Immunol, 2006. **6**(7): p. 520-31.

44. Yokoyama, W.M. and S. Kim, *Licensing of natural killer cells by self-major histocompatibility complex class I.* Immunol Rev, 2006. **214**: p. 143-54.

45. Anfossi, N., et al., *Human NK cell education by inhibitory receptors for MHC class I.* Immunity, 2006. **25**(2): p. 331-42.

46. Bahram, S., et al., *MIC and other NKG2D ligands: from none to too many.* Curr Opin Immunol, 2005. **17**(5): p. 505-9.

47. Eagle, R.A., et al., *Cellular expression, trafficking, and function of two isoforms of human ULBP5/RAET1G.* PLoS One, 2009. **4**(2): p. e4503.

48. Eagle, R.A., et al., *ULBP6/RAET1L is an additional human NKG2D ligand.* Eur J Immunol, 2009. **39**(11): p. 3207-16.

49. Groh, V., et al., *Tumour-derived soluble MIC ligands impair expression of NKG2D and T-cell activation.* Nature, 2002. **419**(6908): p. 734-8.

50. Salih, H.R., H.G. Rammensee, and A. Steinle, *Cutting edge: down-regulation of MICA on human tumors by proteolytic shedding.* J Immunol, 2002. **169**(8): p. 4098-102.

51. Chan, C.J., et al., *DNAM-1/CD155 interactions promote cytokine and NK cell-mediated suppression of poorly immunogenic melanoma metastases.* J Immunol, 2010. **184**(2): p. 902-11.

52. Carlsten, M., et al., *Primary human tumor cells expressing CD155 impair tumor targeting by down-regulating DNAM-1 on NK cells.* J Immunol, 2009. **183**(8): p. 4921-30.

53. Lakshmikanth, T., et al., *NCRs and DNAM-1 mediate NK cell recognition and lysis of human and mouse melanoma cell lines in vitro and in vivo.* J Clin Invest, 2009. **119**(5): p. 1251-63.

54. Mizushima, N., *The pleiotropic role of autophagy: from protein metabolism to bactericide.* Cell Death Differ, 2005. **12 Suppl 2**: p. 1535-41.

55. Axe, E.L., et al., *Autophagosome formation from membrane compartments enriched in phosphatidylinositol 3-phosphate and dynamically connected to the endoplasmic reticulum.* J Cell Biol, 2008. **182**(4): p. 685-701.

56. Simonsen, A. and S.A. Tooze, *Coordination of membrane events during autophagy by multiple class III PI3-kinase complexes.* J Cell Biol, 2009. **186**(6): p. 773-82.

57. Kim, J., W.P. Huang, and D.J. Klionsky, *Membrane recruitment of Aut7p in the autophagy and cytoplasm to vacuole targeting pathways requires Aut1p, Aut2p, and the autophagy conjugation complex.* J Cell Biol, 2001. **152**(1): p. 51-64.

58. Mizushima, N., *Autophagy: process and function.* Genes Dev, 2007. **21**(22): p. 2861-73.

59. Kabeya, Y., et al., *LC3, a mammalian homologue of yeast Apg8p, is localized in autophagosome membranes after processing.* Embo J, 2000. **19**(21): p. 5720-8.

60. Klionsky, D.J., et al., *Guidelines for the use and interpretation of assays for monitoring autophagy in higher eukaryotes.* Autophagy, 2008. **4**(2): p. 151-75.

61. Rubinsztein, D.C., et al., *In search of an "autophagomometer".* Autophagy, 2009. **5**(5): p. 585-9.

62. Funderburk, S.F., Q.J. Wang, and Z. Yue, *The Beclin 1-VPS34 complex - at the crossroads of autophagy and beyond.* Trends Cell Biol, 2010.

63. Pattingre, S., et al., *Bcl-2 antiapoptotic proteins inhibit Beclin 1-dependent autophagy.* Cell, 2005. **122**(6): p. 927-39.

64. Brady, N.R., et al., *The autophagic response to nutrient deprivation in the hl-1 cardiac myocyte is modulated by Bcl-2 and sarco/endoplasmic reticulum calcium stores.* Febs J, 2007. **274**(12): p. 3184-97.

65. Hoyer-Hansen, M., et al., *Control of macroautophagy by calcium, calmodulin-dependent kinase kinase-beta, and Bcl-2.* Mol Cell, 2007. **25**(2): p. 193-205.

66. Maiuri, M.C., et al., *BH3-only proteins and BH3 mimetics induce autophagy by competitively disrupting the interaction between Beclin 1 and Bcl-2/Bcl-X(L).* Autophagy, 2007. **3**(4): p. 374-6.

67. Wei, Y., S. Sinha, and B. Levine, *Dual role of JNK1-mediated phosphorylation of Bcl-2 in autophagy and apoptosis regulation.* Autophagy, 2008. **4**(7): p. 949-51.

68. Pattingre, S., et al., *Role of JNK1-dependent Bcl-2 Phosphorylation in Ceramide-induced Macroautophagy.* J Biol Chem, 2009. **284**(5): p. 2719-28.

69. Djavaheri-Mergny, M., et al., *NF-kappaB activation represses tumor necrosis factor-alpha-induced autophagy.* J Biol Chem, 2006. **281**(41): p. 30373-82.

70. Schlottmann, S., et al., *Prolonged classical NF-kappaB activation prevents autophagy upon E. coli stimulation in vitro: a potential resolving mechanism of inflammation.* Mediators Inflamm, 2008. **2008**: p. 725854.

71. Copetti, T., F. Demarchi, and C. Schneider, *p65/RelA binds and activates the beclin 1 promoter.* Autophagy, 2009. **5**(6).

72. Criollo, A., et al., *IKK connects autophagy to major stress pathways.* Autophagy, 2010. **6**(1): p. 189-91.

73. Tasdemir, E., et al., *Regulation of autophagy by cytoplasmic p53.* Nat Cell Biol, 2008. **10**(6): p. 676-87.

74. Tasdemir, E., et al., *p53 represses autophagy in a cell cycle-dependent fashion.* Cell Cycle, 2008. **7**(19): p. 3006-11.

75. Maiuri, M.C., et al., *Control of autophagy by oncogenes and tumor suppressor genes.* Cell Death Differ, 2009. **16**(1): p. 87-93.

76. Dikic, I., T. Johansen, and V. Kirkin, *Selective Autophagy in Cancer Development and Therapy.* Cancer Res, 2010.

77. Maddodi, N., et al., *Induction of Autophagy and Inhibition of Melanoma Growth In Vitro and In Vivo by Hyperactivation of Oncogenic BRAF.* J Invest Dermatol, 2010.

78. Zuba-Surma, E.K., et al., *The ImageStream System: a key step to a new era in imaging.* Folia Histochem Cytobiol, 2007. **45**(4): p. 279-90.

79. Wilhelm, S.M., et al., *BAY 43-9006 exhibits broad spectrum oral antitumor activity and targets the RAF/MEK/ERK pathway and receptor tyrosine kinases involved in tumor progression and angiogenesis.* Cancer Res, 2004. **64**(19): p. 7099-109.

80. Davies, B.R., et al., *AZD6244 (ARRY-142886), a potent inhibitor of mitogen-activated protein kinase/extracellular signal-regulated kinase kinase 1/2 kinases: mechanism of action in vivo, pharmacokinetic/pharmacodynamic relationship, and potential for combination in preclinical models.* Mol Cancer Ther, 2007. **6**(8): p. 2209-19.

81. Alter, G., J.M. Malenfant, and M. Altfeld, *CD107a as a functional marker for the identification of natural killer cell activity.* J Immunol Methods, 2004. **294**(1-2): p. 15-22.

82. George, T.C., et al., *Distinguishing modes of cell death using the ImageStream multispectral imaging flow cytometer.* Cytometry A, 2004. **59**(2): p. 237-45.

83. George, T.C., et al., *Quantitative measurement of nuclear translocation events using similarity analysis of multispectral cellular images obtained in flow.* J Immunol Methods, 2006. **311**(1-2): p. 117-29.

84. Henery, S., et al., *Quantitative image based apoptotic index measurement using multispectral imaging flow cytometry: a comparison with standard photometric methods.* Apoptosis, 2008. **13**(8): p. 1054-63.

85. Atienza, J.M., et al., *Dynamic monitoring of cell adhesion and spreading on microelectronic sensor arrays.* J Biomol Screen, 2005. **10**(8): p. 795-805.

86. Kirstein, S.L., et al., *Live cell quality control and utility of real-time cell electronic sensing for assay development.* Assay Drug Dev Technol, 2006. **4**(5): p. 545-53.

87. Zitzmann, K., et al., *Compensatory activation of Akt in response to mTOR and Raf inhibitors - a rationale for dual-targeted therapy approaches in neuroendocrine tumor disease.* Cancer Lett, 2010. **295**(1): p. 100-9.

88. Shimizu, S., et al., *Involvement of JNK in the regulation of autophagic cell death.* Oncogene, 2010. **29**(14): p. 2070-82.

89. Glick, D., S. Barth, and K.F. Macleod, *Autophagy: cellular and molecular mechanisms.* J Pathol, 2010. **221**(1): p. 3-12.

90. Mizushima, N. and T. Yoshimori, *How to interpret LC3 immunoblotting.* Autophagy, 2007. **3**(6): p. 542-5.

91. Klionsky, D.J. and S.D. Emr, *Autophagy as a regulated pathway of cellular degradation.* Science, 2000. **290**(5497): p. 1717-21.

92. Powis, G., et al., *Wortmannin, a potent and selective inhibitor of phosphatidylinositol-3-kinase.* Cancer Res, 1994. **54**(9): p. 2419-23.

93. Petiot, A., et al., *Distinct classes of phosphatidylinositol 3'-kinases are involved in signaling pathways that control macroautophagy in HT-29 cells.* J Biol Chem, 2000. **275**(2): p. 992-8.

94. Corcelle, E., et al., *Disruption of autophagy at the maturation step by the carcinogen lindane is associated with the sustained mitogen-activated protein kinase/extracellular signal-regulated kinase activity.* Cancer Res, 2006. **66**(13): p. 6861-70.

95. Sharma, A., et al., *Targeting mitogen-activated protein kinase/extracellular signal-regulated kinase kinase in the mutant (V600E) B-Raf signaling cascade effectively inhibits melanoma lung metastases.* Cancer Res, 2006. **66**(16): p. 8200-9.

96. Hingorani, S.R., et al., *Suppression of BRAF(V599E) in human melanoma abrogates transformation.* Cancer Res, 2003. **63**(17): p. 5198-202.

97. Iguchi-Manaka, A., et al., *Accelerated tumor growth in mice deficient in DNAM-1 receptor.* J Exp Med, 2008. **205**(13): p. 2959-64.

98. Mendelsohn, C.L., E. Wimmer, and V.R. Racaniello, *Cellular receptor for poliovirus: molecular cloning, nucleotide sequence, and expression of a new member of the immunoglobulin superfamily.* Cell, 1989. **56**(5): p. 855-65.

99. Mueller, S. and E. Wimmer, *Recruitment of nectin-3 to cell-cell junctions through trans-heterophilic interaction with CD155, a vitronectin and poliovirus receptor that localizes to alpha(v)beta3 integrin-containing membrane microdomains.* J Biol Chem, 2003. **278**(33): p. 31251-60.

100. Sloan, K.E., et al., *CD155/PVR plays a key role in cell motility during tumor cell invasion and migration.* BMC Cancer, 2004. **4**: p. 73.

101. Masson, D., et al., *Overexpression of the CD155 gene in human colorectal carcinoma.* Gut, 2001. **49**(2): p. 236-40.

102. Sloan, K.E., et al., *CD155/PVR enhances glioma cell dispersal by regulating adhesion signaling and focal adhesion dynamics.* Cancer Res, 2005. **65**(23): p. 10930-7.

103. Oda, T., S. Ohka, and A. Nomoto, *Ligand stimulation of CD155alpha inhibits cell adhesion and enhances cell migration in fibroblasts.* Biochem Biophys Res Commun, 2004. **319**(4): p. 1253-64.

104. Kakunaga, S., et al., *Enhancement of serum- and platelet-derived growth factor-induced cell proliferation by Necl-5/Tage4/poliovirus receptor/CD155 through the Ras-Raf-MEK-ERK signaling.* J Biol Chem, 2004. **279**(35): p. 36419-25.

105. Kono, T., et al., *The CD155/poliovirus receptor enhances the proliferation of ras-mutated cells.* Int J Cancer, 2008. **122**(2): p. 317-24.

106. Packer, L.M., et al., *Identification of direct transcriptional targets of (V600E)BRAF/MEK signalling in melanoma.* Pigment Cell Melanoma Res, 2009. **22**(6): p. 785-98.

107. Yang, S.K., et al., *Differential and regulated expression of C-X-C, C-C, and C-chemokines by human colon epithelial cells.* Gastroenterology, 1997. **113**(4): p. 1214-23.

108. Viac, J., D. Schmitt, and A. Claudy, *Circulating vascular endothelial growth factor (VEGF) is not a prognostic indicator in malignant melanoma.* Cancer Lett, 1998. **125**(1-2): p. 35-8.

109. Rofstad, E.K. and E.F. Halsor, *Vascular endothelial growth factor, interleukin 8, platelet-derived endothelial cell growth factor, and basic fibroblast growth factor promote angiogenesis and metastasis in human melanoma xenografts.* Cancer Res, 2000. **60**(17): p. 4932-8.

110. Straume, O. and L.A. Akslen, *Expresson of vascular endothelial growth factor, its receptors (FLT-1, KDR) and TSP-1 related to microvessel density and patient outcome in vertical growth phase melanomas.* Am J Pathol, 2001. **159**(1): p. 223-35.

111. Einspahr, J.G., et al., *Expression of vascular endothelial growth factor in early cutaneous melanocytic lesion progression.* Cancer, 2007. **110**(11): p. 2519-27.

112. Meyer-Siegler, K.L., M.A. Bellino, and M. Tannenbaum, *Macrophage migration inhibitory factor evaluation compared with prostate specific antigen as a biomarker in patients with prostate carcinoma.* Cancer, 2002. **94**(5): p. 1449-56.

113. Hudson, J.D., et al., *A proinflammatory cytokine inhibits p53 tumor suppressor activity.* J Exp Med, 1999. **190**(10): p. 1375-82.

114. Fingerle-Rowson, G., et al., *The p53-dependent effects of macrophage migration inhibitory factor revealed by gene targeting.* Proc Natl Acad Sci U S A, 2003. **100**(16): p. 9354-9.

115. Krockenberger, M., et al., *Macrophage migration inhibitory factor contributes to the immune escape of ovarian cancer by down-regulating NKG2D.* J Immunol, 2008. **180**(11): p. 7338-48.

116. Gast, A., et al., *Somatic alterations in the melanoma genome: a high-resolution array-based comparative genomic hybridization study.* Genes Chromosomes Cancer, 2010. **49**(8): p. 733-45.

117. Daniotti, M., et al., *BRAF alterations are associated with complex mutational profiles in malignant melanoma.* Oncogene, 2004. **23**(35): p. 5968-77.

118. Alexaki, V.I., D. Javelaud, and A. Mauviel, *JNK supports survival in melanoma cells by controlling cell cycle arrest and apoptosis.* Pigment Cell Melanoma Res, 2008. **21**(4): p. 429-38.

119. Liu, P., et al., *Targeting the phosphoinositide 3-kinase pathway in cancer.* Nat Rev Drug Discov, 2009. **8**(8): p. 627-44.

120. Persad, S., et al., *Regulation of protein kinase B/Akt-serine 473 phosphorylation by integrin-linked kinase: critical roles for kinase activity and amino acids arginine 211 and serine 343.* J Biol Chem, 2001. **276**(29): p. 27462-9.

121. Chresta, C.M., et al., *AZD8055 is a potent, selective, and orally bioavailable ATP-competitive mammalian target of rapamycin kinase inhibitor with in vitro and in vivo antitumor activity.* Cancer Res, 2010. **70**(1): p. 288-98.

122. Davies, M.A., et al., *A novel AKT3 mutation in melanoma tumours and cell lines.* Br J Cancer, 2008. **99**(8): p. 1265-8.

123. Jin, S. and A.J. Levine, *The p53 functional circuit.* J Cell Sci, 2001. **114**(Pt 23): p. 4139-40.

124. Giaccia, A.J. and M.B. Kastan, *The complexity of p53 modulation: emerging patterns from divergent signals.* Genes Dev, 1998. **12**(19): p. 2973-83.

125. Rubinsztein, D.C., et al., *In search of an "autophagomometer".* Autophagy, 2009. **5**(5).

126. Jia, L., et al., *Inhibition of autophagy abrogates tumour necrosis factor alpha induced apoptosis in human T-lymphoblastic leukaemic cells.* Br J Haematol, 1997. **98**(3): p. 673-85.

127. Fung, C., et al., *Induction of autophagy during extracellular matrix detachment promotes cell survival.* Mol Biol Cell, 2008. **19**(3): p. 797-806.

128. Hamacher-Brady, A., N.R. Brady, and R.A. Gottlieb, *Enhancing macroautophagy protects against ischemia/reperfusion injury in cardiac myocytes.* J Biol Chem, 2006. **281**(40): p. 29776-87.

129. Ciechomska, I.A., et al., *Bcl-2 complexed with Beclin-1 maintains full anti-apoptotic function.* Oncogene, 2009. **28**(21): p. 2128-41.

130. Shimizu, S., et al., *Role of Bcl-2 family proteins in a non-apoptotic programmed cell death dependent on autophagy genes.* Nat Cell Biol, 2004. **6**(12): p. 1221-8.

131. Copetti, T., et al., *p65/RelA modulates BECN1 transcription and autophagy.* Mol Cell Biol, 2009. **29**(10): p. 2594-608.

132. Fabre, C., et al., *NF-kappaB inhibition sensitizes to starvation-induced cell death in high-risk myelodysplastic syndrome and acute myeloid leukemia.* Oncogene, 2007. **26**(28): p. 4071-83.

133. Ogata, M., et al., *Autophagy is activated for cell survival after endoplasmic reticulum stress.* Mol Cell Biol, 2006. **26**(24): p. 9220-31.

134. Zhang, Y., et al., *Fas-mediated autophagy requires JNK activation in HeLa cells.* Biochem Biophys Res Commun, 2008. **377**(4): p. 1205-10.

135. Li, D.D., et al., *The pivotal role of c-Jun NH2-terminal kinase-mediated Beclin 1 expression during anticancer agents-induced autophagy in cancer cells.* Oncogene, 2009. **28**(6): p. 886-98.

136. Gomez-Santos, C., et al., *Dopamine induces autophagic cell death and alpha-synuclein increase in human neuroblastoma SH-SY5Y cells.* J Neurosci Res, 2003. **73**(3): p. 341-50.

137. Rodriguez-Enriquez, S., et al., *Tracker dyes to probe mitochondrial autophagy (mitophagy) in rat hepatocytes.* Autophagy, 2006. **2**(1): p. 39-46.

138. Herrero-Martin, G., et al., *TAK1 activates AMPK-dependent cytoprotective autophagy in TRAIL-treated epithelial cells.* EMBO J, 2009. **28**(6): p. 677-85.

139. Cheng, Y., et al., *ERK and JNK mediate TNFalpha-induced p53 activation in apoptotic and autophagic L929 cell death.* Biochem Biophys Res Commun, 2008. **376**(3): p. 483-8.

140. Eisenberg-Lerner, A. and A. Kimchi, *DAP kinase regulates JNK signaling by binding and activating protein kinase D under oxidative stress.* Cell Death Differ, 2007. **14**(11): p. 1908-15.

141. Cohen, O., et al., *DAP-kinase participates in TNF-alpha- and Fas-induced apoptosis and its function requires the death domain.* J Cell Biol, 1999. **146**(1): p. 141-8.

142. Bentele, M., et al., *Mathematical modeling reveals threshold mechanism in CD95-induced apoptosis.* J Cell Biol, 2004. **166**(6): p. 839-51.

143. Schmidt-Glenewinkel, H., et al., *Systems biological analysis of EGF receptor internalization dynamics for altered receptor levels.* J Biol Chem, 2009.

144. Claerhout, S., et al., *Concomitant inhibition of AKT and autophagy is required for efficient cisplatin-induced apoptosis of metastatic skin carcinoma.* Int J Cancer, 2010.

Acknowledgements

I would like to thank Prof. Dr. Stephan Urban for the representation of this work at the biological faculty of the University of Heidelberg.

To Christine, I want to thank you so much for the great time I had during my dissertation and diploma thesis. Working together with you is a ton of fun, and I greatly enjoyed the freedom you have given, and the trust you have shown me over the last couple of years. You bring so much energy and enthusiasm with you, it is hard to not like science. Actually, I like it - which is a rare finding among PhD students. I am looking forward to being back in the lab to put finishing touches to some parts of this work.

Barb, Browning and Eve, members of the original quartet of abbreviated lab members I am now the last man standing of, it was so much fun around you. I am pretty sure we have been laughing so much at times, it was hard to concentrate for Christine and our neighbours. But I can't help it - ISCH BIN DE BUBBLES. Christian, Ludmila, Tina, Bernadette and Susan you have shown me, that life in the lab could be just as much fun without Bubbles. It is great working with you. Special thanks to Tina and Ludmila for their great work on this project, you have helped a lot.
A great thank you also goes to Guido Wabnitz and Nathan Brady. It is great working together with you guys, thank you for sharing your knowledge and supporting me in this project.

Thank you to all my friends for being great friends!

Of course, I can't thank my parents and my brother and sister enough. Thank you for everything you have given me - support, confidence and love. You have always given me the feeling that I could achieve everything I really want.

Clara you have been so understanding and caring during the last couple of months – thank you for all the "Überraschung!", for always being there for me, and the excitement you bring to my life every day! Without you I certainly would not be half as happy as I am today. Crazy in love!

Appendix

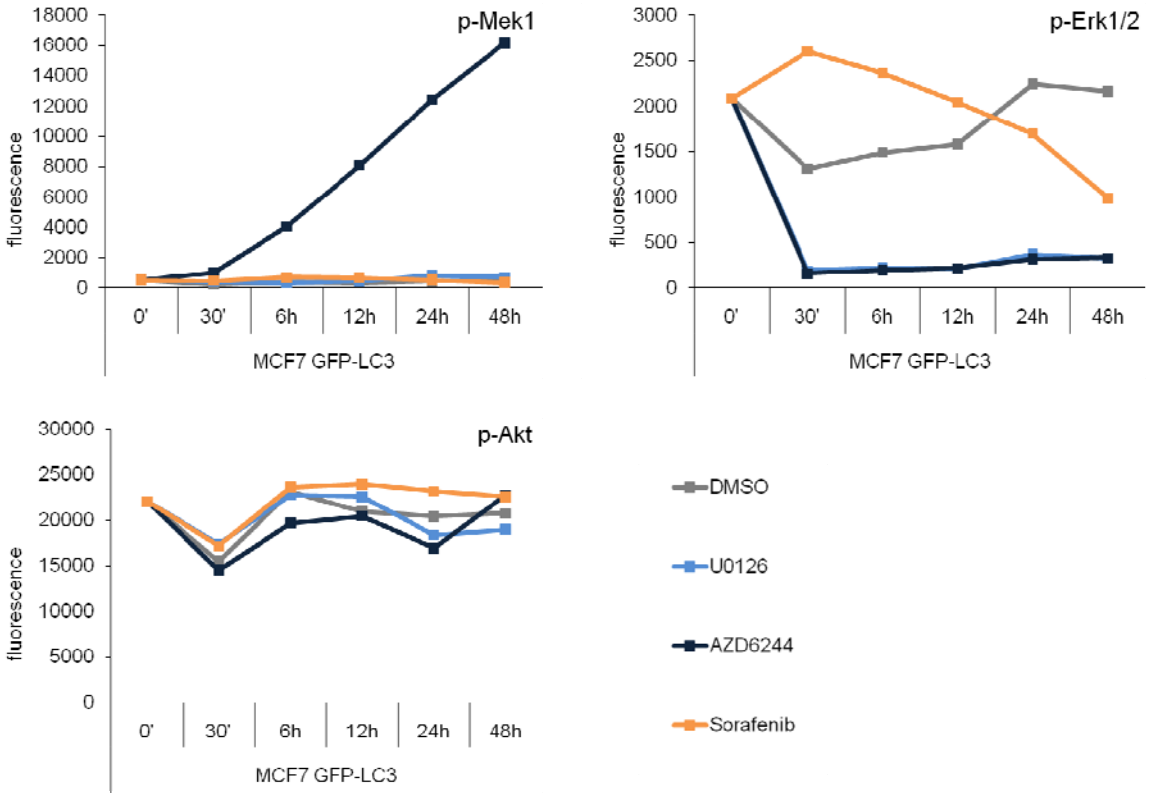

Appendix Figure 1 MCF7 GFP-LC3 cells are BRaf wild-type, but have a constitutively active PI3K pathway. Cells have been treated with U0126 (10µM), AZD6244 (3µM) and Sorafenib (5µM) for 48 hours. AZD6244 displays, as in melanoma cells, increasing phosphorylation of MEK1 upon treatment. Both, MEK1 and ERK1/2 phosphorylation is rather low, underlining the wild-type BRaf signaling. Phosphorylation of ERK1/2 is effectively inhibited with both MEK inhibitors, but Sorafenib, of note, leads to increased phosphorylation of ERK1/2 until 24 hours of treatment. The analysis of Akt phosphorylation displays the constitutively active PI3K signaling, not altered upon inhibition of the MAPK pathway.